



# **Selection and Characterization of Binding Proteins Specific for Amyloidogenic Proteins of Alzheimer Disease**

Inaugural-Dissertation

zur Erlangung des Doktorgrades  
der Mathematisch-Naturwissenschaftlichen Fakultät  
der Heinrich-Heine-Universität Düsseldorf

vorgelegt von

**Clara Sophie Rebecca Grüning**

aus Essen

Düsseldorf, April 2014

aus dem Institut für Physikalische Biologie  
der Heinrich-Heine-Universität Düsseldorf

Gedruckt mit der Genehmigung der  
Mathematisch-Naturwissenschaftlichen Fakultät  
der Heinrich-Heine-Universität Düsseldorf

Referent: Dr. Wolfgang Hoyer

Koreferent: Prof. Dr. Dieter Willbold

Tag der mündlichen Prüfung:

*Für meine Eltern*

---

**CONTENT**

Content.....	I
Summary (Theses).....	III
Zusammenfassung (Thesen).....	V
Introduction.....	7
1.1 Protein Misfolding and Amyloid Diseases .....	7
1.2 Amyloid in Neurodegenerative Diseases.....	7
1.2.1 Amyloid- $\beta$ Peptide.....	10
1.2.2 Tau protein .....	11
1.3 Commonalities between Amyloidogenic Proteins Involved in Neurodegeneration. 13	
1.3.1 The Amyloid-Fold .....	13
1.3.2 The Aggregation Pathway .....	16
1.3.3 Reasons of Misfolding .....	18
1.3.4 Toxic Species.....	20
1.3.5 Mechanism of Toxicity .....	21
1.3.6 Transmission of Toxicity .....	23
1.3.7 Engineered Binding Proteins in Research on Amyloid Diseases .....	24
1.4 Engineered Binding Proteins .....	24
1.4.1 Adnectins.....	26
1.4.2 Anticalins .....	26
1.4.3 Kunitz Domains.....	26
1.4.4 Fynomers.....	28
1.4.5 Affibodies .....	28
1.4.6 ZA $\beta_3$ - an Affibody against A $\beta$ .....	28
1.5 Selection of an Engineered Binding Protein .....	30

---

1.5.1 Phage Display .....	30
Aim of this Work.....	33
Chapter 1 .....	34
Chapter 2 .....	43
Chapter 3 .....	56
Discussion .....	80
2.1 Two Proteins Involved in Alzheimer Disease.....	80
2.2 Characterization of Amyloid- $\beta$ Aggregation Intermediates .....	81
2.2.1 Outlook.....	84
2.3 A Novel Binding Protein to tau .....	84
2.3.1 Outlook.....	87
2.4 Diverse Applications of Engineered Binding Proteins .....	87
References.....	90
Abbreviations .....	103
List of Figures and Tables .....	104
Danksagung .....	105

---

## SUMMARY (THESES)

### **Selection and Characterization of Binding Proteins specific for Amyloidogenic Proteins of Alzheimer Disease**

Alzheimer disease (AD) is a fatal neurological disorder with increasing case numbers worldwide. The AD brain is characterized by progressive neuronal loss along with protein aggregates, senile plaques and neurofibrillary tangles, built up of two major proteins, namely the amyloid- $\beta$  peptide ( $A\beta$ ), a cleavage product of the amyloid precursor protein, and the microtubule-binding protein tau, respectively. Several lines of evidence suggest a neurotoxic role for aggregation intermediates of  $A\beta$  and tau in the course of AD pathogenesis, which emphasize the importance of their characterization to understand and modulate AD progression.

Chapter 1 and chapter 2 of this doctoral thesis are dedicated to the characterization of aggregation intermediates of the  $A\beta$  peptide. Both chapters rely on an engineered binding protein, the affibody  $ZA\beta_3$ , as a co-expression agent for purification of non-aggregated  $A\beta$  from bacterial expression.  $ZA\beta_3$  is a disulfide-linked homodimer that protects  $A\beta$  from aggregation by shielding it in a tunnel-like cavity. This feature also proved successful for the purification of a synthetic covalently-linked  $A\beta$ -dimer (chapter 2). Chapter 1 describes the modification of  $ZA\beta_3$  to a fluorescent detector of monomeric  $A\beta$  by introduction of a tryptophan at a position susceptible to structural changes induced by binding of  $A\beta$ . This  $ZA\beta_3$ -variant,  $ZA\beta_3W$ , enabled the highly specific and quantitative detection of monomeric  $A\beta$  in a dissolution assay of a neurotoxic high molecular weight  $A\beta$  aggregation intermediate, the protofibril.  $ZA\beta_3W$  also impeded the reverse reaction from monomers associating onto the protofibril, a prerequisite for the analysis of the protofibril dissolution. The derived dissociation kinetics of the protofibril followed an exponential decay with a time constant of approximately two hours (25°C), which underlines the high kinetic stability of  $A\beta$  protofibrils. The observed exponential decay is not in agreement with a dissociation of monomers only from the protofibrils' ends, but suggests a dissociation of subunits from all positions of the protofibril.

Chapter 3 deals with the selection of a highly specific binding protein for tau, denoted TP4, from a scaffold library based on ZA $\beta$ <sub>3</sub>. Although elucidation of the TP4:tau complex structure by NMR was impeded by the absence of tau resonance signals in the TP4-bound form, titration experiments and proline mutants of tau demonstrated that two alternative conformations of tau are bound with the same frequency by TP4. These conformations contain regions of high sequence similarity important for tangle formation, PHF6, PHF6\* and PHF6\*\*. Conformation 1 encompasses PHF6 and PHF6\* and conformation 2 encompasses PHF6 and PHF6\*\*. TP4 inhibits tau aggregation, which underlines the importance of these motifs for tangle formation and suggests an interaction of these motifs in tangle formation.

This thesis exemplifies the usage of engineered binding proteins to elucidate structural and mechanistical insights of the amyloidogenic proteins A $\beta$  and tau.

---

## ZUSAMMENFASSUNG (THESEN)

### **Selektion und Charakterisierung spezifischer Bindeproteine für amyloidogene Proteine der Alzheimer-Krankheit**

Die Alzheimer-Krankheit (AD) ist eine tödlich verlaufende neurologische Krankheit mit weltweit ansteigender Fallzahl. Das Alzheimer-Gehirn ist geprägt von dem Verlust von Neuronen und der Ansammlung von Aggregaten (senile Plaques und neurofibrilläre Bündel) zweier Proteine, dem Amyloid- $\beta$  Peptid ( $A\beta$ ), einem Spaltprodukt des Amyloid-Vorläuferproteins (APP), und dem Mikrotubuli-Bindeprotein tau. Mehrere Anhaltspunkte weisen auf eine neurotoxische Rolle von Intermediaten des Aggregationsprozesses beider Proteine im Verlauf der AD hin. Daher ist die Charakterisierung dieser Intermediate essentiell um die molekularen Prozesse der AD zu verstehen und in sie eingreifen zu können.

In den Kapiteln 1 und 2 dieser Dissertation wurden Aggregationsintermediate des  $A\beta$ -Peptids charakterisiert. Beide Kapitel bauen auf der Benutzung eines Bindeproteins, des Affibody  $ZA\beta_3$ , zur Ko-Expression und anschließenden Reinigung von nicht-aggregiertem  $A\beta$  aus Bakterien auf.  $ZA\beta_3$  ist ein durch eine Disulfidbrücke verbundenes Homodimer, das  $A\beta$  durch Abschirmen in einer Tunnel-ähnlichen Vertiefung von der Aggregation abhält. Diese Eigenschaft hat sich, wie in Kapitel 2 gezeigt, auch für die Expression und Reinigung eines kovalent verknüpften  $A\beta$  Dimers bewährt. In Kapitel 1 wurde  $ZA\beta_3$  durch Einfügen eines Tryptophans an eine Position, die bei  $A\beta$ -Bindung strukturellen Veränderungen unterliegt, zu einem fluoreszenten Detektor für monomeres  $A\beta$  modifiziert. Diese  $ZA\beta_3$ -Variante,  $ZA\beta_3W$ , ermöglichte die spezifische und quantitative Detektion von monomerem  $A\beta$  in einem Zerfallsversuch eines  $A\beta$ -Aggregationsintermediats mit hohem Molekulargewicht, der Protofibrille. Voraussetzung für die Verfolgung des Zerfalls der Protofibrille in monomere Bestandteile war dabei, dass  $ZA\beta_3W$  die Rückreaktion der Monomere zur Protofibrille unterband. Die erhaltenen Dissoziationskinetiken entsprechen einem exponentiellen Zerfall mit einer Halbwertszeit von circa zwei Stunden (25°C) und weisen damit auf eine hohe Stabilität der Protofibrille hin. Der exponentielle Zerfall ist nicht vereinbar mit einer

---

Auflösung der Fibrille ausschließlich von den Enden her, sondern weist auf eine Dissoziation von Untereinheiten an jeder Position der Protofibrille hin.

In Kapitel 3 wurde aus einer Proteinbibliothek basierend auf  $\text{ZA}\beta_3$  ein Bindeprotein für tau selektiert, benannt TP4. Auch wenn die Struktur des TP4:tau Komplexes mittels NMR auf Grund des Verschwindens von tau Signalen nach Zugabe von TP4 nicht möglich war, gelang es durch Titrationsexperimente und Prolinmutanten zu zeigen, dass TP4 tau in zwei alternativen Konformationen mit gleicher Häufigkeit bindet. Diese Konformationen enthalten Regionen hoher Sequenzähnlichkeit, die für die Aggregation wichtig sind: PHF6, PHF6\* und PHF6\*\*. Konformation 1 enthält PHF6 und PHF6\* und Konformation 2 enthält PHF6 und PHF6\*\*. Dass die Aggregation von tau durch TP4 unterbunden werden kann, betont die Bedeutung dieser Sequenzmotive und legt eine Interaktion zwischen den Motiven während der Aggregation von tau nahe.

In dieser Dissertation wurden Bindeproteine erfolgreich genutzt um die an der Alzheimer Krankheit beteiligten Proteine, A $\beta$  und tau, strukturell zu untersuchen.

---

## INTRODUCTION

### 1.1 Protein Misfolding and Amyloid Diseases

The proper function of proteins strongly depends upon their three-dimensional folding, ensured through quality control measures, e.g. chaperones, already during translation (1). Misfolding of proteins leads to non-functional proteins that are degraded or accumulate in insoluble aggregates (e.g. inclusion bodies during heterologous protein expression in bacteria (2)). A number of diseases, called amyloidoses, are characterized by the accumulation and deposition of proteins misfolded in an alternative conformation (1). To date, around 20 different proteins and peptides have been associated with amyloidosis, for example the human islet amyloid polypeptide in diabetes II, lysozyme in familial amyloidosis, the peptide amyloid- $\beta$  (A $\beta$ ) in Alzheimer disease (AD) and the Prion protein (PrP) in transmissible spongiform encephalopathies (TSEs). Although these proteins display no primary sequence homology, nor functional or structural similarities in their native conformation, their aggregates share structural characteristics (explained in 1.3.1), which led to their organization into the amyloidosis sub-group of protein misfolding diseases.

### 1.2 Amyloid in Neurodegenerative Diseases

Amyloidosis includes the most common forms of neurodegenerative diseases, such as AD accounting for 60-70% of dementia cases worldwide (corresponding to around 21 to 25 million affected people worldwide (3)). As these diseases are often age-related, their frequency in an aging population is increasing and therefore the problem of their treatment needs to be tackled, which requires the understanding of the aggregation mechanism of the involved proteins, their toxic interactions, and an early diagnosis of the disease.

The clinical symptoms of brain amyloidosis include dementia, other psychiatric problems and movement disabilities, resulting from neurodegeneration and synaptic dysfunction in the

---

central nervous system (1). Post-mortem brain examination of patients unveils the accumulation of normally soluble proteins in filamentous deposits located in characteristic brain areas (Table 1) suggesting a common cause and mechanism for these diseases (4). For example, AD is manifested by neuronal loss and senile plaques in the hippocampus and cerebral cortex (Table 1). Although some neurodegenerative disorders have common protein aggregates, e.g. Parkinson disease and dementia with Lewy bodies (Table 1), the different clinical phenotypes have led to a wide range of names, primarily describing the observed symptoms (5). The diverse phenotypes of the diseases may be explained by the different temporal and brain regional deposition of the involved protein(s) in different cell types or extracellular. In 95% of the AD cases, the malady occurs sporadically (without identified genetic background), whereas in 5% of the cases, a familial genetic background leads to an earlier onset and a greater severity of the disease (1). Remarkably, the deposition of one insoluble protein may be accompanied by the deposition of another protein. For example in AD, the extracellular deposition of A $\beta$  is accompanied by intracellular tau tangle formation. This double amyloidosis applies to around 50% of the sporadic and familial AD cases, whereas the other 50% show a triple amyloidosis, including  $\alpha$ -synuclein aggregates as a third hallmark (AD with Lewy bodies, Table 1, (5)).  $\alpha$ -synuclein aggregates are also found in several other neuronal disorders such as Parkinson disease, dementia with Lewy bodies and multiple system atrophy. Tau pathology is not only a prominent feature of AD, but its deposits are also hallmarks of several other neurodegenerative disorders such as Pick disease, corticobasal degeneration and frontotemporal dementia with parkinsonism linked to chromosome-17 (FTDP-17). The various tauopathies are characterized by tau inclusions of diverse shapes including paired helical filaments (PHFs), straight or ribbon-like filaments (6). FTDP-17 is a hereditary form of tauopathy in which mutations in the tau gene increase tau's tendency to aggregate *in vitro* (7). In fact, familiar forms of dementia, e.g. FTDP-17, AD and others, have helped to link the clinical phenotype and the pathological hallmarks of diseased brains.

**Table 1: Selected features of some neurodegenerative diseases associated with amyloid deposition.** The information is based on (1,5,8-10).

Disease	Mode of Transmission	Clinical Symptoms	Affected Brain Regions	Protein Involved	Microscopic Lesions	Location of Aggregates
Alzheimer disease (AD)	sporadic (95%) or inherited (5%)	progressive dementia	hippocampus, cerebral cortex	amyloid- $\beta$ (A $\beta$ ) tau	amyloid plaques neurofibrillary tangles	extracellular  intracytoplasmic (neurons)
AD with Lewy bodies	mostly sporadic, rarely inherited	progressive dementia, movement disorder	various, in particular cerebral cortex, hippocampus, substantia nigra	$\alpha$ -synuclein	Lewy bodies	intracytoplasmic (neurons)
Parkinson disease	mostly sporadic, rarely inherited	movement disorder	substantia nigra, hypothalamus	$\alpha$ -synuclein	Lewy bodies	intracytoplasmic (neurons)
Corticobasal degeneration, progressive nuclear palsy	mostly sporadic, rarely inherited	cognitive impairment, movement disorder	temporal lobe, cerebral cortex, basal ganglia, substantia nigra	tau (4R)	tau positive inclusions	intracytoplasmic (neurons, oligodendroglia and astrocytes)
Pick disease	mostly sporadic, rarely inherited	behavioural changes, dementia	hippocampus	tau (3R)	Pick bodies	intracytoplasmic (neurons)
Frontotemporal dementia with parkinsonism linked to chromosome 17 (FTDP-17)	inherited	cognitive impairment, personality changes, movement disorder	various, depending on mutation	tau	fibrillar aggregates	intracytoplasmic (neurons)
Transmissible spongiform encephalopathies (TSEs)	sporadic (90%), inherited (8%) or infectious (2%)	dementia, ataxia, psychiatric problems or insomnia	various regions depending on disease, spongiform degeneration	prion protein	prion plaques	extracellular
Amyotrophic lateral sclerosis	sporadic (90%) or inherited (10%)	movement disorder	motor cortex, brainstem	superoxide dismutase	hyaline inclusions	intracytoplasmic (neurons)
Huntington disease	inherited	dementia, motor and psychiatric problems	striatum, cerebral cortex	huntingtin	neuronal inclusions	intranuclear (neurons)

Research is heavily trying to identify drug candidates to treat and prevent neurodegenerative diseases. For this purpose, the understanding of the aggregation mechanism and its linkage to neuronal damage is essential. As the different proteins involved in these neurodegenerative diseases do not share an elevated primary sequence homology, and yet all show an increased tendency to aggregate in a similar structure, a common aggregation mechanism and a common treatment are thinkable (5).

The following sections are discussing general principles of neurodegenerative diseases with the focus on A $\beta$  and tau protein, whose aggregates- senile plaques and neurofibrillary tangles (NFTs) - are the *sine qua non* of AD. Therefore, these two proteins are shortly introduced in the following paragraphs.

### 1.2.1 Amyloid- $\beta$ Peptide

A $\beta$  is a cleavage product of the amyloid precursor protein (APP). APP is an ubiquitously expressed transmembrane protein type I, which is considered to play a role in cell growth, cell adhesion, brain development and maturation, and neuronal calcium homeostasis (11). APP appears in three isoforms due to alternative splicing. The shortest isoform, APP695, is the dominating isoform in neurons and its processing contributes mostly to A $\beta$  release (11). APP belongs to a superfamily of proteins that is found in diverse organisms. Its amino acid sequence is rather conserved, for example rodent APP differs by only three amino acids in the region of the A $\beta$  peptide from the human APP sequence, but this exchange of three amino acids is sufficient to prevent proteolytic A $\beta$  liberation in rodents (11). A $\beta$  is released from APP through a general physiological mechanism: the regulated intramembrane proteolysis (12). The proteinases involved in this process are membrane-bound and consecutively act on APP. The proteolysis can proceed in two divergent pathways the minor of which is called the amyloidogenic pathway (11,13). This pathway involves the consecutive cleavage of APP by two aspartic proteinases,  $\beta$ -secretase (BACE-1) and  $\gamma$ -secretase. BACE-1 cuts APP at the  $\beta$ -site (Fig. 1). The multi-protein complex  $\gamma$ -secretase has diverse cleavage sites, resulting in the generation of A $\beta$  peptides of varying length. The major soluble A $\beta$  peptides ending at residues Val-40 or Ala-42 are generated by cleavage at the  $\gamma$ -site. Other cleavage sites are  $\epsilon$ - and  $\zeta$ -sites which release longer peptides. A current assumption is that

$\gamma$ -secretase first cleaves at the  $\epsilon$ -sites, then  $\zeta$ -sites and the  $\gamma$ -sites, going from A $\beta$ 49 ( $\epsilon$ ) over A $\beta$ 46 ( $\zeta$ ) to A $\beta$ 42 and A $\beta$ 40 ( $\gamma$ ) or from A $\beta$ 48 ( $\epsilon$ ) over A $\beta$ 45 ( $\zeta$ ) to A $\beta$ 42 ( $\gamma$ ) (13). The second and major pathway of APP processing involves the initial cleavage through  $\alpha$ -secretase, a zinc metalloproteinase, in the A $\beta$  peptide region and consecutive cleavage by  $\gamma$ -secretase.

The proteolytic processing of APP not only generates A $\beta$  but also other peptides that might be physiologically active and contribute to disease development e.g. the intracellular domain AICD. Environmental factors and aging influence the APP metabolism and thus might contribute to the sporadic appearance of AD (11,13).

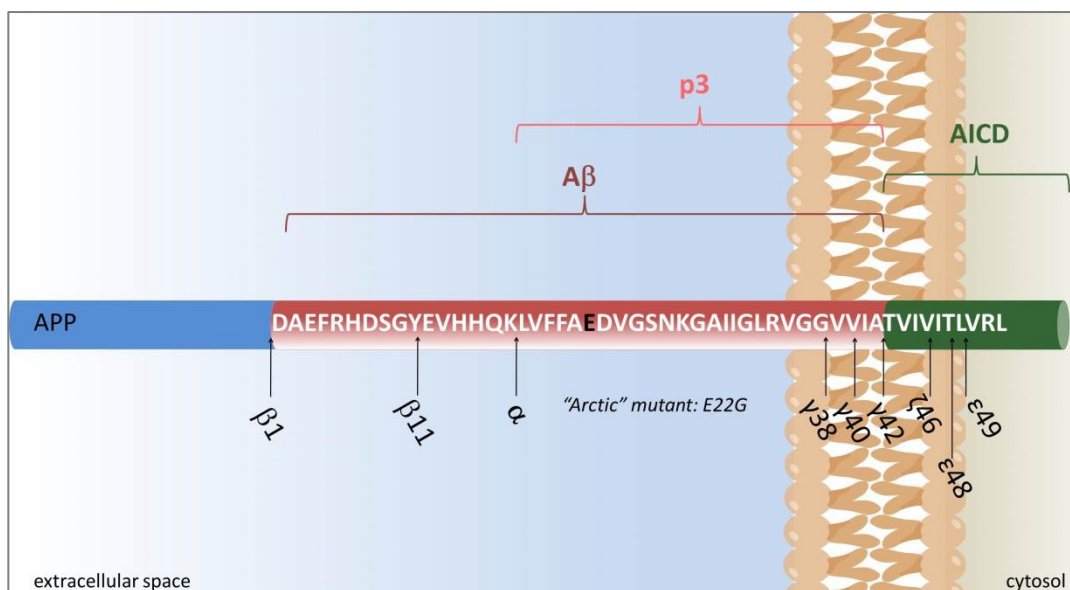


**Figure 1: Cleavage of APP.** APP is processed by three proteases,  $\alpha$ -,  $\beta$ - and  $\gamma$ -secretase yielding several peptides. A $\beta$  peptides of varying length are generated by consecutive cleavage of  $\beta$ - and  $\gamma$ -secretase.  $\beta$ -secretase cuts at D1 ( $\beta$ 1) and rarely between Y10 and E11 ( $\beta$ 11).  $\gamma$ -secretase has several cleavage sites ( $\gamma$ 38,  $\gamma$ 40,  $\gamma$ 42,  $\zeta$ 46,  $\epsilon$ 48,  $\epsilon$ 49). The peptides p3 and AICD are the products of consecutive  $\alpha$ -secretase and  $\gamma$ -secretase action.  $\alpha$ -secretase cuts between K16 and L17 ( $\alpha$ ). The aggregation-promoting mutation E22G, called Arctic mutant, is shown in black. Figure is based on (12,13).

### 1.2.2 Tau protein

The best-studied biological function of tau is its binding to and stabilization of microtubules in the mature neuron, but other cellular functions, such as its role in neuronal signaling pathways have been suggested as well (reviewed in (14)). In the developing brain, tau has been associated with axonogenesis (15,16). The various functions of tau are executed by different regions of the protein: The N-terminal projection domain associates with the cell membrane to regulate microtubule spacing (17), the proline-rich domain mediates

interaction with SH3 domains of other proteins, for example of the non-receptor tyrosine kinase Fyn (18), and the microtubule-binding domain (MTBR), consisting of either three (3R) or four (4R) imperfect repeats, mediates binding to microtubules (19). Tau is expressed from a single gene on chromosome 17 and alternative splicing yields six major isoforms in the adult brain differing in the number of N-terminal inserts and the number of repeats in the MTBR. The longest tau isoform (htau40) consists of 441 amino acids (Fig. 2). The ratio of 4R to 3R tau in the adult brain is 1:1, but can vary characteristically for different tauopathies (13,20,21).

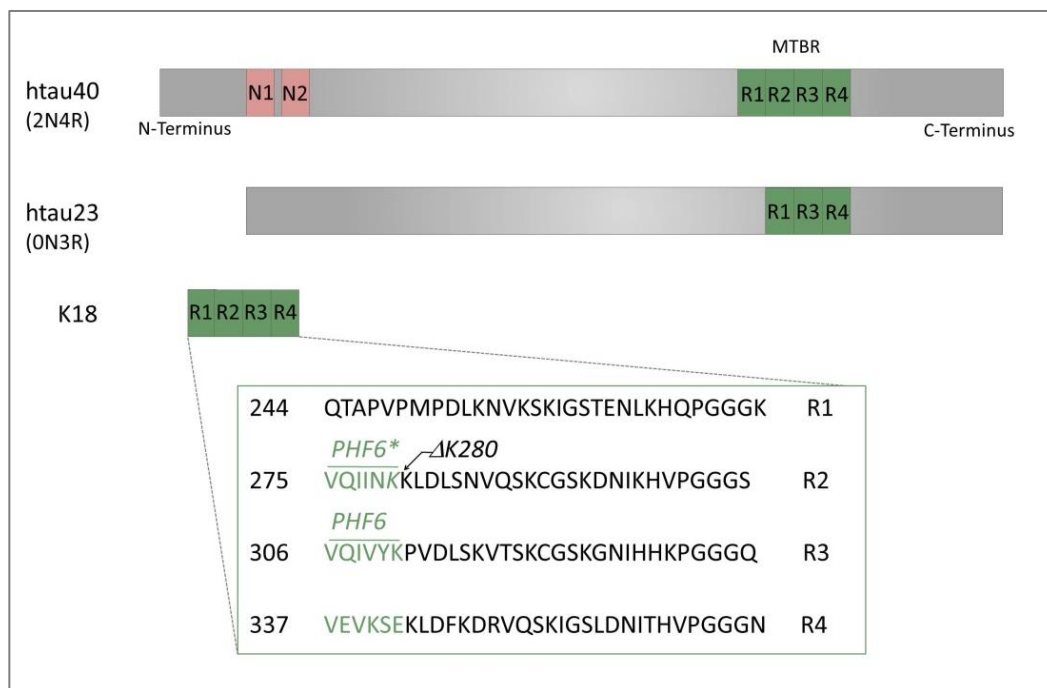


**Figure 2: Isoforms and constructs of tau.** tau is expressed in six isoforms in the adult human brain of which two are shown here. The isoforms differ in the N-terminal inserts and the number of repeat domains (presence of absence of repeat R2). htau40 is the longest tau-isoform harboring two N-terminal inserts, N1 and N2 (red), and four imperfect repeat domains, R1-R4 (green), that build up the microtubule-binding region (MTBR). htau23 differs from htau40 by the lack of the N-terminal inserts and the repeat R2. The construct K18 includes only the four repeat domains; its sequence is depicted in the lower part. The regions of high sequence similarity and high  $\beta$ -sheet propensity are shown in green. The position of the aggregation-promoting mutation  $\Delta$ K280 found in FTDP-17 cases is also indicated.

Soluble tau is an intrinsically disordered protein (22), although particular hexapeptide motifs, denoted PHF6\* and PHF6, in the repeat 2 (R2) and repeat 3 (R3), respectively, exhibit higher  $\beta$ -sheet propensity (23) (Fig. 2). PHF6 and PHF6\* have been identified as the aggregation initiators in the tau sequence (24,25). Furthermore, the phosphorylation state of tau is thought to be relevant for tau's propensity to aggregation. In addition to an intrinsic

regulation by the number of repeat domains, phosphorylation of tau regulates the affinity of tau towards microtubules. Phosphorylation at sites flanking the MTBR decreases tau's affinity for microtubules, whereas phosphorylation at specific sites within the MTBR abolishes binding to microtubules completely (26). Tau phosphorylation leads to an increased pool of soluble tau and might affect tau's conformational behavior and thus contribute in several ways to tau tangle formation.

Research has demonstrated that the aggregation and neurotoxic mechanisms of amyloidogenic proteins share common characteristics, which will be described in the following sections with a focus on A $\beta$  and tau.

### 1.3 Commonalities between Amyloidogenic Proteins Involved in Neurodegeneration

#### 1.3.1 *The Amyloid-Fold*

The pathological definition of amyloid is that the filamentous aggregates are unbranched, found *in vivo*, bind certain dyes, such as Congo Red and Thioflavine T or S, and that they are extracellular. This definition includes the aggregates of A $\beta$ , PrP and human islet amyloid polypeptide. With increasing evidence that also other protein aggregates share the electron-microscopic picture, the structural composition, and tinctorial properties of these typical amyloids, structural biologists have softened this definition to include intracellular aggregates as well as non-disease related aggregates, because the structural elucidation of amyloid structures of all types of proteins helps to understand the cause of aggregation (27). This wider definition includes the tau protein and therefore is the basis of this thesis. The structural feature that describes all amyloid aggregates is the cross- $\beta$  conformation (28). As the native proteins are  $\alpha$ -helical or unordered in structure, large conformational changes are necessary to adopt a  $\beta$ -sheet dominated structure. The  $\beta$ -sheet conformation is stabilized by protein-protein interactions and the bigger the aggregates, the more stable they are (29). Under the electron microscope the filamentous aggregates are observed as long, unbranched fibers with a diameter of 40-185 Å depending on the protein composition. The tau fibril, for example has a thickness of 185 Å as measured by atomic force microscopy (AFM) (30). The core of the fibril is composed of the MTBR region (31-33), which can also

produce fibrils without the N-terminal and C-terminal parts of the protein, construct K18 (32) (Fig. 2). Fibrils of the MTBR region have a diameter of 160 Å in AFM. This small difference was rather surprising as the missing C- and N-terminal domains of the protein make up the majority of the protein, but further AFM studies have demonstrated that the core of the tau filaments is surrounded by a flexible “fuzzy coat” (34). This large unstructured shield exacerbated the elucidation of the  $\beta$ -sheet core of tau fibrils. X-ray diffraction and solid-state NMR studies of truncated tau constructs have revealed that the  $\beta$ -sheet core of NFTs is formed by the MTBR, whereas the N- and C-terminal segments remain unfolded (35-39).

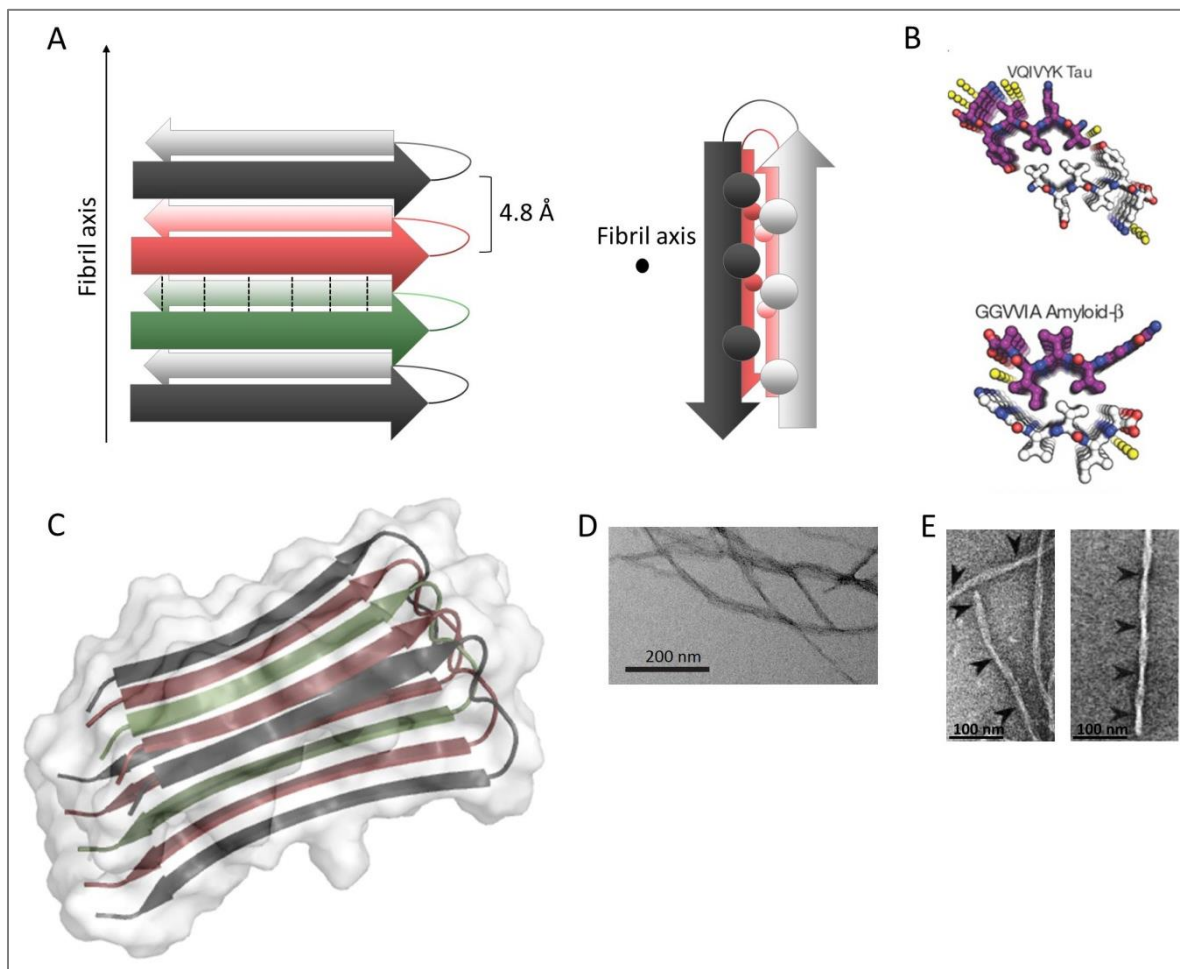


**Figure 3: The amyloid fibril structure.** **A**, the amyloid fibril is composed of parallel in register  $\beta$ -strands perpendicular to the fibril axis here shown schematically as side view (left) and top view (right), where the dots represent amino acid side chains; **B**, dry steric zipper formed by short sequences of tau and A $\beta$ , taken from (40); **C**, model of the A $\beta$  fibril involving residues 18-42 of A $\beta$ 1-42 ((41), PDB code 2BEG, generated using Pymol software); **D**, electron micrograph of A $\beta$ 1-42 fibrils, taken from (42); **E**, electron micrograph of httau40 (left) and K18 (right) PHFs, taken from (43).

The cross- $\beta$  spine of proteins was first described by Astbury (44), when studying denatured egg white in the X-ray beam. He observed a characteristic diffraction pattern with a vertical reflection at 4.8 Å spacing and a diffuse horizontal reflection at around 10 Å spacing (27). Later on, this diffraction pattern was also observed by other researchers investigating the composition of amyloid plaques (28,35,45). As the arrangement of proteins inside the fibril is not as ordered as in a crystal structure, the further elucidation of molecular details of the fibril structure has been challenging. Today, it is generally accepted that the fibril is composed of a set of  $\beta$ -sheets that are parallel to the fiber axis with their extended strands almost perpendicular to the axis (Fig. 3A). The  $\beta$ -strands in the  $\beta$ -sheets build up hydrogen bonds between their amide residues conveying stability to the  $\beta$ -sheet, which can either be parallel or antiparallel. The spacing between parallel strands of the  $\beta$ -sheet is 4.8 Å in line with the vertical 4.8 Å-diffraction. Usually, the side chains of the  $\beta$ -strands are perfectly lying on top of each other (in register) providing further stability to the sheet and facilitating hydrogen bonding between side chain amid groups. The strength of these hydrogen bonds is enhanced by polarization of the adjacent hydrogen bond (46). The interface of the two sheets has mainly been analyzed by short segments of amyloidogenic proteins important for aggregation. Isolated from the rest of the protein, these segments aggregate into microcrystal-like fibers with high morphological similarity to the full-length protein (43,47). These studies (40,48) have revealed that the side-chains of the two opposed  $\beta$ -sheets are tightly interdigitated, comparable to a zipper. This interface is that tightly packed that it is devoid of water molecules and therefore has been named a dry steric zipper (27) (Fig. 3B). If the primary sequence is built of unpolar amino acids, a hydrophobic core between the sheets is formed that stabilizes the filament in addition to the aforementioned hydrogen bonds (29,49). The zipper can be formed either by self-complementary sequences or by different complementary segments of the protein. For A $\beta$ , several dry steric zippers have been described (50) and different segments of A $\beta$ 1-42, e.g. A $\beta$ 10-35, are able to fibrillize *in vitro*. For tau, both hexapeptide motifs, PHF6\* and PHF6, are able to promote aggregation of tau (24,25) and therefore both might also form a dry steric zipper. For one of the hexapeptide motifs, PHF6, Sawaya *et al.* (40) elucidated the dry steric zipper conformation. Siddiqua *et al.* (51) found that the presence of the PHF6\* motif in R2 leads to structural differences between 3R, 4R or mixed 3R and 4R tau aggregates associated with different tauopathies. Thus, the complexity of amyloid fibril structural determination is increased by

---

the possible formation of various dry steric zippers. Furthermore, environmental factors such as temperature, concentration, pH, metal ions, agitation and lipids can also influence the structural characteristics of protein filaments (29). Clarifying the structural polymorphism helps to understand the aggregation process of the amyloidogenic proteins, in particular how the filamentous aggregates of the same protein adopt different shapes in different diseases, and how protein “strains”, like prion strains (27), can appear (52).

### 1.3.2 *The Aggregation Pathway*

Amyloidosis starts with the production of a native protein, which subsequently adopts an alternative  $\beta$ -sheet-rich secondary structure; this conformational change is either induced by interactions with similar protein monomers leading to oligomers, or the conformational change precedes aggregation (1). Most likely, the two initiating steps - structural rearrangement and oligomerization - are dependent on each other and happen simultaneously, in a way that the conformational change towards an increased  $\beta$ -strand population is stabilized by interactions with other proteins of the same species. A further rearrangement going along with a further increase of  $\beta$ -sheet content then produces a fibrillar structure (1,53) (Fig. 4). In this model, the aggregation-initiating step is the rearrangement of the soluble monomer to an aggregation competent conformation. For tau it is suggested that this conformation involves the compaction of the MTBR due to the loss of intramolecular contacts between the MTBR and the N- and C-terminal regions (54,55).

To form a nucleus, it is hypothesized that at least three to four monomers must undergo a conformational rearrangement at the same time and in proximity to each other (56), which makes nucleation obviously a rare event. The binding of matching conformers stabilizes the conformation and generates a nucleus. The aggregation-nucleus recruits and serves as a template for the misfolding of additional protein monomers stabilizing the growing oligomeric structure (29). In the course of the aggregation, a first intermediate species supposedly are protein dimers (57) extending to higher order oligomers and to fibrils by addition of monomers or by coalescence of oligomers (57,58) (Fig. 4A). It is thought that the attachment of a new monomer follows a two-step kinetic process. In the first step, the “dock”-phase, the monomer attaches loosely and reversibly to the growing aggregate; in the second step, the “lock” phase, the deposited molecule is irreversibly attached to the

template (29). For most of the proteins, including A $\beta$  and tau, intermediate species of different size could be isolated from brain material as well as be produced *in vitro* (57,59-61). These species will be further discussed in section 1.3.4. As the increasing  $\beta$ -sheet structures, which are characteristic for certain oligomers and for the fibrils, specifically bind dyes, such as the fluorescence dye Thioflavine T (ThT), the aggregation kinetics can be followed by fluorescence measurements (62,63) (Fig. 4B). The fluorescence experiments first show a lag time depending on protein concentration, temperature, salt concentration, agitation and other factors and then an exponential signal increase indicating the presence of cross- $\beta$  sheet species (63-66). In agreement with a nucleation-dependent aggregation, the addition of a nucleus seed shortens the lag time and accelerates aggregation (65,67).

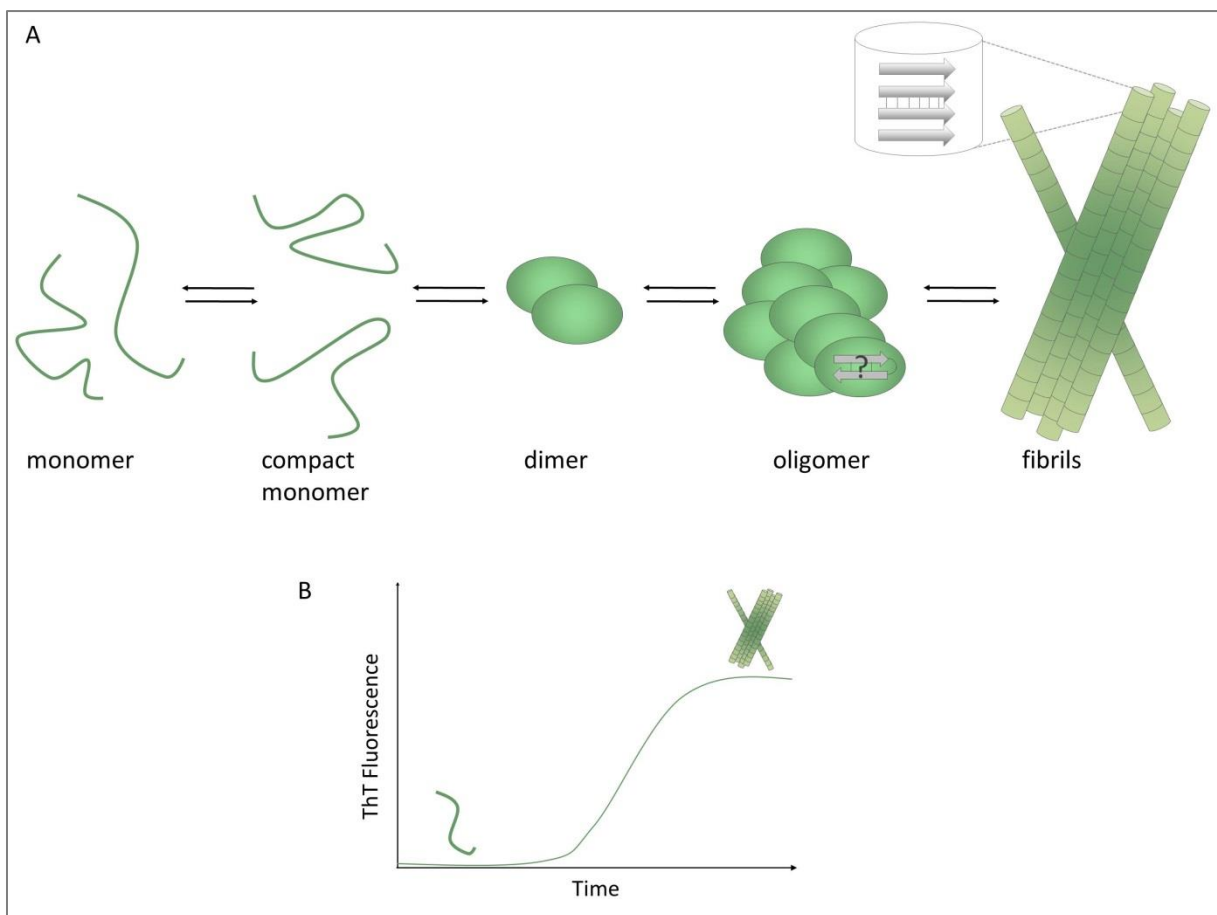


**Figure 4: Amyloid aggregation.** **A**, the amyloid aggregation pathway. Protein monomers fold into a more compact conformation that is stabilized by oligomerization. Oligomers continue to aggregate into fibrils, most likely including a structural rearrangement from antiparallel to parallel  $\beta$ -sheets. **B**, Time course of a typical aggregation experiment followed by the fluorescent dye Thioflavine T. ThT fluorescence increases when intercalated into  $\beta$ -sheet structures that are present in fibrils in contrast to monomers.

### 1.3.3 Reasons of Misfolding

Several influence factors of the aggregation process are discussed in the literature, including environmental factors such as oxidative stress and metal ions (reviewed in (68)), increased protein concentration, posttranslational modifications and genetic mutations. Indeed, first evidence that the proteinaceous aggregates are linked to the clinical symptoms of patients has been provided by familial cases of neurodegenerative diseases. Hereditary forms of tauopathy, for example, are caused mainly by point or deletion mutations in proximity to and within the MTBR. These mutations either diminish the affinity of tau to microtubules and thus, increase the soluble protein concentration, or enhance tau's  $\beta$ -sheet propensity as for example the deletion of Lys-280 (7). Another genetic factor that has recently been discovered is the H1 haplotype, which affects the overall expression level of tau (6). For the rare familiar cases of AD, mutations in the APP gene itself or in the genes of the processing secretases, in particular in the catalytic subunit, presenilin-1, of  $\gamma$ -secretase, can shift the cleavage pattern towards the more aggregation-prone peptide A $\beta$ 1-42. Mutations in the A $\beta$ -region of the APP gene can furthermore influence aggregational properties of the peptide, such as the "Arctic" mutant (APP E693G, A $\beta$  E22G), which accelerates aggregation and protofibril formation (69,70). Thus, mutations contribute to an increased protein concentration of the amyloidogenic proteins in several ways. However, in sporadic cases of AD other factors are supposed to contribute to an increased pool of misfolded protein species; posttranslational modifications are suspected to be one of those various factors. In the case of tau, the protein is extensively posttranslationally modified. The predominant alterations are truncation, oxidation of cysteines and phosphorylation at serine, threonine and tyrosine residues. 4R tau has two cysteines that can form either inter- or intramolecular disulfide bonds under oxidizing conditions. Intramolecular cystins are believed to place tau in an aggregation-incompetent conformation, whereas intermolecular cystins do not interfere with aggregation (71,72). Phosphorylation regulates tau's affinity for the microtubules; phosphorylation at sites flanking the MTBR diminishes tau's affinity for the microtubule, whereas phosphorylation at sites within the MTBR abolishes tau's binding potential to the microtubules completely (26). In NFTs tau has been found to be hyperphosphorylated (more than 10 or more moles of phosphate per tau molecules (6)) indicating a link between tau phosphorylation and aggregation. Several studies investigating the influence of phosphorylation on tau for example through mutations imitating phosphorylation

---

(pseudophosphorylation) have shown that phosphorylation modulates the aggregation process and stabilizes mature fibrils (73,74). N- and C-terminally truncated versions of tau have also been isolated from NFTs (6) and findings that the N- and C-terminal parts of the protein fold to the MTBR and thus retard aggregation (54,55,75) in correlation with the observation that the MTBR alone aggregates faster (7,72) and forms the core of the fibril (33), support a role of proteolysis of tau in AD. Furthermore, Klistunova *et al.* (76) observed fragmentation of tau prior to aggregate formation in cell culture experiments and Park *et al.* (77) identified a neurotoxic tau fragment generated by the activity of the protease calpain.

N-terminal truncations also play a significant role in the aggregation of A $\beta$  (13) and are a prerequisite for further modifications of A $\beta$  such as pyro-glutamate formation of Glu-3 or Glu-11 (78,79). Pyro-glutamate A $\beta$  is discussed to be gravely toxic (80,81) and the removal of the N-terminal charge increases the hydrophobicity of the peptide and may thus increase aggregation propensity (13). In addition, the p3 fragments, A $\beta$ 17-40 and A $\beta$ 17-42, resulting from the consecutive action of  $\alpha$ - and  $\gamma$ -secretase in the non-amyloidogenic pathway, have been found in the AD brain. They show increased hydrophobicity and tend to aggregate (13). Other posttranslational modifications of A $\beta$  observed in the AD brain include isomerization of Asp-residues and oxidation of Met-35 (13,82,83).

Another highly discussed influence factor is oxidative stress, which can either be the cause or consequence of the aggregation and deposition of the amyloidogenic proteins. In fact many of the alterations described are associated with aging, especially oxidative stress, which may explain the late on-set of the sporadic cases of neurodegenerative diseases (1,84).

In the laboratory, the aggregation process of amyloidogenic proteins, such as A $\beta$ , tau and  $\alpha$ -synuclein, can be emulated (cp. 1.3.2). This facilitates testing a variety of factors, such as metal ions, salt concentration, macromolecular crowding, lipids and others on their effect on the protein aggregation kinetics (e.g. (63,65,85-90)). For example, several metal ions have been shown *in vitro* to influence the aggregation kinetics of A $\beta$  (85) and the aggregation of tau can be accelerated by polyanionic cofactors such as heparin or RNA (89).

#### 1.3.4 Toxic Species

Although the hallmarks of AD are senile plaques or neurofibrillary tangles in the brain of patients, increasing evidence suggests that not the insoluble aggregates are the main neurotoxic species, but soluble aggregation intermediates. This hypothesis is based on the observation of patients that suffered from severe cognitive dysfunction but had no protein deposits in the brain (91), and on autopsy brain material that displayed amyloid plaques without recognized clinical symptoms of AD of the patient (92). Nowadays, it is postulated that the insoluble aggregates are rather a dump of misfolded protein, protecting the brain from further damage through soluble toxic oligomers (1,6). The observed cerebral damage in the surroundings of the deposits might result from the dynamic equilibrium between fibril-associated protein, oligomeric species and the respective soluble protein (93). Studies assessing the AD brain load with soluble A $\beta$  oligomers revealed that the presence of soluble oligomeric species correlates more strongly with the observed degree of dementia than do amyloid plaques (94-97). The findings of Lasagna-Reeves *et al.* (98) suggest a similar correlation between tau oligomers and cytotoxicity.

The soluble oligomeric species that have been identified so far are low-molecular weight oligomers (dimers to dodecamers) and higher molecular weight oligomers. These aggregation intermediates have been isolated from human brain material and could be produced *in vitro* (60,61). Their characterization is rather difficult as they are transient and either disassemble or produce fibrils. For tau as well as for A $\beta$ , it is supposed that oligomerization starts with dimerization (57,63,99,100). For A $\beta$ , SDS-stable, neurotoxic dimers could be isolated from human AD brain (99). Ongoing aggregation produces a variety of higher order oligomers, which have been isolated and prepared of A $\beta$  (reviewed by (12)) as well as of tau (reviewed by (101)).

The A $\beta$  oligomeric species show higher toxicity in cell culture compared to fibrils (102,103) and they can induce synaptic alterations when injected into the rodent brain (104,105) underlining that the aggregation intermediates rather than the mature fibrils are the culprits in neurodegenerative diseases (106). Although some of the oligomeric species summarized by Haass & Selkoe (12) are off-pathway, they might share structural properties with fibrils. It has been shown that they contain increased  $\beta$ -sheet content and a NMR study also indicated a parallel in register  $\beta$ -sheet of the A $\beta$  C-terminus in one of the intermediates (107). An

---

engineered binding protein, ZAB<sub>3</sub>, selected to specifically bind Aβ, trapped a transiently adopted β-hairpin conformation of the Aβ monomer (108-110). This β-hairpin conformation most likely represents the conformation of an Aβ monomer in a soluble oligomer (108,110,111). This is underlined by the fact that the stabilized β-hairpin conformation (an Aβ monomer arrested by a disulfide bond) forms stable oligomers that do not produce fibrils (112), which would require a reorientation of the β-strands (108,113).

Tau oligomeric species were also isolated from AD brain and produced *in vitro* (57,98,114). Mouse models of tauopathy indicate that soluble aggregates preceding NFT formation are responsible for neurotoxicity rather than NFTs themselves (115,116). *In vitro* application of tau oligomers in comparison to monomeric and fibrillar tau on SH-SY5Y cells demonstrated an elevated toxicity of the oligomeric species (61). Tau oligomers were found to be β-sheet rich (61) and it is supposed that interactions between PHF6 and PHF6\* stabilize these oligomers (117).

Presumably, some oligomeric structures share a common structure and thus might mediate toxicity through a similar pathway (118,119), but it remains to be elucidated if the increase in toxicity is due to a greater diffusion capability of the soluble intermediates compared to large insoluble fibrils, or if structural properties (120,121), or the oligomers' interactions lead to neuronal death (5).

### 1.3.5 Mechanism of Toxicity

In neurodegenerative diseases, the occurrence of proteinaceous deposits is accompanied by neuronal loss, synaptic dysfunction and neuroinflammation. The affected brain regions differ among the different clinical diseases (Table 1). Neuronal loss can occur via programmed cell death or apoptosis (122).

Generally, three basic theories of the toxic mechanism as the cause for neuronal loss can be distinguished (1). The first hypothesis is the loss-of-function hypothesis, in which neurodegeneration is the result of the loss of regular activity of the protein, because it misfolds and aggregates. This hypothesis is underlined by observations of impairments in axonal transport if the microtubule binding protein tau aggregates (123-126).

The second hypothesis is the gain-of-toxic activity hypothesis, which suggests that due to misfolding the protein adopts a neurotoxic function. This hypothesis is based on studies

---

demonstrating direct induction of apoptosis by aggregated proteins *in vitro* (61,127), toxicity of A $\beta$  aggregates (oligomers, protofibrils, fibrils) in cell culture (128), and on the realization that  $\beta$ -sheet oligomerization in general, i.e. also of non-disease-related proteins, can be cytotoxic (118).

The third hypothesis suggests that the large protein deposits induce chronic neuroinflammation, which in turn causes synaptic damage and neuronal loss. Observed extensive astrogliosis and microglial activation in the brain of patients indicate an inflammatory process (129).

Most likely several aspects of these hypotheses act jointly and cause neuronal damage (5). Various conditions, genetic factors as well as environmental factors (compare 1.3.3), high protein production, and insufficient protein removal lead to an increased protein concentration promoting misfolding and aggregation. The aggregation intermediates and neglected cellular functions initiate a cascade of cellular events that finally result in neuronal death. Recently, special attention has been paid to the role of tau in this cascade of events. Tau pathology often accompanies the deposition of A $\beta$  or  $\alpha$ -synuclein in neurodegenerative diseases and a single A $\beta$  brain amyloidosis has not been identified so far in contrast to single tauopathies. This gives tau a central role of a common pathway leading to neurodegeneration (5). Recent research has demonstrated that tau expression is crucial for A $\beta$ -mediated toxicity (130,131).

As amyloid deposits such as A $\beta$  plaques are in a dynamic equilibrium with their proteinaceous constituents, they are thought to be responsible for local neuritic dystrophy, gliosis and synaptic alterations (132,133). Additionally, they may act as a source providing constantly smaller, soluble intermediates that function as neurotoxins (99,134,135). For these smaller aggregates a toxic activity has been demonstrated (102,104,136). How the oligomeric species execute their toxic activity is rather unknown so far.

For A $\beta$ , receptor-mediated and non-receptor mediated membrane toxic activity has been reported. A $\beta$  oligomers may interact with membrane-bound receptors such as PrP (137) or epidermal growth factor receptor (138) and initiate an intracellular signaling cascade including the protein-kinase Fyn (139), which has been linked to tau phosphorylation (compare 1.2.2). Or A $\beta$  oligomers may insert into the membrane, forming a pore and acting

as a neurotoxin through cell leakage (4,140). The isoform APP695 is also supposed to exercise a receptor-like function and to be involved in neurodegeneration through G<sub>o</sub>-protein activation (11). Furthermore, APP and A $\beta$  are also accumulated in mitochondria of AD patients connected with mitochondrial dysfunction and impairment of cell metabolism, which results e.g. in an increase of reactive oxygen species (11). The cleavage product AICD of APP is also suspected to induce neuronal cell death (11).

For tau, a neurotoxic function through muscarinic receptor activation (141,142), mitochondrial damage or cellular leakage is proposed as well (6).

For both proteins, however, a clear concept of how toxicity is exercised is still missing.

### 1.3.6 *Transmission of Toxicity*

Understanding the toxic origin and mechanism of a disease is also important from the epidemic perspective. The observation that an aggregation seed (nucleus) can minimize the lag time of fibril formation *in vitro* renders amyloids as transmissible per se (27). It is thus important to investigate if a seed can have the same effect in a cell, tissue or in an organism. The question of the transmissibility of a misfolded protein has thus two perspectives: The first one concerns the propagation of a misfolded template protein from cell to cell, the second one assesses the transmission of a proteinaceous seed from organism to organism. In this field of investigation the prion-diseases (TSEs) have demonstrated that in fact proteinaceous particles can be infective (143,144). In certain cases, a prion can even induce the aggregation of a heterologous protein. For example, misfolded bovine PrP can induce misfolding of human PrP, leading to Creutzfeld-Jakob disease (145). For the case of AD, a transmission between organisms has not been observed so far. But rodent studies have demonstrated that the onset of neurodegeneration can be accelerated by the injection of diseased brain material of AD patients or aged APP-mice into the brain of young human APP-expressing mice (146,147). A $\beta$  plaques first occurred in the brain region of injection and then spread into neighboring areas. Another study has demonstrated that A $\beta$  pathology can also be induced by intraperitoneal injection of A $\beta$  brain material (148). For tau, similar experiments produced comparable results. Brain injections of tau tangles induced tau misfolding of recipient mice expressing human tau (149,150) and a spreading from the injection area to anatomically connected regions was observed. This suggests a cell-to-cell based propagation mechanism of misfolded protein (151,152).

### 1.3.7 *Engineered Binding Proteins in Research on Amyloid Diseases*

Several of the studies presented herein rely on the usage of binding proteins especially antibodies for sensitive and specific protein detection or isolation (e.g. (99,146,151,152)). Moreover, binding proteins have also delivered other important insights into AD research. For example, a conformational antibody generated to synthetic A $\beta$  oligomers was able to detect oligomers of other amyloidogenic proteins as well indicating that these species have a similar structural basis (119). Furthermore, one prominent therapeutic approach to AD is immunotherapy based on vaccination or direct administration of antibodies (reviewed in (153)). Besides antibodies, engineered binding proteins have demonstrated to be useful instruments in immunotherapy as well as in structural biology. In immunotherapy, antibody fragments may help to reduce side effects of the antibody treatment (153) and in structural biology engineered binding proteins help to obtain structural information. For example, an engineered binding protein to A $\beta$  trapped the A $\beta$  monomer in an antiparallel  $\beta$ -sheet conformation that involves comparable residues to the parallel  $\beta$ -sheet in the fibril (108) (cp. 1.3.4). Thus, binding proteins offer a great variety of possible applications and a great gain of information. Therefore, this thesis relies on engineered binding proteins to gain insights into AD pathology. The following sections will introduce binding proteins in a general manner and explain one way of how an engineered binding protein can be obtained.

## 1.4 **Engineered Binding Proteins**

The best known binding proteins are antibodies or immunoglobulins, produced by vertebrates' immune system to disarm foreign molecules, particles or microorganisms. The antibody's binding site consists of six loops, the complementarity-determining regions (CDRs) that address their target (antigen) with high specificity. The CDRs length and amino acid composition is highly variable and fitted through a natural selection process (154). The CDRs represent only a minor part of the antibody, while the major part conveys stability to the antibody and serves other functions, e.g. phagocytosis activation. The antibody is composed of two different polypeptide chains, the heavy and the light chain. Two chains of each type build up the antibody and each polypeptide chain contributes to antigen binding

with one of its  $\beta$ -sheet immunoglobulin domains ( $V_H$  and  $V_L$  domains) (Fig. 5A). The relatively big size (around 150 kDa) of these glycoproteins and the disulfide bonding between the polypeptide chains complicates recombinant production and limits the usage of antibodies (155). Nevertheless, immunoglobulins dominate the range of available affinity proteins employed for research, diagnostics and medical therapy (156,157). To circumvent the limitations of antibodies, smaller constructs were designed that maintain the high affinity towards antigens but are smaller in size. An example is the Fab fragment with a size of approximately 55 kDa which contains the complete light chain connected to a fragment of the heavy chain by a disulfide bridge and importantly the intact antigen binding site (Fig. 5B). As the constant region (Fc) interacts with other components of the immune system, the Fab construct missing the Fc region is preferable when communication to the immune system is not desirable. An even smaller immunoglobulin fragment is the single-chain antibody (scFv) with a size of 28 kDa. The scFv is composed of the variable domains of the heavy ( $V_H$ ) and the light chain ( $V_L$ ) connected by a polypeptide linker. Fab and scFv fragments have been further adapted and optimized to provide multivalent binders gaining affinity through avidity effects, e.g. a dimeric scFv called diabody (158), or bispecific antibodies that can target two different antigens, e.g. the bispecific T-cell engager BiTE (159). A further reduction of size was obtained by limiting the construct to one single immunoglobulin domain, either  $V_H$  or  $V_L$  (160-162). In nature, examples of these single domain antibodies (sdAbs) can be found in camelids or cartilaginous fish. In sdAbs a single immunoglobulin domain is responsible for antigen binding (in camelids VHH or in sharks V-NAR), which as well shows good solubility and stability as an independent protein of 15 kDa (160,163). scFv and sdAbs have been used successfully for selection of novel binding proteins (e.g. (164), reviewed in (160)).

As molecular recognition and highly specific binding is not limited to immunoglobulins, but are core features of protein interactions in nature, researchers have tried to engineer affinity proteins based on other protein frameworks as well. These protein backbones, the so-called scaffolds, have to tolerate variations in their amino acid sequence to a certain extent without loss of stability and solubility. In the past, over 50 protein scaffolds have been suggested (165). Preferably, the scaffold is small in size and is composed of a single polypeptide chain facilitating recombinant production. Furthermore, the scaffolds have to fulfil particular criteria depending on their intended usage, e.g. as an imaging agent, the affinity protein besides being small in size to enable tissue penetration, has to be cleared

---

rapidly from blood *in vivo* to reduce background signal and has to withstand harsh labelling conditions. Some examples of proteins that were derived from alternative scaffolds are adnectins, anticalins, Kunitz domains, fynomers, and affibodies, which will be shortly described in the following as a selection of alternative scaffold proteins (Fig. 5C-H).

#### 1.4.1 *Adnectins*

Adnectins were engineered from the 10th fibronectin type III domain, which is a 10 kDa,  $\beta$ -sheet folded domain resembling an immunoglobulin domain, by randomization of two or three surface loops (167,168) (Fig. 5C). A successful example of an adnectin is CT-322, which binds to VEGFR2 (human vascular endothelial growth factor receptor 2), relevant in carcinosis, with subnanomolar affinity and thus blocks VEGFR2's receptor function. CT-322 is currently in phase II of clinical trials for cancer therapy (169).

#### 1.4.2 *Anticalins*

Anticalins are affinity proteins derived from the bilin-binding protein, a lipocalin transport protein (Fig. 5D). Lipocalins are able to transport a great variety of molecules by their highly adaptive binding cavity formed by four flexible loops inside a rigid  $\beta$ -barrel conveying the necessary stability. By varying 16 residues in these four loops, anticalins against low molecular weight components, such as fluorescein and the steroid digoxigenin, were selected (170,171). Based on other lipocalins, further libraries were designed and used to select anticalins targeting other low molecular weight components or proteins (reviewed in (172)).

#### 1.4.3 *Kunitz Domains*

The protease inhibitor domain of the amyloid- $\beta$  precursor protein is the scaffold behind the Kunitz domain (Fig. 5E). It is only one example of a protease inhibitor modified to generate specific binders against pharmaceutical relevant targets, mostly proteases (173). Kunitz domains are small in size (60 amino acids) and are stabilized by three disulfide bonds. Their binding site is positioned in one exposed loop, which facilitates randomization and library creation (173).

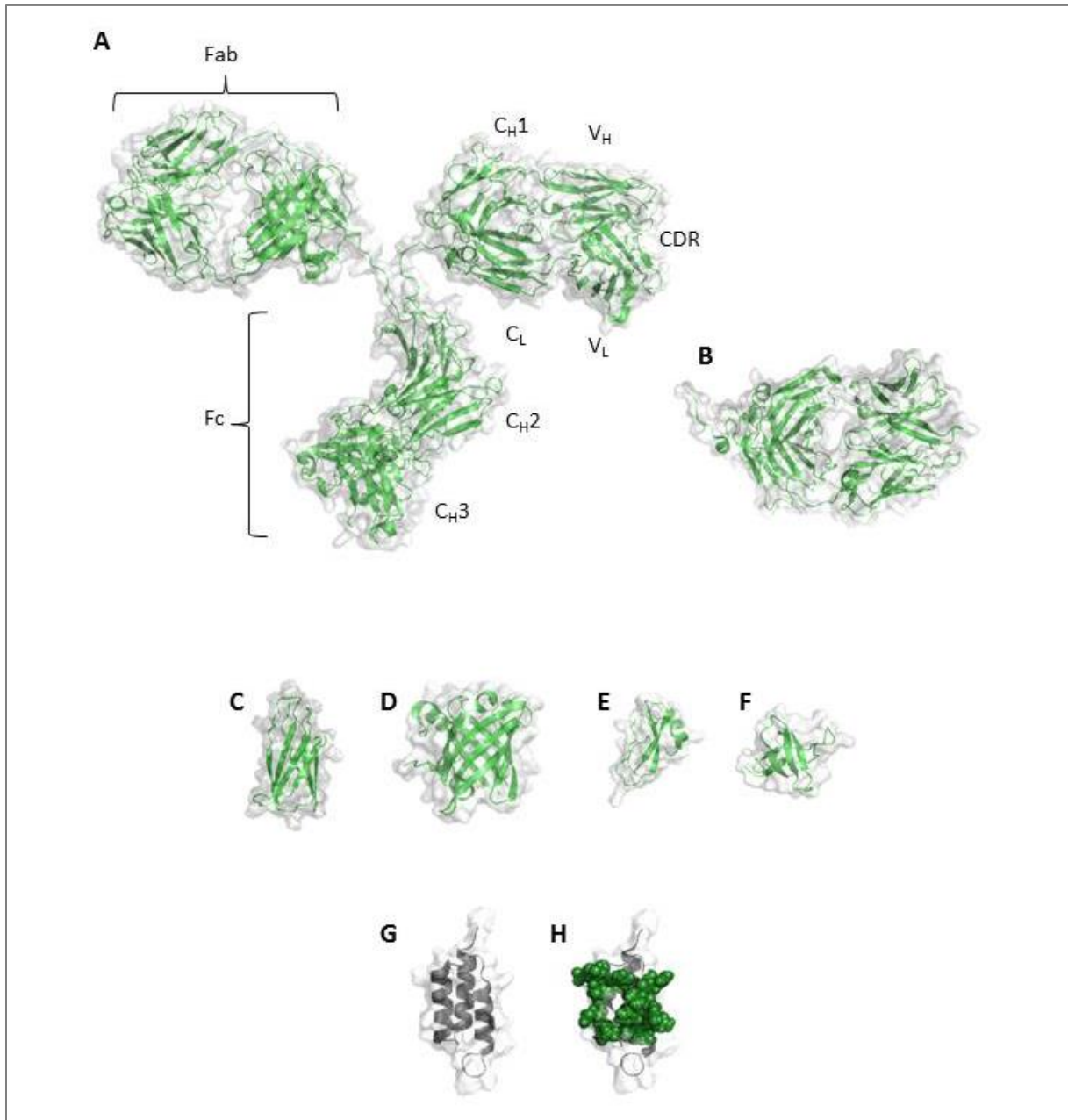


**Figure 5: Representative illustrations of selected binding protein scaffolds.** The surface of each molecule and the backbone chain are depicted, generated using Pymol software. **A**, a typical antibody (PDB code 1IGT) composed of two light chains of two immunoglobulin domains ( $C_L$  and  $V_L$ ) each and two heavy chains composed of four immunoglobulin domains each ( $V_H$ ,  $C_{H1}$ - $C_{H3}$ ). The complementarity-determining region (CDR) is built up by the N-terminal variable immunoglobulin domains of the heavy and the light chain ( $V_H$  and  $V_L$ ). By cleavage with papain two antibody fragments, Fab and Fc, respectively, are obtained. The Fab fragment provides binding affinity whereas the Fc fragment interacts with other components, e.g. macrophages, of the immune system; **B**, a Fab fragment (PDB code 3AAZ); **C**, adnectin, based on the 10th fibronectin type III domain, which is depicted here (PDB code 1TTG); **D**, anticalin, derived from a lipocalin, here an anticalin tailored to target dioxigenin is depicted (PDB code 1LKE); **E**, Kunitz domain, based on the protease inhibitor domain of APP, which is depicted here (PDB code 1AAP); **F**, fynomer, based on the Fyn SH3 domain, which is depicted here (PDB code 1M27); **G+H**, Z-domain (PDB code 1Q2N), diversified residues for generation of a library from which  $Z\alpha\beta_3$  (166) originates are depicted in green spheres.

#### 1.4.4 Fynomers

Fynomers are affinity proteins derived from the human Fyn SH3 domain by randomization of surface-exposed loops and subsequent selection by phage display (Fig. 5F). They are small in size (7 kDa) and contain no disulfide bonds. Furthermore, as the Fyn SH3 domain is conserved from mice to humans their immunogenicity is evaluated as low (174).

#### 1.4.5 Affibodies

The affibody scaffold is derived from a 58 amino acid domain of a cell wall protein from *Staphylococcus aureus*. This protein, denoted protein A, enables the bacterium to hide from the immune system by binding the Fc-part of immunoglobulins and thus inverting the orientation of the antibodies. The so disguised *Staphylococcus* is protected from opsonisation and phagocytosis. Because of protein A's capacity to bind a great variety of immunoglobulins, protein A has been used in a wide range of biotechnological applications such as antibody extraction. Protein A is built of five immunoglobulin-binding domains, of which one was used to engineer a stable and highly soluble protein denoted Z-domain which differs by one amino acid substitution from the original protein A domain (substitution of glycine 29 by alanine, (175), Fig. 5G). By randomization of 13 surface-exposed residues in two of the three  $\alpha$ -helices responsible for binding of the Fc-part of immunoglobulins, a library was generated from the Z-domain (166) (Fig. 5H). From this library, several affinity proteins, called affibodies, have been selected by *in vitro* selection techniques targeting a great variety of proteins, e.g. the Alzheimer disease-related A $\beta$  peptides (109) and the breast cancer-related receptor HER2 (human epidermal growth factor receptor 2) (176). A HER2-affibody is currently in development as an imaging reagent for tumor visualization (177). Affibodies have been employed for a wide range of applications in areas of imaging (diagnostics), medical therapy, and biotechnological research and production (reviewed in (178)).

#### 1.4.6 ZA $\beta_3$ - an Affibody against A $\beta$

As A $\beta$  peptides are strongly related to the pathogenesis of Alzheimer disease (cp. 1.3), current therapeutic research aims at i) inhibiting the production of A $\beta$  peptides, e.g. by blocking protease activity; ii) reversing or inhibiting A $\beta$  aggregation; iii) increasing A $\beta$  clearance or iv) disarming the potential toxic oligomeric species (179). Immunotherapy has contributed to drug development through various approaches, including active

immunization and passive immunization with various affinity proteins derived from different frameworks, which target different epitopes and exhibit different modes of action (153). Several antibodies, targeting different linear epitopes or a conformational epitope are in clinical trials (reviewed in (153)). Some antibodies produced severe side effects in clinical trials, which could be circumvented by reducing the antibody's affinity to its cell-membrane receptor (180) demonstrating that also smaller antibody fragments could be valuable tools in AD treatment. scFvs, Fabs and dAbs have been identified, some selected by phage display, that had anti-aggregatory and neuroprotective function (181-183).

An alternative scaffold protein selected to bind A $\beta$  peptides with high affinity is the affibody ZA $\beta_3$  that resulted from phage display selection against A $\beta$ 1-40 (109) (Fig. 6A). ZA $\beta_3$  binds the central and C-terminal residues (17-36) of the A $\beta$  peptide with nanomolar affinity (17 nM according to isothermal titration calorimetry (184)). During the *in vitro* evolution process, a cysteine residue at position 28 in the ZA $\beta_3$  sequence was selected enabling ZA $\beta_3$  to form a disulfide-linked homodimer (the term ZA $\beta_3$  refers to the dimeric form (108,109)) that generates a cavity to bind A $\beta$  by coupled-folding (108,184). This is in contrast to the flat binding surface offered by the original Z-domain and to most of the other alternative scaffold proteins presented above, which bind their targets through surface-exposed loops. Only, the anticalin-scaffold offers a binding cavity adapted particularly to the binding of small molecules. Moreover, the binding mechanism of ZA $\beta_3$ , coupled-folding, is unique in the range of scaffold proteins presented herein.

The A $\beta$  peptide in complex with ZA $\beta_3$  adopts a  $\beta$ -hairpin fold that is characterized by two antiparallel  $\beta$ -strands formed by residues 17-23 and 30-36 and a linker given by residues 24-29. The hairpin of A $\beta$  is flanked on each site by a short  $\beta$ -strand formed by residues of 15-18 of each ZA $\beta_3$  molecule. This  $\beta$ -strand replaces helix three of the three  $\alpha$ -helices bundle (108). The hairpin-fold of A $\beta$  in complex with ZA $\beta_3$  resembles the structure of A $\beta$  within the amyloid fibril, which is also characterized by a  $\beta$ -strand-turn- $\beta$ -strand arrangement (108). ZA $\beta_3$  is able to capture A $\beta$  in plasma and serum (109) and to inhibit A $\beta$  aggregation *in vitro* (108). In a *Drosophila* AD model, ZA $\beta_3$  co-expression led to a prolonged life time of flies (185) due to the sequestration of the aggregation-prone central part of the A $\beta$  peptide.

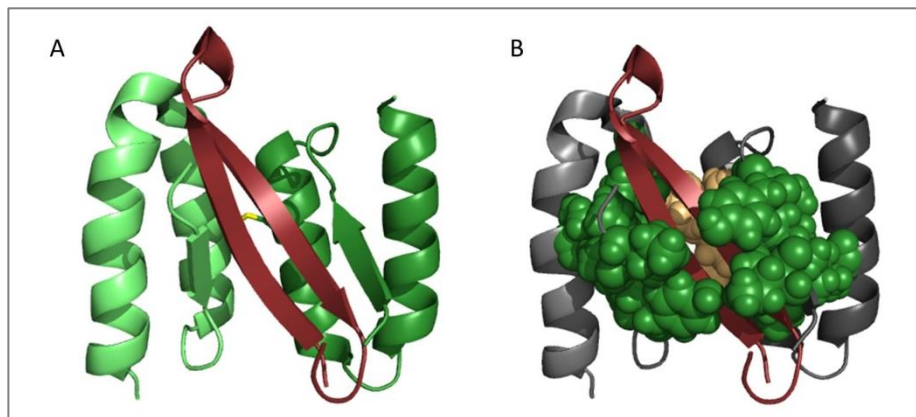


**Figure 6: The ZAβ<sub>3</sub>:Aβ<sub>1-40</sub> complex.** **A**, NMR structure of the ZAβ<sub>3</sub> homodimer (green) linked by a disulfide bridge (yellow) bound to Aβ<sub>1-40</sub> (red). Aβ<sub>1-40</sub> adopts a β-hairpin fold that is supported by short β-strands of ZAβ<sub>3</sub>. **B**, ZAβ<sub>3</sub> as scaffold protein. The residues that contribute to the binding of Aβ were substituted by all amino acids (residues 16, 17, 18, 19, 30, 34, 45, green) or only hydrophobic amino acids (residues 27 and 31, orange) to maintain the hydrophobic core of the homodimer around the disulfide bridge (PDB code 2OTK, generated using Pymol software).

## 1.5 Selection of an Engineered Binding Protein

Isolation of a protein with the desired binding properties from a large library requires techniques that allow fast screening of the library, especially as the necessary changes to induce binding are rarely predictable. To date, a great variety of selection systems have been developed, which can be categorized into three categories: cell-dependent systems, e.g. phage display and yeast display, cell-free systems, e.g. ribosomal display and mRNA display, and non-display systems, e.g. yeast-two-hybrid (165). Each of these selection systems has its advantages and limitations, but all are based on a linkage between genotype, protein sequence and binding propensity. The selection procedure itself relies on several selection and amplification cycles with the aim to enrich variants binding the target. As this thesis is based on phage display technology, this procedure will be explained in more detail in the following.

### 1.5.1 Phage Display

Among all developed selection procedures phage display using M13 filamentous phage is used most widely (165). For phage display, the gene variants of the scaffold protein are inserted into a phagemid vector fused to the C-terminus of a phage coat protein enabling

---

exposure of a library member on the phage surface. Mostly, the phage coat protein pIII is used as a fusion partner as the phage rather tolerates bigger proteins fused to pIII probably because only five copies of pIII are localized at the tip of the phage (186). The M13 origin of replication present on the phagemid vector allows production of single-stranded DNA, packed into the phage, whereas the standard origin of replication (*oriC*) allows replication of the vector in *E. coli* (187,188). The translated fusion protein is directed to the bacterial periplasm by the C-terminally fused leader sequence, where pIII plugs (together with protein pVI) the assembled phage before it detaches from the bacterial surface. As the phagemid vector only delivers the pIII gene, helper phages, e.g. M13KO7, are needed to generate phage particles. In average, only one copy of the fusion-protein is incorporated into the tip together with wild-type pIII (189). *E. coli* cells harboring the phagemid vector are thus infected with helper phages, whose genome is less efficiently replicated due to a mutation in the *pII* gene, which results in secreted phage particles displaying and encoding simultaneously a single scaffold library member. These phages are subsequently employed in a selection process, referred to as panning (165) (Fig. 7). In the first step of the selection procedure, the phages are incubated with the target protein. A common procedure is the biotinylation of the target protein enabling the formation of phage:target protein complexes in solution and the isolation of these complexes by addition of a streptavidin surface, e.g. on magnetic beads. Phages are eluted from the streptavidin surface and used to infect new *E. coli* cells creating an enriched library of affinity proteins, which is the initial library for a subsequent selection round. Typically, three to five rounds of panning are performed with increasing stringency, e.g. decreased target concentration, to produce high affinity binders. Finally, the library enriched in target-specific proteins is analyzed clone-by-clone for the binding properties and protein sequence.

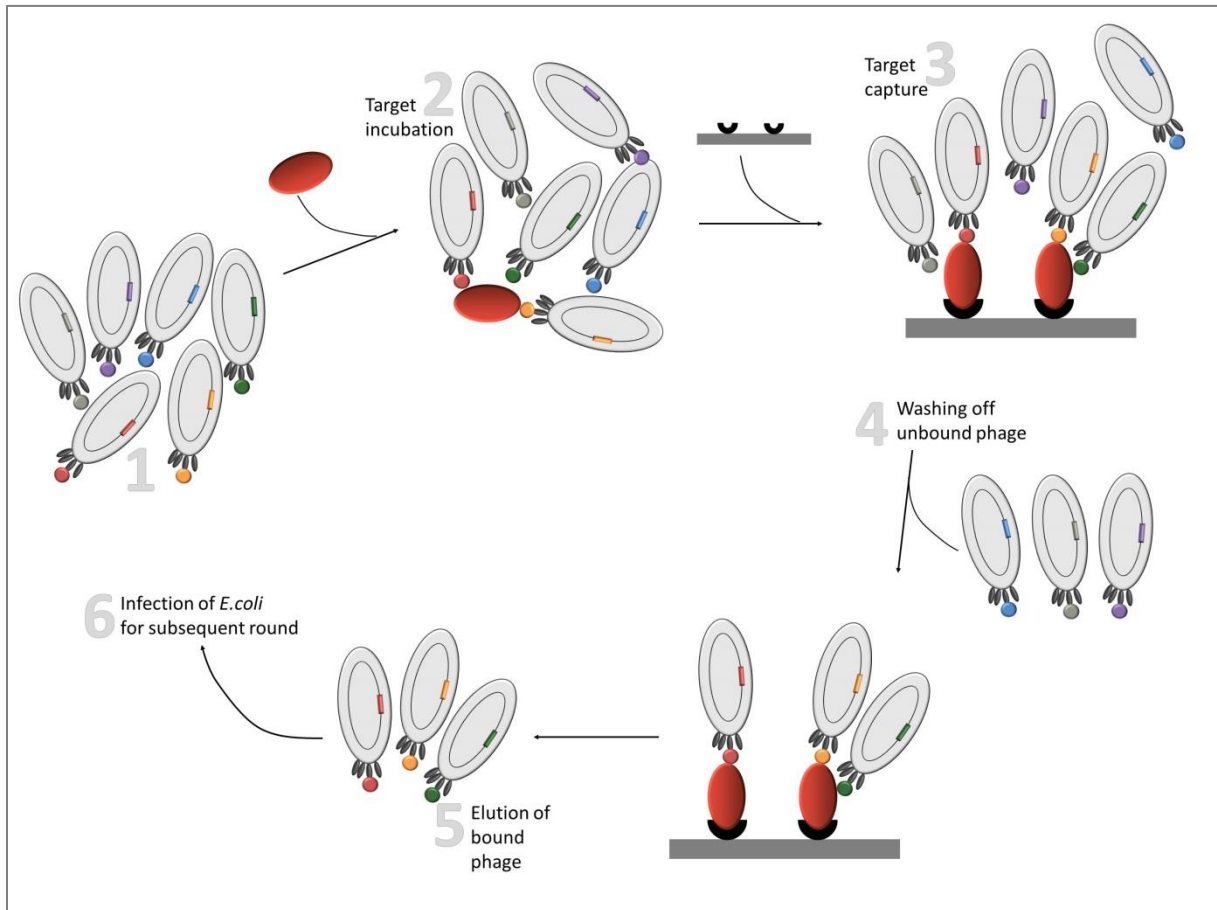


**Figure 7: Schematic of the phage display procedure.** **1**, the library inserted into a phagemid vector as a fusion protein to the pIII phage protein is packed into phages by superinfection of *E. coli* cells with helper phages; **2**, the prepared phage library is incubated with the target yielding phage:target protein complexes; **3**, the biotinylated target protein: phage complex is captured by streptavidin magnetic beads; **4**, unbound phages are washed off and **5**, phages are eluted from the biotinylated target protein by lowering the pH; **6**, eluted phages are used to infect *E. coli* cells for a subsequent round of panning.

---

## AIM OF THIS WORK

The deposits of the proteins A $\beta$  and tau are the neuropathological hallmarks of AD. Evidence from hereditary forms of AD suggests an involvement of these proteins in the course of the disease, most likely connected to the misfolding and oligomerization of these proteins. To be able to provide therapeutic treatment and early diagnosis, it is essential to understand the toxic mechanism and the aggregational properties of the proteins involved. Binding proteins largely contributed to the understanding of these features; the engineered binding protein ZA $\beta$ <sub>3</sub> for example has helped to understand conformational properties of the A $\beta$  peptide. ZA $\beta$ <sub>3</sub> is in several ways the basis of this work: It is employed as a detection tool, as a co-expression and purification agent, and as a scaffold protein to derive new binding proteins.

A first goal of this thesis is to assess the kinetic properties of A $\beta$  oligomer dissolution by exploiting the ability of ZA $\beta$ <sub>3</sub> to bind specifically monomeric A $\beta$ . As a dynamic equilibrium between monomers, oligomeric species and fibrils is supposed for A $\beta$  *in vivo*, the analysis of the kinetics of this process is fundamental, especially as oligomeric species are suspected to be the main toxic species.

A second intention of this thesis is to find a binding protein to tau, the second hallmark protein of AD. For this purpose, ZA $\beta$ <sub>3</sub> is an ideal scaffold as it possesses already affinity to an amyloid protein. In addition, fibrils of amyloid proteins share a common fold (the amyloid-fold) and aggregation intermediates of several amyloid proteins can be detected by the same conformational antibody (119), it is nearby to assume that randomization of ZA $\beta$ <sub>3</sub> might generate binders to other amyloidogenic proteins. The binding cavity and the binding mechanism of ZA $\beta$ <sub>3</sub> are quite unique and might thus provide binding properties specialized to the binding of amyloidogenic proteins. This project includes the selection of a ZA $\beta$ <sub>3</sub> variant to the protein tau and the subsequent characterization of the selected ZA $\beta$ <sub>3</sub> variant.

---

**CHAPTER 1****THE OFF-RATE OF MONOMERS DISSOCIATING FROM AMYLOID-BETA PROTOFIBRILS**

Clara S. R. Grüning\*, Stefan Klinker\*, Martin Wolff, Mario Schneider, Küpra Töksöz, Antonia N. Klein, Luitgard Nagel-Steger, Dieter Willbold, and Wolfgang Hoyer

\* Both authors contributed equally to this work

**Status:** published in *Journal of Biological Chemistry* on November 18, 2013

**Impact Factor:** 4.651 (2012)

**Own proportion to this work:** 45%

Design, cloning, expression and purification of ZA $\beta_3$ W, expression and purification of A $\beta$ , preparation and isolation of A $\beta$  oligomers and fibrils, preparation and analysis of fluorescence dissolution assay of A $\beta$  oligomers and fibrils, preparation of transmission electron microscopic samples.

## The Off-rate of Monomers Dissociating from Amyloid- $\beta$ Protofibrils\*

Received for publication, August 23, 2013, and in revised form, October 30, 2013. Published, JBC Papers in Press, November 18, 2013, DOI 10.1074/jbc.M113.513432

Clara S. R. Grüning<sup>+1</sup>, Stefan Klinker<sup>+1</sup>, Martin Wolff<sup>+5</sup>, Mario Schneider<sup>+</sup>, Küpra Toksöz<sup>+</sup>, Antonia N. Klein<sup>5</sup>, Luitgard Nagel-Steger<sup>+5</sup>, Dieter Willbold<sup>+5</sup>, and Wolfgang Hoyer<sup>+5,2</sup>

From the <sup>+</sup>Institute of Physical Biology, Heinrich-Heine-Universität, 40204 Düsseldorf and the <sup>5</sup>Institute of Structural Biochemistry (ICS-6), Research Centre Jülich, 52425 Jülich, Germany

**Background:** Protofibrils of the amyloid- $\beta$  peptide (A $\beta$ ) are neurotoxic oligomers implicated in development and progression of Alzheimer disease.

**Results:** The dissociation of A $\beta$  protofibrils into their monomeric subunits is a slow process, occurring on the time scale of hours.

**Conclusion:** A $\beta$  protofibrils possess a high kinetic stability toward dissociation into monomers.

**Significance:** The longevity of A $\beta$  protofibrils permits sustained toxic effects.

The interconversion of monomers, oligomers, and amyloid fibrils of the amyloid- $\beta$  peptide (A $\beta$ ) has been implicated in the pathogenesis of Alzheimer disease. The determination of the kinetics of the individual association and dissociation reactions is hampered by the fact that forward and reverse reactions to/from different aggregation states occur simultaneously. Here, we report the kinetics of dissociation of A $\beta$  monomers from protofibrils, prefibrillar high molecular weight oligomers previously shown to possess pronounced neurotoxicity. An engineered binding protein sequestering specifically monomeric A $\beta$  was employed to follow protofibril dissociation by tryptophan fluorescence, precluding confounding effects of reverse or competing reactions. A $\beta$  protofibril dissociation into monomers follows exponential decay kinetics with a time constant of  $\sim 2$  h at 25 °C and an activation energy of 80 kJ/mol, values typical for high affinity biomolecular interactions. This study demonstrates the high kinetic stability of A $\beta$  protofibrils toward dissociation into monomers and supports the delineation of the A $\beta$  folding and assembly energy landscape.

Amyloid fibrils composed of amyloid- $\beta$  peptide (A $\beta$ )<sup>3</sup> are the main protein component of senile plaques found in the brains of Alzheimer disease patients (1, 2). Genetics, cell culture studies, and animal models support a critical role of A $\beta$  in Alzheimer disease pathogenesis, with the 42-amino acid A $\beta$ 42 peptide being more aggregation-prone and neurotoxic than the more common 40-amino acid A $\beta$ 40 variant. A $\beta$  forms different types of prefibrillar oligomers, which, according to several lines of evidence, include the most toxic A $\beta$  species (3, 4). Neurotoxic high molecular weight oligomers referred to as protofibrils or A $\beta$ -derived diffusible ligands have been purified by size

exclusion chromatography (SEC) of A $\beta$  incubations (4–10). A $\beta$  protofibrils are heterogeneous in size (in the range of 50–1500 kDa) and morphology, comprising spherical, annular, and curvilinear assemblies. The protofibrils are in equilibrium with both monomers and fibrils (7). The dynamics of the monomer-protofibril-fibril equilibrium is crucial for A $\beta$  toxicity, as (i) the different association states exhibit different toxicities (2, 3), and (ii) toxicity emanates from the polymerization reaction itself (11). It is thus valuable to gain kinetic information on the individual interconversion steps. Knowledge of the kinetic stability of the involved species furthermore aids in the delineation of the amyloid folding and assembly energy landscape (12, 13).

In this study, we determined the off-rate of monomers dissociating from A $\beta$  protofibrils by tryptophan fluorescence using a tryptophan-containing variant of the engineered A $\beta$ -binding protein ZA $\beta$ 3. ZA $\beta$ 3, which has been selected previously from an Affibody protein library, specifically binds monomeric A $\beta$  with an affinity of  $K_d = 17$  nM (14, 15). ZA $\beta$ 3 is a dimer of two identical subunits composed of 58 amino acids covalently linked by a disulfide bond. ZA $\beta$ 3 inhibits A $\beta$  oligomerization and aggregation by sequestering the aggregation-prone central and C-terminal sequence regions of monomeric A $\beta$  (15, 16). The addition of an excess of the tryptophan-containing variant ZA $\beta$ 3W to SEC-purified A $\beta$  protofibrils enabled the detection of monomeric A $\beta$  dissociating from protofibrils while preventing the reverse reaction from monomers to protofibrils as well as the reaction to amyloid fibrils. The temperature-dependent kinetic stability of A $\beta$  protofibrils toward dissociation into monomers could thus be assessed.

### EXPERIMENTAL PROCEDURES

**Cloning of ZA $\beta$ 3W**—Site-directed mutagenesis was achieved by back-to-back primer PCR (17). Plasmid pAY442 containing the ZA $\beta$ 3 gene (14) was amplified with phosphorylated primers, one of which carried the mutation for the Y18W exchange at the 5'-end. The vector was religated, and the mutation was verified by sequencing.

**Expression and Purification of ZA $\beta$ 3W**—Expression and purification were done as described previously (18) with minor

\* This work was supported by the Ministerium für Innovation, Wissenschaft und Forschung des Landes Nordrhein-Westfalen.

<sup>1</sup> Both authors contributed equally to this work.

<sup>2</sup> To whom correspondence should be addressed: Inst. of Physical Biology, Heinrich-Heine-Universität, 40204 Düsseldorf, Germany. Tel.: 49-211-811-5153; Fax: 49-211-811-5167; E-mail: wolfgang.hoyer@uni-duesseldorf.de.

<sup>3</sup> The abbreviations used are: A $\beta$ , amyloid- $\beta$  peptide; SEC, size exclusion chromatography; AUC, analytical ultracentrifugation.

modifications. For cell lysis, high pressure (2.9 kilobars; Constant Systems) was used. After affinity chromatography, SEC (Superdex 75 16/60, GE Healthcare) was performed in 20 mM sodium phosphate and 50 mM NaCl (pH 7.2).

**Expression, Purification, and Protofibril Formation of A $\beta$ —**A $\beta$ 40 and A $\beta$ 42 were produced with an N-terminal methionine by recombinant coexpression with ZA $\beta$ 3 (19). For protein expression, unlabeled M9 medium without Celtone was used. The cell pellet was resuspended in 50 mM sodium phosphate, 200 mM NaCl, and 20 mM imidazole (pH 8.0). For cell disruption, high pressure (2.9 kilobars) was used. Affinity chromatography was performed on an ÄKTA Purifier system using a 5-ml HisTrap FF column (GE Healthcare). A $\beta$  was eluted from the ZA $\beta$ 3-A $\beta$  complex bound on the column with 8 M urea and 20 mM sodium phosphate (pH 7.6). The eluted A $\beta$  was washed over a 1-ml HisTrap FF column equilibrated in urea to remove any residual ZA $\beta$ 3. Buffer exchange to 20 mM sodium phosphate (pH 7.0) was achieved by SEC (Superdex 75 16/60). The pH was adjusted to 10 to prevent aggregation during storage (4 °C) and during concentration (Vivaspin 20 3000 MWCO PES, Sartorius AG). For preparation of protofibrils, the pH was titrated back to 7. At room temperature, A $\beta$ 42 was incubated at a concentration of  $\sim$ 100  $\mu$ M for 1–4 h, whereas A $\beta$ 40 was incubated at a concentration of  $\sim$ 500  $\mu$ M for 24 h. The formation of protofibrils was monitored by analytical SEC runs (Superdex 75 10/300; 20 mM sodium phosphate (pH 7.0)). Protofibrils were purified by SEC and immediately employed in the fluorescence assay. The A $\beta$  concentration of the freshly eluted protofibril fractions was determined by UV absorption at 280 nm. A protofibril batch referred to in this study is defined as one particular protofibril preparation starting from an individual A $\beta$  expression cell pellet. To test fibril dissociation, amyloid fibrils were prepared by incubation of 650  $\mu$ l of 380  $\mu$ M A $\beta$ 42 in 20 mM sodium phosphate (pH 7.0) and 0.03% sodium azide for 1 week at 37 °C in a 2-ml glass vial, with stirring at 300 rpm using a micro stir bar.

**Fluorescence Assay**—Protofibril dissociation samples with a volume of  $\sim$ 500  $\mu$ l were prepared in 5  $\times$  5-mm fluorescence cells (101.016-QS, Hellma) and sealed with Parafilm. An air-water interface was present at the top of the solutions. The samples were equipped with crown magnetic stirring bars (Jasco) and stirred at 500 rpm. A $\beta$  concentrations between 4 and 35  $\mu$ M were employed in the dissociation assay, and ZA $\beta$ 3W was added at an excess of  $\sim$ 25% to ensure removal of dissociated A $\beta$  monomers from the monomer-protofibril equilibrium. The time elapsed between protofibril elution from SEC and the addition of ZA $\beta$ 3W was  $\sim$ 15 min.

Tryptophan fluorescence was excited at 295 nm, and emission spectra were recorded from 330 to 360 nm on a Jasco FP-6500 spectrofluorometer. The excitation and emission bandwidths were 5 and 1 nm, respectively, and the data pitch was 0.2 nm. The fluorescence was repeatedly measured over  $\sim$ 12 h, during which time the sample temperature was kept constant using external water-jacketed cell holders. For fluorescence measurements, cells were transferred to the spectrofluorometer cell holder, which was thermostatted at 25 °C.

The  $\lambda_{\text{max}}$  values of the fluorescence emission spectra were determined by fitting the fluorescence intensity to an empirical

## Kinetic Stability of A $\beta$ Protofibrils

fitting function (1) using a trust region reflective algorithm implemented in MATLAB 2011 (MathWorks) (Equation 1),

$$F = F_0 + \Delta F e^{-e^{-\left(\frac{\lambda - \lambda_{\text{max}}}{\Gamma}\right) - \frac{\lambda - \lambda_{\text{max}}}{\Gamma} + 1}} \quad (\text{Eq. 1})$$

where  $F_0$  is the fluorescence intensity offset,  $F_0 + \Delta F$  is the fluorescence intensity at  $\lambda_{\text{max}}$ , and  $\Gamma$  is the peak width. The fraction of free ZA $\beta$ 3W was determined from  $\lambda_{\text{max}}$  as explained under “Results,” employing the fit shown in Fig. 1D and complying with Equation 2.

$$\frac{[\text{ZA}\beta 3\text{W}_{\text{free}}]}{[\text{ZA}\beta 3\text{W}_{\text{total}}]} = 1.935 - 1.1143 \cdot 10^{14} e^{-0.09311 \lambda_{\text{max}}} \quad (\text{Eq. 2})$$

The fraction of free ZA $\beta$ 3W dependent on incubation time was plotted, and a monoexponential fit to Equation 3 was employed to obtain individual apparent  $k_{\text{off}}$  values for each dissociation experiment using OriginPro 8.6 (OriginLab) (Equation 3).

$$\frac{[\text{ZA}\beta 3\text{W}_{\text{free}}]}{[\text{ZA}\beta 3\text{W}_{\text{total}}]} = A_1 e^{-k_{\text{off}} t} + y_0 \quad (\text{Eq. 3})$$

A global fit of all A $\beta$ 42 protofibril dissociation data sets recorded at 25 °C to a triexponential decay with individual amplitudes  $A_1$ ,  $A_2$ , and  $A_3$  and offset  $y_0$  but shared rate constants  $k_{\text{off},1}$ ,  $k_{\text{off},2}$ , and  $k_{\text{off},3}$  was performed according to Equation 4.

$$\frac{[\text{ZA}\beta 3\text{W}_{\text{free}}]}{[\text{ZA}\beta 3\text{W}_{\text{total}}]} = A_1 e^{-k_{\text{off},1} t} + A_2 e^{-k_{\text{off},2} t} + A_3 e^{-k_{\text{off},3} t} + y_0 \quad (\text{Eq. 4})$$

The fraction of A $\beta$  in protofibrils was calculated according to Equation 5.

$$\frac{[\text{A}\beta_{\text{in protofibrils}}]}{[\text{A}\beta_{\text{total}}]} = \left( \frac{[\text{ZA}\beta 3\text{W}_{\text{free}}]}{[\text{ZA}\beta 3\text{W}_{\text{total}}]} - y_0 \right) / (1 - y_0) \quad (\text{Eq. 5})$$

**Transmission Electron Microscopy**—A $\beta$  samples were diluted to 1  $\mu$ M and incubated for 3 min on a Formvar/carbon-coated copper grid (S162, Plano). The grid was washed three times with H<sub>2</sub>O and one time with 2% aqueous uranyl acetate before incubation for 1 min with 2% aqueous uranyl acetate for negative staining, followed by drying overnight. The samples were examined with a Libra 120 electron microscope (Zeiss) operating at 120 kV.

**Analytical Ultracentrifugation**—Analytical ultracentrifugation (AUC) was performed in an Optima XL-A analytical ultracentrifuge (Beckman Coulter) with absorbance optics using an An-60 Ti rotor with aluminum 2-channel centerpiece cells. Sedimentation velocity centrifugation was done at 40,000 rpm and 20 °C. The intensity at 230 nm was recorded (radial resolution, 0.03 cm; continuous mode; no replicate; one scan/3 min). The run duration was 5 h for the protofibril sample and 10 h for the samples containing ZA $\beta$ 3W. Data were fitted using the continuous distribution ( $c(s)$ ) Lamm equation model with a  $\bar{v}$  of 0.738 cm<sup>3</sup>/g based on the A $\beta$ 42 sequence for the protofibril sample and a  $\bar{v}$  of 0.721 cm<sup>3</sup>/g based on the ZA $\beta$ 3W sequence for the ZA $\beta$ 3W samples in the software package Sedfit. An  $s$ -value resolution of 0.3 or 0.025 S was chosen for the fit of the

### Kinetic Stability of A $\beta$ Protofibrils

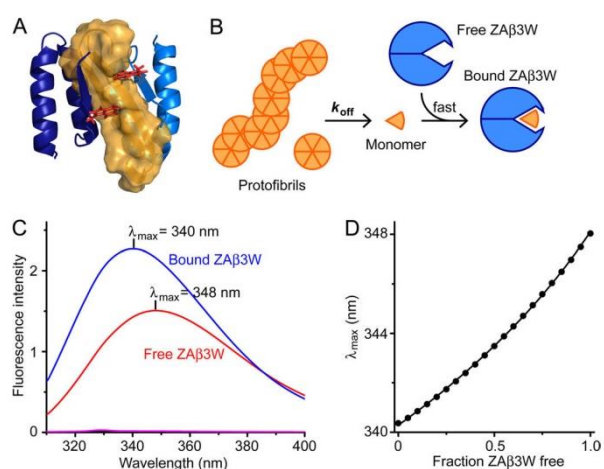


**FIGURE 1. ZAB3W as a probe for A $\beta$  protofibril dissociation.** *A*, model of the ZAB3W-A $\beta$  complex. Tyr-18 in both subunits (*blue* and *marine*) of ZAB3 (Protein Data Bank entry 2OTK) was replaced by tryptophan (*red sticks*). A $\beta$ (16–40) is shown in *orange*. *B*, scheme of protofibril dissociation monitored by binding of A $\beta$  monomers to ZAB3W. *C*, fluorescence emission spectra of ZAB3W in the absence (*red*) and presence (*blue*) of a stoichiometric amount of A $\beta$ 42 monomers and spectra of free A $\beta$ 42 (*magenta*) and buffer (*black*). *D*,  $\lambda_{\max}$  of fluorescence emission spectra of simulated mixtures of free and bound ZAB3W (●). The *line* represents a fit to an exponential function employed to calculate the fraction of free ZAB3W from experimentally determined  $\lambda_{\max}$  values.

protofibril sample or the ZAB3W samples, respectively. The quality of the fits was confirmed by low root mean square deviations below  $A_{230} = 0.005$ . Specified amounts of species in the protofibril sample resulted from the  $c(s)$  distribution exclusive of the area below 0.6 S, which contains a base-line deconvolution artifact. The  $s$ -values determined were corrected for water at 20 °C.

**Isothermal Titration Calorimetry**—Isothermal titration calorimetry was performed essentially as described previously (15) using an iTC200 calorimeter (GE Healthcare).

## RESULTS

**ZAB3W Is a Tryptophan Fluorescence Probe for Monomeric A $\beta$** —Binding of ZAB3 to A $\beta$  is accompanied by a decrease in tyrosine fluorescence (18), presumably due to altered fluorescence properties of Tyr-18 in both ZAB3 subunits, which are located at the binding interface. To exploit the higher extinction coefficient, higher quantum yield, and greater environmental sensitivity of tryptophan compared with tyrosine, a ZAB3 variant termed ZAB3W was generated by site-directed mutagenesis of Tyr-18 to Trp-18 (Fig. 1A). ZAB3W bound monomeric A $\beta$ 40 with an affinity of  $K_d = 20$  nM as determined by isothermal titration calorimetry, which is close to the value of  $K_d = 17$  nM obtained for ZAB3 (15). Thus, the Y18W mutation did not significantly affect the affinity. The fluorescence emission spectrum of free ZAB3W had a maximum at 348 nm (Fig. 1C), indicative of water exposure of the tryptophan side chains (20). Upon A $\beta$  binding, the fluorescence intensity increased, and the emission maximum was blue-shifted to a wavelength of  $\lambda_{\max} = 340$  nm, in agreement with a less polar environment of the tryptophan indole groups in the bound state. Because of the spectral differences between its free

and bound states, ZAB3W could be employed to detect and quantify monomeric A $\beta$  by sequestering it into the ZAB3W-A $\beta$  complex. Both the fluorescence intensity and  $\lambda_{\max}$  could in principle be evaluated for this purpose. However, the fluorescence intensity decreased upon repeated measurements of free and bound ZAB3W, indicative of photobleaching, whereas  $\lambda_{\max}$  remained constant. Therefore,  $\lambda_{\max}$  was chosen as the spectral property to evaluate for the detection of monomeric A $\beta$ . However,  $\lambda_{\max}$  does not linearly depend on the fraction of free/bound ZAB3W (21). To derive the relationship between  $\lambda_{\max}$  and the fraction of free/bound ZAB3W, the simulated spectra of mixtures of free and bound ZAB3W were calculated from the spectra of free and bound ZAB3W, and the resulting  $\lambda_{\max}$  values dependent on the fraction of free ZAB3W were plotted (Fig. 1D). A fit to an exponential function was employed for the calculation of the fraction of free ZAB3W from experimentally determined  $\lambda_{\max}$  values. In conclusion, ZAB3W addition to test solutions permits the detection and quantification of monomeric A $\beta$ . In particular, the concentration of monomeric A $\beta$  in a test solution corresponds to the concentration of bound ZAB3W if an excess of ZAB3W is added, ensuring a concentration of free ZAB3W of  $[ZAB3W]_{\text{free}} \gg K_d = 20$  nM.

**Exponential Decay Kinetics of A $\beta$  Protofibril Dissociation**—ZAB3W was employed to study the dissociation kinetics of A $\beta$  protofibrils as schematically shown in Fig. 1B. Monomers dissociating from protofibrils were captured by ZAB3W. The ZAB3W binding kinetics were sufficiently fast (time constant on the order of seconds (18)) not to obscure the slow protofibril dissociation kinetics. Sequestration of monomeric A $\beta$  by ZAB3W effectively inhibited fibril formation, which otherwise is a competing reaction of protofibril dissociation (11, 16). Under the experimental conditions, the decrease in the fraction of free ZAB3W was proportional to the decrease in the fraction of A $\beta$  within protofibrils and to the amount of A $\beta$  monomers dissociated from protofibrils.

A $\beta$  protofibrils were prepared by SEC of incubated samples of monomeric A $\beta$  as described previously (4–8, 10, 16). Fresh samples of monomeric A $\beta$ 42 or A $\beta$ 40 were incubated at 25 °C in 20 mM sodium phosphate (pH 7.0), followed by injection of the solution onto a Superdex 75 10/300 SEC column and isolation of the protofibril fraction, which eluted close to the void volume of the column (Fig. 2A). The protofibrils exhibited mainly curvilinear but also spherical and annular morphologies in transmission electron microscopy (Fig. 2B), in agreement with previous studies (4–9). AUC of the A $\beta$ 42 protofibril fraction detected a monomer content of ~30% of total A $\beta$ , in accordance with dissociation of protofibrils on the time scale of AUC sample preparation and measurement. Of the remaining A $\beta$ , the majority (~50% of total A $\beta$ ) could be resolved by sedimentation velocity AUC at 40,000 rpm and 20 °C, yielding a size distribution from 2 to 13 S with an average  $s_{20,w} = 7.6$  S (Fig. 2C). These values are in agreement with literature AUC data for the high molecular weight SEC fraction of A $\beta$ 42 (10). An additional A $\beta$  fraction (~20% of total A $\beta$ ) sedimented too fast for reliable determination of  $s$ -values, possibly comprising larger protofibrils as well as mature amyloid fibrils.

Protofibril dissociation samples containing between 4 and 35  $\mu$ M A $\beta$  were prepared in fluorescence cells. The time of

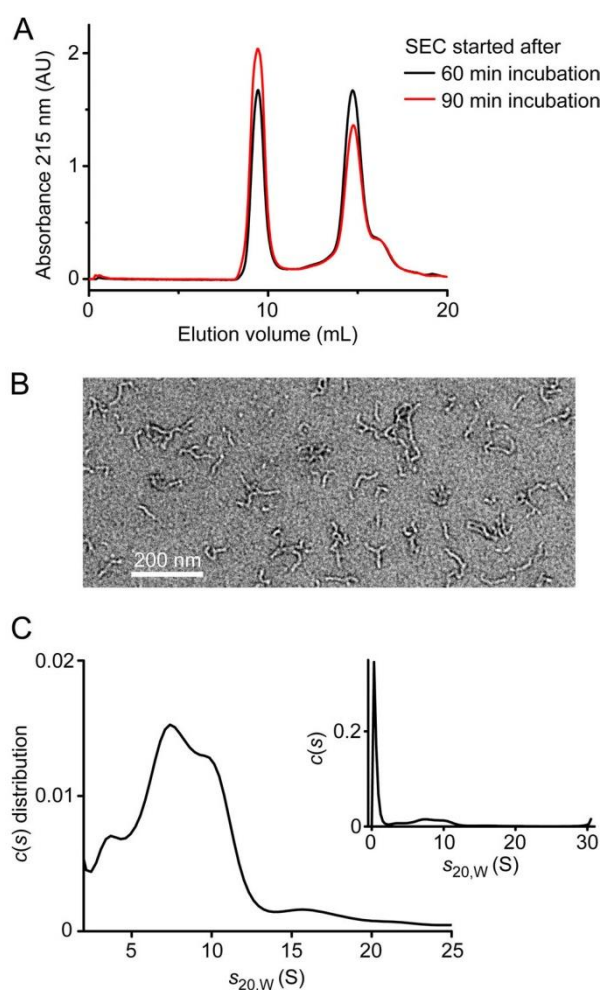
Kinetic Stability of A $\beta$  Protofibrils

FIGURE 2. **A $\beta$  protofibrils.** A, SEC of A $\beta$ 42 monomer samples incubated at 25 °C for the indicated times. The protofibril fraction eluted at ~9 ml, and the monomer fraction eluted at ~14.5 ml on a Superdex 75 10/300 column. AU, absorbance units. B, transmission electron microscopy of A $\beta$ 42 protofibrils prepared for the dissociation assay. C, sedimentation coefficient distribution of the A $\beta$ 42 protofibril fraction obtained from sedimentation velocity AUC analyzed with a continuous  $c(s)$  distribution model. The complete distribution, including the monomer peak, is shown in the inset.

ZA $\beta$ 3W addition was taken as the starting time of the protofibril dissociation reaction. Fluorescence emission spectra showed a blue shift of the tryptophan fluorescence with time, reporting the binding of ZA $\beta$ 3W to monomeric A $\beta$  dissociated from protofibrils on the time scale of minutes to hours (Fig. 3A). This is in agreement with the appearance of an A $\beta$  monomer peak on this time scale after reinjection of the protofibril fraction onto an SEC column (Fig. 3B) as reported previously (16, 22). At the end of the dissociation experiments, protofibrils or other protein aggregates were not detected by transmission electron microscopy (Fig. 3C). In contrast, a protofibril sample incubated for the same time without ZA $\beta$ 3W contained amyloid fibrils. AUC performed at the end of protofibril dissociation experiment showed that protofibrils were dissociated and that A $\beta$  was bound to ZA $\beta$ 3W (Fig. 3E).

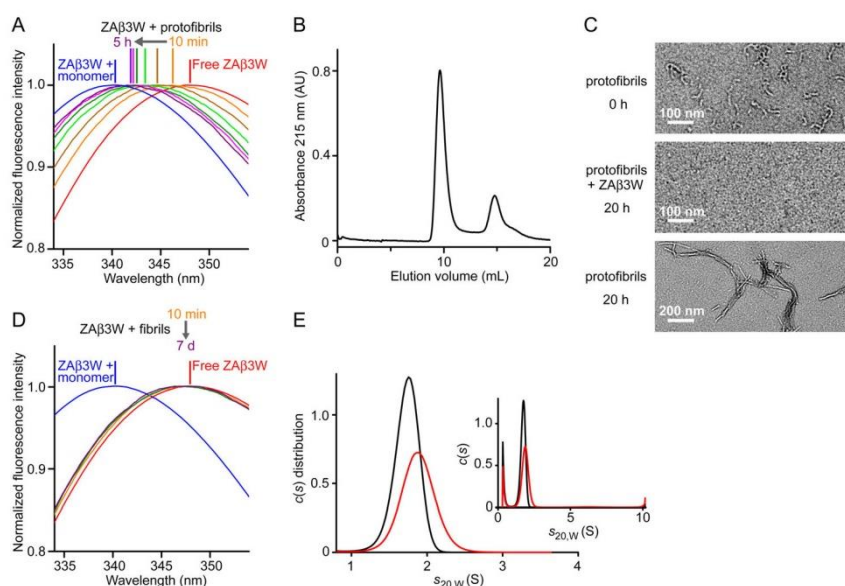
In contrast to protofibrils, A $\beta$  amyloid fibrils did not cause a significant blue shift of ZA $\beta$ 3W tryptophan fluorescence after prolonged incubation (Fig. 3D). This is in agreement with previous data obtained by NMR-detected binding of ZA $\beta$ 3 to A $\beta$ , which showed a very high kinetic stability of A $\beta$  fibrils prepared *in vitro* (16).

For the kinetic analysis of protofibril dissociation, the fraction of free ZA $\beta$ 3W was calculated from the  $\lambda_{\max}$  values of the fluorescence emission spectra. The time traces of the fraction of free ZA $\beta$ 3W revealed that protofibril dissociation was a rather slow reaction, occurring on the time scale of minutes to hours (Fig. 4). The dissociation kinetics were not affected by agitation, as expected for a dissociation reaction occurring in solution (Fig. 4). The time traces could be fitted to a monoexponential decay function, providing individual  $k_{\text{off}}$  values for each protofibril dissociation sample (Figs. 4A and 5). The fits did not cover the complete amplitude of the decay of the fraction of A $\beta$  in protofibrils, explainable by (i) the dissociation of protofibrils during the time elapsed between protofibril elution from SEC and addition of ZA $\beta$ 3W and (ii) the fast dissociation of a fraction of A $\beta$  monomers loosely bound to the protofibril surface, which has been detected before by dark-state exchange saturation transfer NMR (23).

The average  $k_{\text{off}}$  at 25 °C determined from 12 A $\beta$ 42 protofibril dissociation experiments of six independent protofibril batches was  $(1.4 \pm 0.7) \times 10^{-4} \text{ s}^{-1}$ . The  $k_{\text{off}}$  values obtained for different protofibril batches varied considerably, ranging from  $0.8 \times 10^{-4}$  to  $3.5 \times 10^{-4} \text{ s}^{-1}$  (Figs. 4A and 5). The  $k_{\text{off}}$  value did not correlate with the A $\beta$  concentration in the protofibril preparation (Fig. 5).  $k_{\text{off}}$  did also not vary with the protofibril maturation time, as protofibril fractions harvested at two different times from the same A $\beta$  incubation did not exhibit different dissociation kinetics within the error of the experiment (Figs. 4 and 5). One possible explanation for the heterogeneity in  $k_{\text{off}}$  values would be a high sensitivity of the energy barrier of a defined rate-limiting step of protofibril dissociation to subtle differences in the solution conditions of different protofibril preparations. Alternatively, protofibril batches might be variably composed of a set of protofibrillar structures, each associated with a distinct individual energy barrier of the rate-limiting step of dissociation. A global fit of the 12 A $\beta$ 42 protofibril dissociation data sets recorded at 25 °C to a triexponential decay with shared rate constants performed similarly to the individual monoexponential fits, yielding the rate constants  $k_{\text{off},1} = 0.77 \times 10^{-4} \text{ s}^{-1}$ ,  $k_{\text{off},2} = 1.5 \times 10^{-4} \text{ s}^{-1}$ , and  $k_{\text{off},3} = 3.5 \times 10^{-4} \text{ s}^{-1}$  (Fig. 4B). Our data are thus compatible with the existence of a set of protofibrillar structures of different kinetic stabilities, with variable distribution in different protofibril batches.

**A $\beta$ 40 and A $\beta$ 42 Protofibrils Possess Similar Kinetic Stabilities**—The  $k_{\text{off}}$  values of three protofibril dissociation experiments of an A $\beta$ 40 protofibril batch were within the range of those observed for A $\beta$ 42 protofibrils, with an average  $k_{\text{off}}$  at 25 °C of  $1.2 \times 10^{-4} \text{ s}^{-1}$  for A $\beta$ 40 (Fig. 5). A $\beta$ 40 and A $\beta$ 42 protofibrils thus possess similar kinetic stabilities.

**Activation Energy of Protofibril Dissociation**—The temperature dependence of the protofibril dissociation kinetics was investigated in the range of 19–37 °C for three independent A $\beta$ 42

Kinetic Stability of A $\beta$  Protofibrils

**FIGURE 3. Protofibril dissociation.** *A*, normalized fluorescence emission spectra of ZA $\beta$ 3W after the addition of an A $\beta$ 42 protofibril sample and incubation at 25 °C for 10 min or 1, 2, 3, 4, or 5 h. The protein concentrations used were 14.8  $\mu$ M A $\beta$ 42 and 19.6  $\mu$ M ZA $\beta$ 3W. Spectra of free ZA $\beta$ 3W and ZA $\beta$ 3W bound to a stoichiometric amount of A $\beta$ 42 monomers are shown for comparison. *B*, SEC of an A $\beta$ 42 protofibril sample re-injected onto a Superdex 75 10/300 column after incubation for 20 min in the absence of ZA $\beta$ 3W. In addition to protofibrils eluting at  $\sim$ 9 ml, A $\beta$  monomers eluting at  $\sim$ 14.5 ml were detected. AU, absorbance units. *C*, transmission electron microscopy of fresh A $\beta$ 42 protofibrils (*upper panel*), A $\beta$ 42 protofibrils at the end of the dissociation experiment but in the absence of ZA $\beta$ 3W (*middle panel*), and A $\beta$ 42 protofibrils treated as in the dissociation experiment but in the presence of ZA $\beta$ 3W (*lower panel*). *D*, normalized fluorescence emission spectra of ZA $\beta$ 3W after the addition of an A $\beta$ 42 amyloid fibril sample and incubation at 25 °C for 10 min or 2 or 7 days (*d*). The protein concentrations used were 20  $\mu$ M A $\beta$ 42 and 25  $\mu$ M ZA $\beta$ 3W. Spectra of free ZA $\beta$ 3W and ZA $\beta$ 3W bound to a stoichiometric amount of A $\beta$ 42 monomers are shown for comparison. *E*, sedimentation coefficient distribution of ZA $\beta$ 3W (*black*) and of the A $\beta$ 42 protofibril fraction in the presence of ZA $\beta$ 3W at the end of the dissociation experiment (*red*). The shift of the distribution maximum to a higher *s*-value upon addition of protofibrils to ZA $\beta$ 3W demonstrates formation of the ZA $\beta$ 3W-A $\beta$ 42 complex. The complete distribution is shown in the *inset*.

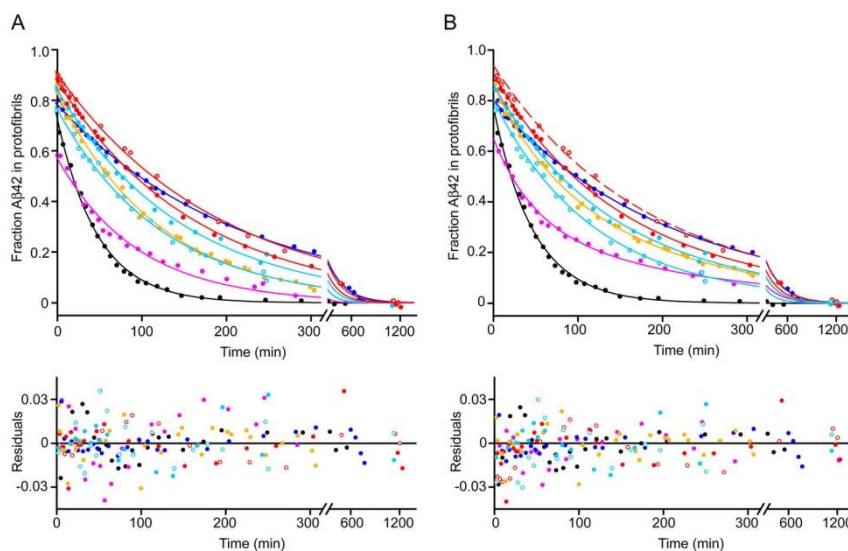


**FIGURE 4. Kinetics of A $\beta$ 42 protofibril dissociation.** Eight exemplary time traces are shown of protofibril-bound A $\beta$ 42 fractions after the addition of ZA $\beta$ 3W to fresh A $\beta$ 42 protofibril preparations at 25 °C. The time traces were obtained for six independent protofibril preparations, with each batch indicated in individual color. For the batch shown in *red*, protofibrils harvested after 60 min of incubation (*closed circles*) or 90 min of incubation (*open circles*) were compared (SEC profiles in Fig. 2A). For the batch shown in *light blue*, protofibril dissociation samples were incubated with agitation (*closed circles*) or quiescent (*open circles*). *A*, *lines* represent local fits for each time trace to single exponential decay functions. *B*, *lines* represent one global fit for all time traces to a triexponential decay with shared rate constants but independent amplitudes for the time traces. The *lower panels* show the residuals of the fits.

protofibril preparations (Fig. 5). The  $k_{\text{off}}$  values were obtained from fits to a monoexponential decay function. The  $\ln(k_{\text{off}})$  versus  $1/T$  plots could be fit linearly, in concordance with Arrhenius law

behavior in this temperature range. The activation energy was obtained from the slope of the linear fits, yielding values between 75 and 89 kJ/mol, with an average of 80 kJ/mol.

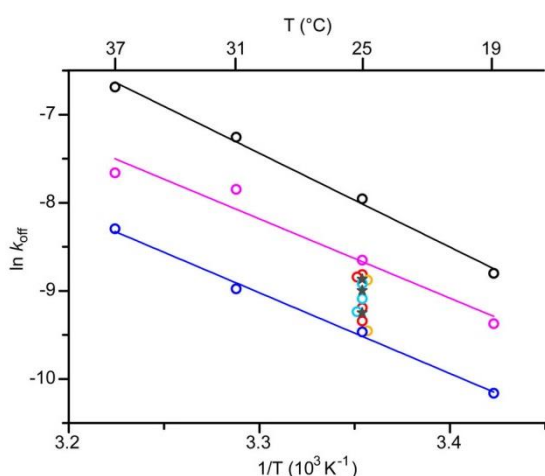


FIGURE 5. **The off-rate of monomers dissociating from A $\beta$  protofibrils.** Shown is a plot of the  $\ln(k_{\text{off}})$  values of A $\beta$ 40 (stars) and A $\beta$ 42 (circles) protofibrils against the inverse of the temperature. Independent protofibril preparations are identified by individual colors. For three A $\beta$ 42 protofibril preparations,  $\ln(k_{\text{off}})$  values were determined at different temperatures and fit linearly according to an Arrhenius temperature dependence. A $\beta$  concentrations in the protofibril dissociation samples were 4.5  $\mu\text{M}$  (magenta circles), 10.0  $\mu\text{M}$  (black circles), 10.5–14.8  $\mu\text{M}$  (red circles), 14.8  $\mu\text{M}$  (orange circles), 20.0  $\mu\text{M}$  (light blue circles and gray stars), and 35.0  $\mu\text{M}$  (dark blue circles).

## DISCUSSION

This study introduces a fluorescence assay for the determination of A $\beta$  protofibril dissociation kinetics, employing the engineered binding protein ZA $\beta$ 3W. ZA $\beta$ 3W is uniquely suited for this purpose because it requires the hydrophobic central region of A $\beta$  comprising residues 17–36 to be accessible to coupled folding-binding (15, 18). This region is buried in the hydrophobic core of A $\beta$  oligomers and amyloid fibrils (24–27), implying that ZA $\beta$ 3W specifically binds monomeric A $\beta$ , a prerequisite for the dissociation assay.

The results from this study reveal that the dissociation of monomers from A $\beta$  protofibrils follows exponential decay kinetics. This is remarkable, inasmuch as the protofibril fraction obtained from SEC includes particles of different sizes, with spherical as well as (curvi)linear morphologies. Exponential decay behavior is not in agreement with a rate-limiting role of processes occurring exclusively at the end of (curvi)linear assemblies. However, it would be compatible with dissociation of (curvi)linear assemblies, e.g. (i) by rate-limiting dissociation of subunits at a rate that is independent of the subunit position within the linear assembly (Fig. 6A) or (ii) through a pre-equilibrium of linear with nonlinear assemblies and a rate-limiting dissociation of the latter into monomers (Fig. 6B). Interestingly, both models require the postulation of an A $\beta$  oligomer as an intermediate unit through which protofibril dissociation occurs. A $\beta$  oligomers potentially fulfilling this role have been identified before, e.g. by ion mobility coupled with mass spectrometry (28). Exponential dissociation kinetics have also been reported for pre-fibrillar oligomers of the SH3 domain of PI3K (29).

A $\beta$  protofibril dissociation is a slow process, with a time constant of  $\sim 2$  h at 25  $^{\circ}\text{C}$ . The low rate of dissociation corresponds to a high free energy barrier that has to be crossed in the rate-limiting step. The energy barrier has a considerable enthalpic

## Kinetic Stability of A $\beta$ Protofibrils

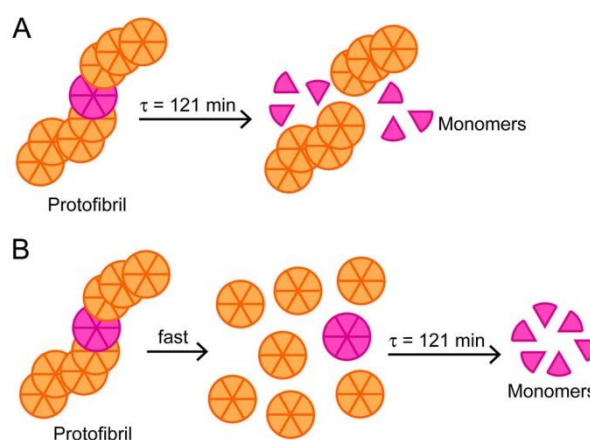


FIGURE 6. **Models of A $\beta$  protofibril dissociation into monomers compatible with exponential decay kinetics.** A, rate-limiting dissociation of protofibril subunits at a rate that is independent of the subunit position within the linear assembly. B, pre-equilibrium of linear and nonlinear protofibrils and rate-limiting dissociation of the latter into monomers. For illustration purposes, only one of the protofibril subunits (shown in magenta) dissociates. The indicated dissociation time constant ( $\tau$ ) was determined for A $\beta$ 42 protofibrils at 25  $^{\circ}\text{C}$ .

component as evidenced by the high activation energy of dissociation of  $\sim 80$  kJ/mol, a value typical for high affinity biomolecular interactions (30, 31). This indicates that a significant number of interactions have to be broken to reach the transition state. A $\beta$  protofibrils contain extended H-bonded and  $\beta$ -sheet structure as detected by hydrogen-deuterium exchange and CD spectroscopy (7, 32, 33). Destruction of this structure can be expected to be associated with a considerable energy barrier, explaining the slow kinetics and high activation energy of protofibril dissociation.

The apparent  $k_{\text{off}}$  values of different protofibril batches varied considerably, indicating the existence of distinct protofibrillar structures with different kinetic stabilities. This is reminiscent of prion/amyloid strains, protein aggregates of different conformation and thermodynamic stabilities that are associated with different phenotypes (34, 35).

Formation of protofibrils by A $\beta$ 40 requires higher monomer concentrations and longer incubation times compared with A $\beta$ 42, reflecting a marked difference in the association kinetics (4). In contrast, the dissociation kinetics of A $\beta$ 40 and A $\beta$ 42 protofibrils provided here are similar. This indicates that the main difference between A $\beta$ 40 and A $\beta$ 42 is the lower monomer solubility and increased oligomerization of the latter (36), whereas the kinetic stabilities of the formed protofibrils are alike.

In contrast to protofibrils, A $\beta$  amyloid fibrils prepared *in vitro* do not dissociate effectively in the presence of ZA $\beta$ 3 over weeks (16). This is in line with an even higher kinetic stability of fibrils compared with protofibrils, probably due to a more ordered and expanded  $\beta$ -sheet core (32).

The data gained by the ZA $\beta$ 3W sequestration approach can be compared with previous data for the dissociation of different A $\beta$  aggregates obtained from other techniques. The dissociation of radiolabeled A $\beta$ 40 deposited onto an amyloid fibril template occurred with dissociation half-times of  $\sim 10$  min or  $\gg 1000$  min depending on the deposition time, providing evi-

## Kinetic Stability of A $\beta$ Protofibrils

dence for two different A $\beta$  association states, a docked and a locked state (37). Dissociation of the weakly bound, docked A $\beta$  is approximately an order of magnitude faster than protofibril dissociation. A $\beta$ 40 fibrils released soluble species at a rate of  $\sim 1 \times 10^{-4} \text{ s}^{-1}$  as detected by two-color coincidence detection fluorescence (38), a value in the range of the rate of A $\beta$  protofibril dissociation reported here. Analysis of hydrogen-deuterium exchange of A $\beta$  fibrils employing a model of a recycling mechanism resulted in comparatively fast monomer off-rates of  $0.6 \times 10^{-2}$  and  $1.0 \times 10^{-2} \text{ s}^{-1}$  for A $\beta$ 40 and A $\beta$ 42 fibrils, respectively (39). The comparability of the data sets is limited, however, inasmuch as ZA $\beta$ 3W sequestration reports on the appearance of monomers, whereas the other techniques detect all soluble particles or hydrogen-deuterium exchangeable species.

This study demonstrates the applicability of a binding molecule obtained by protein engineering for the characterization of a key intermediate in amyloid formation. ZA $\beta$ 3W can further be used to identify conditions and compounds that modulate A $\beta$  aggregation, for example by destabilizing soluble oligomers (40).

## REFERENCES

1. Querfurth, H. W., and LaFerla, F. M. (2010) Alzheimer's disease. *N. Engl. J. Med.* **362**, 329–344
2. Skovronsky, D. M., Lee, V. M., and Trojanowski, J. Q. (2006) Neurodegenerative diseases: new concepts of pathogenesis and their therapeutic implications. *Annu. Rev. Pathol.* **1**, 151–170
3. Haass, C., and Selkoe, D. J. (2007) Soluble protein oligomers in neurodegeneration: lessons from the Alzheimer's amyloid  $\beta$ -peptide. *Nat. Rev. Mol. Cell Biol.* **8**, 101–112
4. Jan, A., Hartley, D. M., and Lashuel, H. A. (2010) Preparation and characterization of toxic A $\beta$  aggregates for structural and functional studies in Alzheimer's disease research. *Nat. Protoc.* **5**, 1186–1209
5. Hartley, D. M., Walsh, D. M., Ye, C. P., Diehl, T., Vasquez, S., Vassilev, P. M., Teplow, D. B., and Selkoe, D. J. (1999) Protofibrillar intermediates of amyloid  $\beta$ -protein induce acute electrophysiological changes and progressive neurotoxicity in cortical neurons. *J. Neurosci.* **19**, 8876–8884
6. Lashuel, H. A., Hartley, D. M., Petre, B. M., Wall, J. S., Simon, M. N., Walz, T., and Lansbury, P. T., Jr. (2003) Mixtures of wild-type and a pathogenic (E22G) form of A $\beta$ 40 *in vitro* accumulate protofibrils, including amyloid pores. *J. Mol. Biol.* **332**, 795–808
7. Walsh, D. M., Hartley, D. M., Kusumoto, Y., Fezoui, Y., Condron, M. M., Lomakin, A., Benedek, G. B., Selkoe, D. J., and Teplow, D. B. (1999) Amyloid  $\beta$ -protein fibrillogenesis. Structure and biological activity of protofibrillar intermediates. *J. Biol. Chem.* **274**, 25945–25952
8. Walsh, D. M., Lomakin, A., Benedek, G. B., Condron, M. M., and Teplow, D. B. (1997) Amyloid  $\beta$ -protein fibrillogenesis. Detection of a protofibrillar intermediate. *J. Biol. Chem.* **272**, 22364–22372
9. Freir, D. B., Nicoll, A. J., Klyubin, I., Panico, S., McDonald, J. M., Risse, E., Asante, E. A., Farrow, M. A., Sessions, R. B., Saibil, H. R., Clarke, A. R., Rowan, M. J., Walsh, D. M., and Collinge, J. (2011) Interaction between prion protein and toxic amyloid  $\beta$  assemblies can be therapeutically targeted at multiple sites. *Nat. Commun.* **2**, 336
10. Hepler, R. W., Grimm, K. M., Nahas, D. D., Breese, R., Dodson, E. C., Acton, P., Keller, P. M., Yeager, M., Wang, H., Shughrue, P., Kinney, G., and Joyce, J. G. (2006) Solution state characterization of amyloid  $\beta$ -derived diffusible ligands. *Biochemistry* **45**, 15157–15167
11. Jan, A., Adolfsen, O., Allaman, I., Buccarelli, A. L., Magistretti, P. J., Pfeifer, A., Muhs, A., and Lashuel, H. A. (2011) A $\beta$ 42 neurotoxicity is mediated by ongoing nucleated polymerization process rather than by discrete A $\beta$ 42 species. *J. Biol. Chem.* **286**, 8585–8596
12. Eichner, T., and Radford, S. E. (2011) A diversity of assembly mechanisms of a generic amyloid fold. *Mol. Cell* **43**, 8–18
13. Baldwin, A. J., Knowles, T. P., Tartaglia, G. G., Fitzpatrick, A. W., Devlin, G. L., Shammass, S. L., Waudby, C. A., Mossuto, M. F., Meehan, S., Gras, S. L., Christodoulou, J., Anthony-Cahill, S. J., Barker, P. D., Vendruscolo, M., and Dobson, C. M. (2011) Metastability of native proteins and the phenomenon of amyloid formation. *J. Am. Chem. Soc.* **133**, 14160–14163
14. Grönwall, C., Jonsson, A., Lindström, S., Gunneriusson, E., Ståhl, S., and Herne, N. (2007) Selection and characterization of Affibody ligands binding to Alzheimer amyloid  $\beta$  peptides. *J. Biotechnol.* **128**, 162–183
15. Hoyer, W., Grönwall, C., Jonsson, A., Ståhl, S., and Härd, T. (2008) Stabilization of a  $\beta$ -hairpin in monomeric Alzheimer's amyloid- $\beta$  peptide inhibits amyloid formation. *Proc. Natl. Acad. Sci. U.S.A.* **105**, 5099–5104
16. Luheshi, L. M., Hoyer, W., de Barros, T. P., van Dijk Härd, I., Brorsson, A. C., Macao, B., Persson, C., Crowther, D. C., Lomas, D. A., Ståhl, S., Dobson, C. M., and Härd, T. (2010) Sequestration of the A $\beta$  peptide prevents toxicity and promotes degradation *in vivo*. *PLoS Biol.* **8**, e1000334
17. Hemsley, A., Arnheim, N., Toney, M. D., Cortopassi, G., and Galas, D. J. (1989) A simple method for site-directed mutagenesis using the polymerase chain reaction. *Nucleic Acids Res.* **17**, 6545–6551
18. Hoyer, W., and Härd, T. (2008) Interaction of Alzheimer's A $\beta$  peptide with an engineered binding protein—thermodynamics and kinetics of coupled folding-binding. *J. Mol. Biol.* **378**, 398–411
19. Macao, B., Hoyer, W., Sandberg, A., Brorsson, A. C., Dobson, C. M., and Härd, T. (2008) Recombinant amyloid  $\beta$ -peptide production by coexpression with an Affibody ligand. *BMC Biotechnol.* **8**, 82
20. Burstein, E. A., Vedenkina, N. S., and Ivkova, M. N. (1973) Fluorescence and the location of tryptophan residues in protein molecules. *Photochem. Photobiol.* **18**, 263–279
21. Ladokhin, A. S., Jayasinghe, S., and White, S. H. (2000) How to measure and analyze tryptophan fluorescence in membranes properly, and why bother? *Anal. Biochem.* **285**, 235–245
22. Jan, A., Gokce, O., Luthi-Carter, R., and Lashuel, H. A. (2008) The ratio of monomeric to aggregated forms of A $\beta$ 40 and A $\beta$ 42 is an important determinant of amyloid- $\beta$  aggregation, fibrillogenesis, and toxicity. *J. Biol. Chem.* **283**, 28176–28189
23. Fawzi, N. L., Ying, J., Ghirlando, R., Torchia, D. A., and Clore, G. M. (2011) Atomic-resolution dynamics on the surface of amyloid- $\beta$  protofibrils probed by solution NMR. *Nature* **480**, 268–272
24. Chimon, S., Shaibat, M. A., Jones, C. R., Calero, D. C., Aizezi, B., and Ishii, Y. (2007) Evidence of fibril-like  $\beta$ -sheet structures in a neurotoxic amyloid intermediate of Alzheimer's  $\beta$ -amyloid. *Nat. Struct. Mol. Biol.* **14**, 1157–1164
25. Lührs, T., Ritter, C., Adrian, M., Riek-Loher, D., Bohrmann, B., Döbeli, H., Schubert, D., and Riek, R. (2005) 3D structure of Alzheimer's amyloid- $\beta$ (1–42) fibrils. *Proc. Natl. Acad. Sci. U.S.A.* **102**, 17342–17347
26. Petkova, A. T., Yau, W. M., and Tycko, R. (2006) Experimental constraints on quaternary structure in Alzheimer's  $\beta$ -amyloid fibrils. *Biochemistry* **45**, 498–512
27. Yu, L., Edalji, R., Harlan, J. E., Holzman, T. F., Lopez, A. P., Labkovsky, B., Hillen, H., Barghorn, S., Ebert, U., Richardson, P. L., Miesbauer, L., Solomon, L., Bartley, D., Walter, K., Johnson, R. W., Hajduk, P. J., and Olejniczak, E. T. (2009) Structural characterization of a soluble amyloid  $\beta$ -peptide oligomer. *Biochemistry* **48**, 1870–1877
28. Bernstein, S. L., Dupuis, N. F., Lazo, N. D., Wyttenbach, T., Condron, M. M., Bitan, G., Teplow, D. B., Shea, J. E., Ruotolo, B. T., Robinson, C. V., and Bowers, M. T. (2009) Amyloid- $\beta$  protein oligomerization and the importance of tetramers and dodecamers in the aetiology of Alzheimer's disease. *Nat. Chem.* **1**, 326–331
29. Orte, A., Birkett, N. R., Clarke, R. W., Devlin, G. L., Dobson, C. M., and Klenerman, D. (2008) Direct characterization of amyloidogenic oligomers by single-molecule fluorescence. *Proc. Natl. Acad. Sci. U.S.A.* **105**, 14424–14429
30. Ojcius, D. M., Gapin, L., and Kourilsky, P. (1993) Dissociation of the peptide/MHC class I complex: pH dependence and effect of endogenous peptides on the activation energy. *Biochem. Biophys. Res. Commun.* **197**, 1216–1222
31. Schwesinger, F., Ros, R., Strunz, T., Anselmetti, D., Güntherodt, H. J., Honegger, A., Jeremius, L., Tiefenauer, L., and Plückthun, A. (2000) Unbinding forces of single antibody-antigen complexes correlate with their thermal dissociation rates. *Proc. Natl. Acad. Sci. U.S.A.* **97**, 9972–9977
32. Kheterpal, I., Chen, M., Cook, K. D., and Wetzel, R. (2006) Structural differences in A $\beta$  amyloid protofibrils and fibrils mapped by hydrogen

**Kinetic Stability of A $\beta$  Protofibrils**

- exchange-mass spectrometry with on-line proteolytic fragmentation. *J. Mol. Biol.* **361**, 785–795
33. Kheterpal, I., Lashuel, H. A., Hartley, D. M., Walz, T., Lansbury, P. T., Jr., and Wetzel, R. (2003) A $\beta$  protofibrils possess a stable core structure resistant to hydrogen exchange. *Biochemistry* **42**, 14092–14098
34. Qiang, W., Kelley, K., and Tycko, R. (2013) Polymorph-specific kinetics and thermodynamics of  $\beta$ -amyloid fibril growth. *J. Am. Chem. Soc.* **135**, 6860–6871
35. Tanaka, M., Chien, P., Naber, N., Cooke, R., and Weissman, J. S. (2004) Conformational variations in an infectious protein determine prion strain differences. *Nature* **428**, 323–328
36. Bitan, G., Kirkitadze, M. D., Lomakin, A., Vollers, S. S., Benedek, G. B., and Teplow, D. B. (2003) Amyloid  $\beta$ -protein (A $\beta$ ) assembly: A $\beta$ 40 and A $\beta$ 42 oligomerize through distinct pathways. *Proc. Natl. Acad. Sci. U.S.A.* **100**, 330–335
37. Esler, W. P., Stimson, E. R., Jennings, J. M., Vinters, H. V., Ghilardi, J. R., Lee, J. P., Mantyh, P. W., and Maggio, J. E. (2000) Alzheimer's disease amyloid propagation by a template-dependent dock-lock mechanism. *Biochemistry* **39**, 6288–6295
38. Narayan, P., Orte, A., Clarke, R. W., Bolognesi, B., Hook, S., Ganzinger, K. A., Meehan, S., Wilson, M. R., Dobson, C. M., and Klenerman, D. (2012) The extracellular chaperone clusterin sequesters oligomeric forms of the amyloid- $\beta$ (1–40) peptide. *Nat. Struct. Mol. Biol.* **19**, 79–83
39. Sánchez, L., Madurga, S., Pukala, T., Vilaseca, M., López-Iglesias, C., Robinson, C. V., Giralt, E., and Carulla, N. (2011) A $\beta$ 40 and A $\beta$ 42 amyloid fibrils exhibit distinct molecular recycling properties. *J. Am. Chem. Soc.* **133**, 6505–6508
40. Ladiwala, A. R., Dordick, J. S., and Tessier, P. M. (2011) Aromatic small molecules remodel toxic soluble oligomers of amyloid  $\beta$  through three independent pathways. *J. Biol. Chem.* **286**, 3209–3218

**CHAPTER 2****CHARACTERIZATION OF A COVALENTLY-LINKED AMYLOID-BETA DIMER**

Clara S. R. Grüning, Philipp Neudecker, and Wolfgang Hoyer

**Status:** in preparation

**Impact Factor:** -

**Own proportion to this work:** 80%

Design, cloning, expression and purification of A $\beta$  dimers, expression and purification of A $\beta$ 1-40, circular dichroism and aggregation experiments, preparation of NMR samples, writing of the manuscript.

## Characterization of a Covalently-linked Amyloid- $\beta$ Dimer

Clara S. R. Grüning<sup>1</sup>, Philipp Neudecker<sup>2</sup> and Wolfgang Hoyer<sup>1</sup>

<sup>1</sup>Institut für Physikalische Biologie, Heinrich-Heine-Universität, 40204 Düsseldorf, Germany

<sup>2</sup>Institute of Structural Biochemistry (ICS-6), Forschungszentrum Jülich, 52425 Jülich, Germany

Corresponding author: Wolfgang Hoyer, Institut für Physikalische Biologie, Heinrich-Heine-Universität, 40204 Düsseldorf, Germany, Phone +49 211 8115153, E-mail: wolfgang.hoyer@hhu.de

### Abstract

Small aggregation intermediates of the Alzheimer disease-associated amyloid- $\beta$  (A $\beta$ ) peptide have been isolated from Alzheimer disease brains and have shown neurotoxic effects. The most prevalent intermediate species were A $\beta$  dimers which were resistant to low concentrations of sodium dodecyl sulfate. As the actual linkage of A $\beta$  monomers to dimers remains obscure, it is necessary to study synthetic dimeric species of the A $\beta$  peptide to derive structural and biochemical knowledge of these synaptotoxic aggregation intermediates. In this work, we characterized a covalently linked A $\beta$  dimer. Linkage was accomplished by a glycine serine linker, which allowed a flexible arrangement of the two subunits as shown by NMR and CD experiments. Aggregation experiments using the fluorescence dye Thioflavine T indicated an inhibitory effect of the A $\beta$  dimer towards the aggregation of the A $\beta$  monomer.

### Introduction

Alzheimer disease (AD) is the most prevalent neurological disorder with around 25 million people affected worldwide (1). The hallmarks of AD are senile plaques and neurofibrillary tangles composed of the amyloid- $\beta$  (A $\beta$ ) peptide and the microtubule-binding protein tau, respectively. Increasing evidence has indicated that not these insoluble aggregates per se but aggregation intermediates whose elongation produces these filaments represent the neurotoxic species (2). A great variety of diffusible A $\beta$  aggregation intermediates have been

isolated from AD brain and neuronal cell culture so far, reaching from dimers and dodecamers to multimers of rod-shaped appearance (reviewed in detail in 2). These oligomers have demonstrated to induce principal features associated with the AD phenotype such as neuronal cell death, altered hippocampal synaptic plasticity and successional memory dysfunction in cell culture and rodent model experiments (3-5). A $\beta$  dimers are the major form of soluble oligomers isolated from human AD brain; treatment of rodent hippocampal slices with purified A $\beta$  dimers in contrast to monomeric A $\beta$  impaired long-term potentiation and induced synapse loss (5,6). These dimers are stable towards low concentrations of sodium dodecyl sulfate (SDS) and easily build up higher-order aggregates (6). As the pathological relevance for A $\beta$  dimers in AD is increasingly realized, particularly as recent studies suggest a link between dimeric A $\beta$  species and tau hyperphosphorylation associated with tangle formation (7), several studies have tried to design dimeric A $\beta$  species and to slow down their aggregation into higher-order oligomers (8-11). Most of these studies relied on the insertion of cysteine residues at selected positions, e.g. serine 26 (10), alanine 21 and alanine 30 (9), to link two A $\beta$  molecules via a disulfide bridge and thus arrest the conformation of A $\beta$  in a protofibrillar arrangement incompatible with fibril formation. Protofibrils resulting from aggregation of the A $\beta$ 1-40 S26C dimer impaired long-term potentiation, but were less potent than human AD brain isolated A $\beta$  dimers (10). Another study assessed the dimerization potential of several cellular factors (glutaraldehyde, transglutaminase and Cu(II)) and thus obtained SDS-stable dimers (12). A third approach to create a covalently bound A $\beta$  dimer is a peptide linker. This approach was followed by Roeder *et al.* (13) connecting C-terminal segments of A $\beta$  in several orientations and varying amino acid linkers with positive charges to increase the solubility of the resulting A $\beta$  dimer. Roeder *et al.* (13) identified variants of A $\beta$  that were toxic in their dimeric but not in their monomeric form.

Besides the aim to study the dimeric A $\beta$  species per se, in this work we aim at investigating the molecular mechanism of primary nucleation, e.g. which amino acid motif is involved in aggregation-initiating intermolecular interactions, by using a synthetic dimer. For these purposes, we expressed and structurally analyzed an A $\beta$  head-to-tail dimer linked with a glycine-serine-linker ((G<sub>4</sub>S)<sub>4</sub>-linker). The (G<sub>4</sub>S)<sub>4</sub>-linker provides a flexible linkage between the two subunits without the necessity of point mutations in the A $\beta$  sequence. We designed

homodimers of both major A $\beta$  peptides, namely the A $\beta$ 1-42 and A $\beta$ 1-40 peptides. Although a co-expression system (14) was employed, the A $\beta$ 1-42 dimer was not expressible in bacteria. The A $\beta$ 1-40 dimer showed a similar secondary structure composition as its parent monomeric form in circular dichroism (CD) experiments. In NMR experiments, the A $\beta$ 1-40 dimer behaved as two independent monomers, but residues 32-34 showed a resonance splitting. Aggregation experiments with A $\beta$ 1-40 indicated a substoichiometric inhibitory effect of the A $\beta$ 1-40 dimer.

## Results

### *Expression and Purification*

A $\beta$  dimers of A $\beta$ 1-40 and A $\beta$ 1-42 were designed as head-to-tail homodimers linked with a (G<sub>4</sub>S)<sub>4</sub>-linker (Fig. 1). Bacterial expression required an N-terminal methionine and was achieved by co-expression of ZA $\beta$ <sub>3</sub>, a binding protein to A $\beta$  that shields the A $\beta$  peptide from the exterior (14,15). Although ZA $\beta$ <sub>3</sub> sequesters A $\beta$  in the bacterial cell, expression of the more toxic and aggregation-prone A $\beta$ 1-42 dimeric variant was not attained (Fig. 2). The co-expression with ZA $\beta$ <sub>3</sub> also facilitated subsequent purification of the A $\beta$ 1-40 dimer via a 6-fold histidine-tag and size exclusion chromatography (SEC) (14). In comparison to the monomeric A $\beta$  construct, SEC purification of A $\beta$ 1-40 dimer was only successful at increased pH (pH 10), probably due to accelerated aggregation at neutral pH.

### *Circular Dichroism*

The secondary structure of the A $\beta$ 1-40 dimer was compared to that of its parent (Fig. 3). The A $\beta$ 1-40 dimer spectrum is characterized by a minimum below 200 nm and a maximum around 220 nm, both indicative of random coil structure, and is thus similar to the spectrum of its monomeric form. The spectra were measured at pH 10 as well as pH 8 and the proteins gave comparable spectra.

### *Nuclear Magnetic Resonance Spectroscopy*

Furthermore, we used Nuclear Magnetic Resonance (NMR) spectroscopy to characterize the A $\beta$ 1-40 dimer. The (<sup>1</sup>H-<sup>15</sup>N)-HSQC spectrum of [*U*-<sup>15</sup>N]-A $\beta$ 1-40 dimer resembled essentially that of its monomeric parent demonstrating that the two subunits act independently from each other; additional resonance signals with typical <sup>1</sup>H and <sup>15</sup>N shifts for glycine and serine

were attributed to the linker between the two subunits of the A $\beta$ 1-40 dimer (Fig. 4). However, the resonance signals for the residues 32-34 are broadened in the A $\beta$ 1-40 dimer spectra compared to the monomer spectra suggesting a possible interaction of the two subunits of the A $\beta$ 1-40 dimer (Fig. 4 B-D).

### *Aggregation*

The fluorescence emission of the dye Thioflavine T (ThT) is increased when bound to  $\beta$ -sheet structures enabling to follow the aggregation of amyloidogenic proteins (16). To test whether the synthetic A $\beta$ 1-40 dimer can accelerate the aggregation of A $\beta$ 1-40, we added substoichiometric concentrations of A $\beta$ 1-40 dimer to monomeric A $\beta$ 1-40. Unexpectedly, the contrary was the case: the A $\beta$ 1-40 dimer prolonged the aggregation of A $\beta$ 1-40 in a concentration-dependent manner (Fig. 5), also substoichiometric addition of A $\beta$ 1-40 dimer affected A $\beta$ 1-40 aggregation.

### **Discussion and Outlook**

This work shows that the co-expression system established for the monomeric A $\beta$  peptides also enables the production of a covalently-linked A $\beta$ 1-40 dimer. In contrast, expression and purification of the A $\beta$ 1-42 dimer have not been successful so far, which is possibly due to its increased aggregation propensity and toxicity. First structural analyses of the A $\beta$ 1-40 dimer indicate an intrinsically disordered conformation of the two subunits as shown by NMR and CD experiments. The ( $^1\text{H}$ - $^{15}\text{N}$ )-HSQC spectrum of A $\beta$ 1-40 dimer demonstrated a signal splitting of some resonances (32-34) in comparison to the A $\beta$ 1-40 monomer thus indicating that these amino acid residues sample different environmental conditions (Fig. 4). The different environments for these residues can either be a result of the introduced linker or due to interactions between the two A $\beta$  subunits. An interaction between the residues 32-34 is in line with the structural model of A $\beta$  preglobulomers by Yu *et al.* (8), who observed a slow NH/ND exchange for these residues by NMR and NOEs between G33 and L34. To clarify if the observed resonance splitting originates from an interaction between the two subunits an assignment of the subunits within the A $\beta$ 1-40 dimer is fundamental. A distinction of the two subunits in NMR can for example be achieved by the introduction of a point mutation only in one of the subunits. Moreover, an effect of the linker has to be excluded. If the splitting of these resonance signals results from an interaction between the two subunits,

this could indicate a region crucial for interaction between two A $\beta$  monomers and thus crucial for initiating A $\beta$  aggregation.

Furthermore, we showed here that the A $\beta$ 1-40 dimer prolongs A $\beta$ 1-40 aggregation in a substoichiometric concentration. The elucidation of the inhibition mechanism of the A $\beta$ 1-40 dimer requires further experimental data; in particular as it seems that the aggregation of the A $\beta$ 1-40/ A $\beta$ 1-40 dimer-mixed sample follows a two-step aggregation kinetic. It is important to elucidate which species induce the difference in ThT signal during the aggregation of a mixture of A $\beta$ 1-40 and A $\beta$ 1-40 dimer. Two possible explanations are: 1) In the first phase, A $\beta$ 1-40-dimer oligomerizes to stable protofibrils but cannot convert into fibrils because the covalently attached second subunit interferes with the arrangement of A $\beta$  units within the fibrillar  $\beta$ -sheet structure. Yu *et al.* (8) also identified a  $\beta$ -sheet arrangement in the preglobulomer different from that in the fibril requiring a rearrangement of secondary structure between the two aggregate species. The second phase characterized by a fast increase of ThT fluorescence is then explained by the independent fibrillization of A $\beta$ 1-40. In this hypothesis, the aggregation of A $\beta$ 1-40 is prolonged by the reduced free concentration of A $\beta$ 1-40, because A $\beta$ 1-40 is also present in the oligomeric structures induced by the A $\beta$ 1-40 dimer, thus this idea implies that there is an interaction between A $\beta$ 1-40 dimer and monomer. 2) On the contrary, the second explanation for the two-phase aggregation is an independent aggregation of the A $\beta$ 1-40 dimer and A $\beta$ 1-40. This hypothesis is strengthened by the low ThT signal of the first phase observed in the A $\beta$ 1-40/A $\beta$ 1-40 dimer-mixed sample, which is comparable to that of the A $\beta$ 1-40 dimer sample. But this explanation does not provide an evident inhibition mechanism for the A $\beta$ 1-40 dimer on the aggregation of A $\beta$ 1-40. To clarify the inhibitory effect of the A $\beta$ 1-40 dimer and its interaction with the parent form, further experiments are necessary. Further investigation of this issue is also especially important in the light of the actual neurotoxic species possibly derived from A $\beta$  dimers, because A $\beta$ -derived dimeric constructs were also shown to facilitate aggregation besides their synoptotoxic activity (17).

The smallest aggregation intermediate of A $\beta$ , a dimer, was linked to AD progression (18), has been isolated from affected AD brains (5,6) and was shown to impair memory (6,19), but their structural characterization remains difficult. Here, we tried to deliver a structural model of a dimeric A $\beta$  species by linking two A $\beta$  molecules with a glycine serine linker. As

the precise chemical structure of the AD brain isolated dimers is still obscure, model systems are needed to analyze and imitate the dimerization of A $\beta$ . Although the molecule presented in this work is synthetic, it might deliver important understanding of dimeric A $\beta$  intermediates, especially as the linker permits a flexible conformation of the two subunits and does not require the insertion of point mutations as in studies relying on disulfide bridge formation. To get a complete understanding of A $\beta$  dimers, studies with different construction approaches of A $\beta$  dimers are necessary and complementary. Furthermore, the investigation of the synthetic A $\beta$  dimer presented in this work can help us to understand the first events of aggregation, e.g. first intermolecular interactions.

## Materials and Methods

### *Cloning, Expression and Purification of the A $\beta$ dimer*

The A $\beta$  dimer sequences were obtained from GeneArt (Life Sciences) and cloned into the vector used for co-expression with the ZA $\beta_3$  gene (14) using NcoI and HindIII restriction sites. For expression, transformed *Escherichia coli* BL21(DE3) cells were grown in minimal medium at 37°C. To obtain protein samples for NMR experiments, 1g/l <sup>15</sup>N ammonium chloride was added. Expression was induced with 1 mM IPTG for 5 h. Cells were harvested by centrifugation (4000x g, 4°C, 10 min). The cell pellet was resuspended in 20 mM sodium phosphate, 200 mM sodium chloride, 20 mM imidazole, pH 7.4 including EDTA-free protease inhibitor (Roche). For cell lysis a high pressure-based system (Constant Systems, 2.9 kbar) was used. The cell lysate was cleared from cell debris by centrifugation (40,000x g, 4°C, 40 min) and loaded onto a 5 ml HisTrap column (GE Healthcare), connected to an Äkta Purifier system (GE Healthcare), to bind the ZA $\beta_3$ :A $\beta$ -dimer complex as described (14). A $\beta$  dimer was eluted from the complex by 8 M urea, 20 mM sodium phosphate, pH 7.5. To remove any residual ZA $\beta_3$ , the eluate was loaded again on a 1 ml HisTrap column (GE Healthcare) pre-equilibrated in 8 M urea, 20 mM sodium phosphate, pH 7.5. The A $\beta$  dimer was stable in 8 M urea at 4°C. Immediately before an experiment, A $\beta$  dimer was eluted from a Superdex 75 10/300 column (GE Healthcare) equilibrated in 20 mM sodium phosphate freshly adjusted to pH 10. For an experiment, the pH was adjusted to selected conditions by dilution in appropriate buffer. Protein concentration was determined by absorption at 280 nm using a calculated extinction coefficient (2980 M<sup>-1</sup> cm<sup>-1</sup>). The success of expression and purification

was verified by SDS-Polyacrylamide gel electrophoresis using 16.5% Tris-Tricine gels (Criterion, Bio-Rad).

#### *Circular Dichroism Spectroscopy*

Spectra of 15  $\mu\text{M}$  A $\beta$ 1-40 dimer or 30  $\mu\text{M}$  A $\beta$ 1-40 were measured in a 1 mm Suprasil Quartz cuvette (Hellma) on a Jasco-J815 spectrophotometer using 50 nm/min scanning speed, 1 nm data pitch and 5 nm bandwidth at 10°C.

#### *Aggregation*

For the aggregation assay the final concentrations employed in the respective samples were 50  $\mu\text{M}$  A $\beta$ 1-40, 5 or 1  $\mu\text{M}$  A $\beta$ 1-40 dimer, 60  $\mu\text{M}$  ThT. The samples were prepared in 20 mM sodium phosphate, 50 mM sodium chloride, pH 7.4 and appropriate volumes of 20 mM sodium phosphate, pH 10 to account for the addition of pH 10 buffer by the A $\beta$ 1-40 dimer. The samples were incubated at 37°C with continuous orbital shaking at 300 rpm in a round-bottom 96-well plate (Nunc) containing 150  $\mu\text{l}$ /well and a 2 mm glass bead per well. ThT emission was recorded at 480 nm (excitation 440 nm) on an Infinite M1000 plate reader (Tecan).

#### *Nuclear Magnetic Resonance Spectroscopy*

[U- $^{15}\text{N}$ ]-A $\beta$ 1-40 dimer was freshly eluted in 20 mM sodium phosphate buffer pH 10 from Superdex 75 10/300 column (GE Healthcare) and diluted to 100  $\mu\text{M}$  with 200 mM NaPi pH 7. NMR data were collected at 5 °C using a 900-MHz spectrometer (Varian) equipped with a cryogenically cooled Z-axis pulse-field-gradient triple resonance probe. NMR data were processed using NMRPipe (20) and analyzed with CcpNmr (21).

## Figures

### A $\beta$ 1-40 dimer :

MDAEFRHDSGYEVHHQKLVFFAEDVGSNKGAIIGLMVGGVVGGGGSGGGSGGGSGGGGSDAEFRHDSGYEVHHQKLVFFAEDVGSNKGAIIGLMVGGVV

### A $\beta$ 1-42 dimer:

MDAEFRHDSGYEVHHQKLVFFAEDVGSNKGAIIGLMVGGVVVIAGGGGSGGGSGGGSGGGGSDAEFRHDSGYEVHHQKLVFFAEDVGSNKGAIIGLMVGGVVIA

**Figure 1: Amino acid sequences of the dimeric A $\beta$  constructs.** The additional N-terminal methionine required for heterologous expression in **green**, representation of the glycine-serine- linker in **red**.

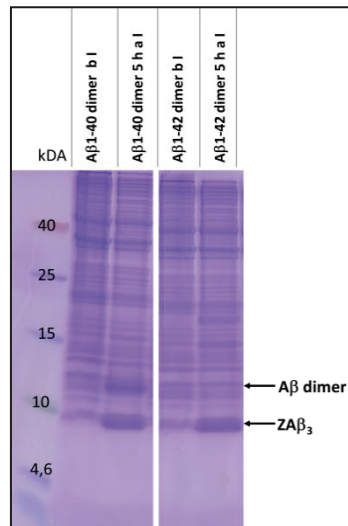


**Figure 2: Expression of A $\beta$  dimers.** Coomassie-stained 16.5% Tris Tricine SDS-PAGE with Spectra Multicolor low range protein ladder (Thermo); b I, before induction; a I, after induction.

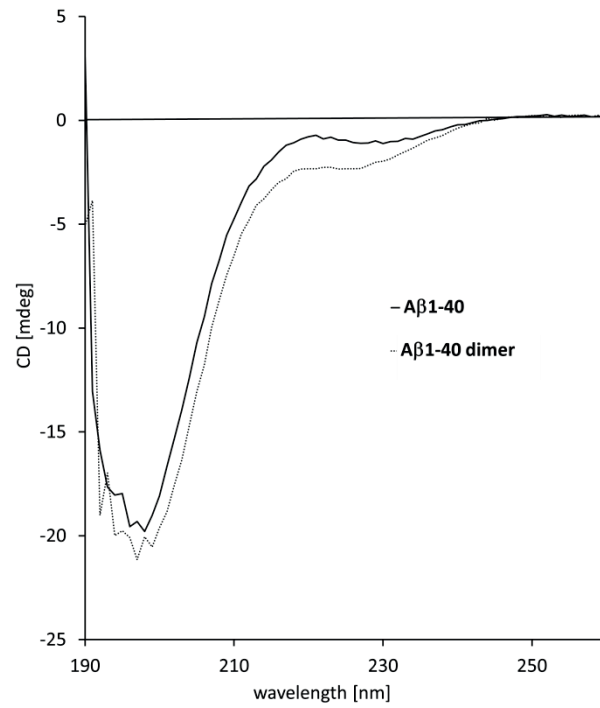


Figure 3: CD spectra of A $\beta$ 1-40 and A $\beta$ 1-40 dimer at pH 8.

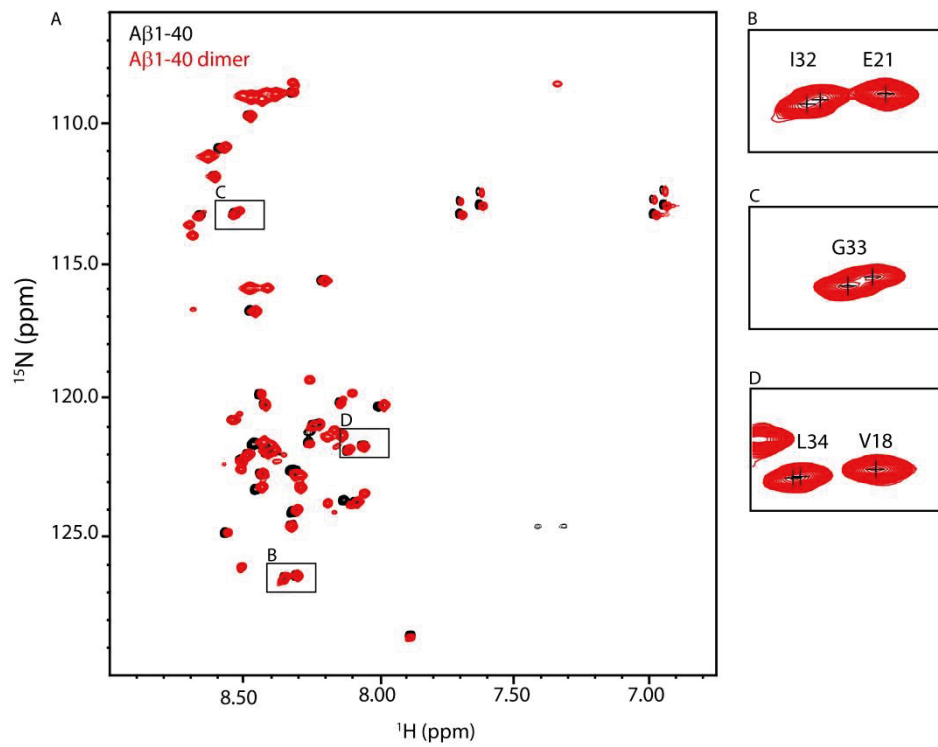
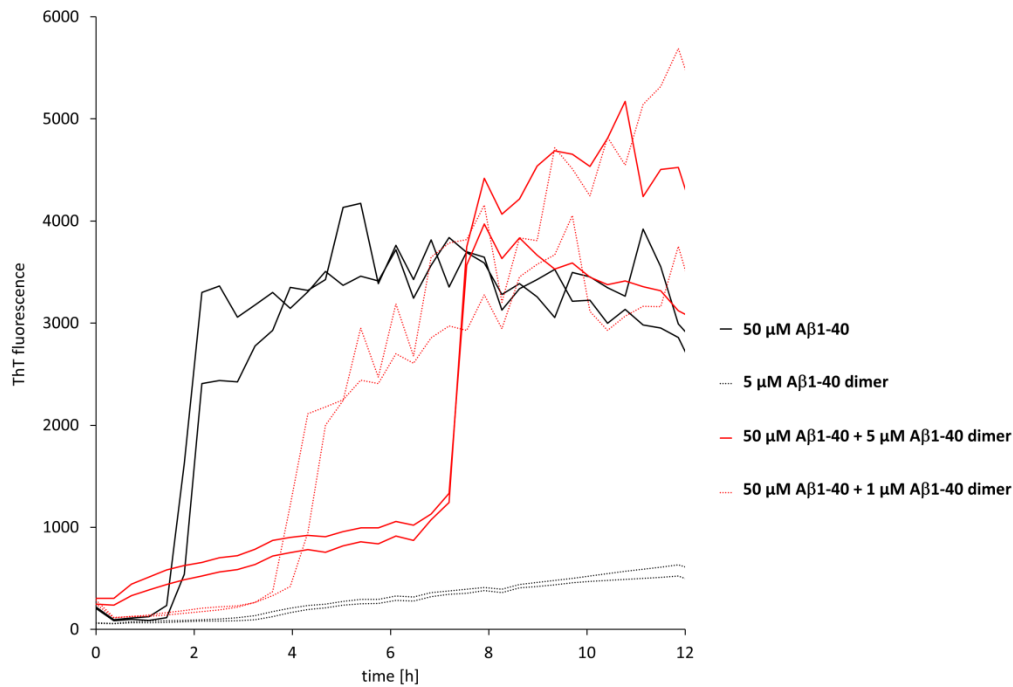


Figure 4: ( $^1\text{H}$ - $^{15}\text{N}$ )-HSQC of A $\beta$ 1-40 dimer. **A**, overlay of A $\beta$ 1-40 dimer (red) and A $\beta$ 1-40 (black); **B-D**, details of A $\beta$ 1-40 dimer resonances.



**Figure 5: Aggregation of Aβ1-40 and Aβ1-40 dimer followed by fluorescence of Thioflavine T.**

## Abbreviations

Aβ, amyloid-β peptide; AD, Alzheimer disease; CD, circular dichroism; (G4S)4, glycine serine linker; NMR, nuclear magnetic resonance; SDS, sodium dodecyl sulfate; ThT, Thioflavine T

## References

1. WHO. (2012) Dementia. World Health Organization, Fact Sheet 362, April 2012.
2. Haass, C., and Selkoe, D. J. (2007) Soluble protein oligomers in neurodegeneration: lessons from the Alzheimer's amyloid beta-peptide. *Nature reviews. Molecular cell biology* **8**, 101-112
3. Lambert, M. P., Barlow, A. K., Chromy, B. A., Edwards, C., Freed, R., Liosatos, M., Morgan, T. E., Rozovsky, I., Trommer, B., Viola, K. L., Wals, P., Zhang, C., Finch, C. E., Krafft, G. A., and Klein, W. L. (1998) Diffusible, nonfibrillar ligands derived from Abeta1-42 are potent central nervous system neurotoxins. *Proceedings of the National Academy of Sciences of the United States of America* **95**, 6448-6453
4. Walsh, D. M., Klyubin, I., Fadeeva, J. V., Cullen, W. K., Anwyl, R., Wolfe, M. S., Rowan, M. J., and Selkoe, D. J. (2002) Naturally secreted oligomers of amyloid beta protein potently inhibit hippocampal long-term potentiation in vivo. *Nature* **416**, 535-539
5. Shankar, G. M., Bloodgood, B. L., Townsend, M., Walsh, D. M., Selkoe, D. J., and Sabatini, B. L. (2007) Natural oligomers of the Alzheimer amyloid-beta protein induce reversible synapse loss by modulating an NMDA-type glutamate receptor-dependent signaling pathway. *The Journal of neuroscience : the official journal of the Society for Neuroscience* **27**, 2866-2875
6. Shankar, G. M., Li, S., Mehta, T. H., Garcia-Munoz, A., Shepardson, N. E., Smith, I., Brett, F. M., Farrell, M. A., Rowan, M. J., Lemere, C. A., Regan, C. M., Walsh, D. M., Sabatini, B. L., and

- Selkoe, D. J. (2008) Amyloid-beta protein dimers isolated directly from Alzheimer's brains impair synaptic plasticity and memory. *Nature medicine* **14**, 837-842
7. Jin, M., Shepardson, N., Yang, T., Chen, G., Walsh, D., and Selkoe, D. J. (2011) Soluble amyloid beta-protein dimers isolated from Alzheimer cortex directly induce Tau hyperphosphorylation and neuritic degeneration. *Proceedings of the National Academy of Sciences of the United States of America* **108**, 5819-5824
  8. Yu, L., Rohinton, E., Harlan, J. E., Holzman, T. F., Lopez, A. P., Labkovsky, B., Hillen, H., Barghorn, S., Ebert, U., Richardson, P. L., Miesbauer, L., Solomon, L., Bartley, D., Walter, K., Johnson, R. W., Hajduk, P. J., and Olejniczak, E. T. (2009) Structural Characterization of a Soluble Amyloid Beta-Peptide Oligomer. *Biochemistry* **48**, 1870-1877
  9. Sandberg, A., Luheshi, L. M., Sollvander, S., Pereira de Barros, T., Macao, B., Knowles, T. P., Biverstal, H., Lendel, C., Ekholm-Petterson, F., Dubnovitsky, A., Lannfelt, L., Dobson, C. M., and Hard, T. (2010) Stabilization of neurotoxic Alzheimer amyloid-beta oligomers by protein engineering. *Proceedings of the National Academy of Sciences of the United States of America* **107**, 15595-15600
  10. O'Nuallain, B., Freir, D. B., Nicoll, A. J., Risse, E., Ferguson, N., Herron, C. E., Collinge, J., and Walsh, D. M. (2010) Amyloid beta-protein dimers rapidly form stable synaptotoxic protofibrils. *The Journal of neuroscience : the official journal of the Society for Neuroscience* **30**, 14411-14419
  11. Muller-Schiffmann, A., Andreyeva, A., Horn, A. H., Gottmann, K., Korth, C., and Sticht, H. (2011) Molecular engineering of a secreted, highly homogeneous, and neurotoxic abeta dimer. *ACS chemical neuroscience* **2**, 242-248
  12. Moore, B. D., Rangachari, V., Tay, W. M., Milkovic, N. M., and Rosenberry, T. L. (2009) Biophysical analyses of synthetic amyloid-beta(1-42) aggregates before and after covalent cross-linking. Implications for deducing the structure of endogenous amyloid-beta oligomers. *Biochemistry* **48**, 11796-11806
  13. Roeder, A. M., Roettger, Y., Stuendel, A., Dodel, R., and Geyer, A. (2013) Synthetic dimeric Abeta28-40 mimics the complex epitope of human anti-Abeta autoantibodies against toxic Abeta oligomers. *The Journal of biological chemistry*
  14. Macao, B., Hoyer, W., Sandberg, A., Brorsson, A. C., Dobson, C. M., and Hard, T. (2008) Recombinant amyloid beta-peptide production by coexpression with an affibody ligand. *BMC biotechnology* **8**, 82
  15. Hoyer, W., Gronwall, C., Jonsson, A., Stahl, S., and Hard, T. (2008) Stabilization of a beta-hairpin in monomeric Alzheimer's amyloid-beta peptide inhibits amyloid formation. *Proceedings of the National Academy of Sciences of the United States of America* **105**, 5099-5104
  16. LeVine, H., 3rd. (1993) Thioflavine T interaction with synthetic Alzheimer's disease beta-amyloid peptides: detection of amyloid aggregation in solution. *Protein science : a publication of the Protein Society* **2**, 404-410
  17. Hard, T. (2011) Protein engineering to stabilize soluble amyloid beta-protein aggregates for structural and functional studies. *The FEBS journal* **278**, 3884-3892
  18. Mc Donald, J. M., Savva, G. M., Brayne, C., Welzel, A. T., Forster, G., Shankar, G. M., Selkoe, D. J., Ince, P. G., Walsh, D. M., Medical Research Council Cognitive, F., and Ageing, S. (2010) The presence of sodium dodecyl sulphate-stable Abeta dimers is strongly associated with Alzheimer-type dementia. *Brain : a journal of neurology* **133**, 1328-1341
  19. Klyubin, I., Betts, V., Welzel, A. T., Blennow, K., Zetterberg, H., Wallin, A., Lemere, C. A., Cullen, W. K., Peng, Y., Wisniewski, T., Selkoe, D. J., Anwyl, R., Walsh, D. M., and Rowan, M. J. (2008) Amyloid beta protein dimer-containing human CSF disrupts synaptic plasticity: prevention by systemic passive immunization. *The Journal of neuroscience : the official journal of the Society for Neuroscience* **28**, 4231-4237

- 
20. Delaglio, F., Grzesiek, S., Vuister, G. W., Zhu, G., Pfeifer, J., and Bax, A. (1995) NMRPipe: a multidimensional spectral processing system based on UNIX pipes. *Journal of biomolecular NMR* **6**, 277-293
  21. Vranken, W. F., Boucher, W., Stevens, T. J., Fogh, R. H., Pajon, A., Llinas, M., Ulrich, E. L., Markley, J. L., Ionides, J., and Laue, E. D. (2005) The CCPN data model for NMR spectroscopy: development of a software pipeline. *Proteins* **59**, 687-696

**CHAPTER 3**

ALTERNATIVE CONFORMATIONS OF THE TAU REPEAT DOMAIN IN COMPLEX  
WITH AN ENGINEERED BINDING PROTEIN

Clara S. R. Grüning, Ewa A. Mirecka, Antonia N. Klein, Stephen F. Marino, Eckhard Mandelkow, Dieter Willbold, Matthias Stoldt, and Wolfgang Hoyer

**Status:** submitted to *Journal of Biological Chemistry* on February 25, 2014

**Impact Factor:** 4.651 (2012)

**Own proportion to this work:** 80%

Design, cloning, expression and purification of tau constructs including proline mutants, biotinylation of tau, expression and purification of htau40 and A $\beta$ 1-40, selection, expression and purification of TP4, preparation of samples for isothermal titration calorimetry, transmission electron microscopy and NMR, NMR resonance assignments, circular dichroism and aggregation experiments, writing of the manuscript.

## Alternative Conformations of the Tau Repeat Domain in Complex with an Engineered Binding Protein\*

Clara S. R. Grüning<sup>1</sup>, Ewa A. Mirecka<sup>1</sup>, Antonia N. Klein<sup>2</sup>, Eckard Mandelkow<sup>3,4</sup>, Dieter Willbold<sup>1,2</sup>, Stephen F. Marino<sup>1,5</sup>, Matthias Stoldt<sup>1,2</sup>, and Wolfgang Hoyer<sup>1,2</sup>

From the <sup>1</sup>Institute of Physical Biology, Heinrich-Heine-Universität, 40204 Düsseldorf, Germany, <sup>2</sup>Institute of Structural Biochemistry (ICS-6), Research Centre Jülich, 52425 Jülich, Germany, <sup>3</sup>CAESAR Research Center, 53175 Bonn, Germany, <sup>4</sup>German Center for Neurodegenerative Diseases (DZNE), 53175 Bonn, Germany

\*Running title: *Alternative conformations of the tau repeat domain*

To whom correspondence should be addressed: Wolfgang Hoyer, Institute of Physical Biology, Heinrich-Heine-Universität, 40204 Düsseldorf, Germany, Phone 0049 211 8115153, Fax 0049 211 8115167, Email: wolfgang.hoyer@uni-duesseldorf.de

**Keywords:** Alzheimer disease; amyloid; nuclear magnetic resonance; protein aggregation; protein conformation; protein engineering; protein misfolding; tau

**Background:** Aggregates of the protein tau are associated with Alzheimer disease and other neurodegenerative diseases.

**Results:** The engineered binding protein TP4, targeting the tau repeat domain, was obtained from a novel  $\beta$ -wrapin protein library.

**Conclusions:** TP4 interacts with two alternative conformations of tau, thereby inhibiting tau aggregation.

**Significance:** Binding of aggregation-prone sequence stretches is an approach to interfere with tau aggregation.

**ABSTRACT**

The aggregation of tau into paired helical filaments is involved in the pathogenesis of several neurodegenerative diseases including Alzheimer disease. The aggregation reaction is characterized by conformational conversion of the repeat domain, which partially adopts a cross- $\beta$  structure in the resulting amyloid-like fibrils. Here we report the selection and characterization of an engineered binding protein,  $\beta$ -wrapin TP4, targeting the tau repeat domain. TP4 was obtained by phage display using the four-repeat tau construct K18 $\Delta$ K280

as a target. TP4 binds K18 $\Delta$ K280 as well as the longest isoform of human tau, htau40, with nanomolar affinity. NMR spectroscopy identified two alternative TP4-binding sites in the four-repeat domain, each including two hexapeptide motifs with high  $\beta$ -sheet propensity. Both binding sites contain the aggregation-determining PHF6 hexapeptide within repeat 3. In addition, one binding site includes the PHF6\* hexapeptide within repeat 2, whereas the other includes the corresponding hexapeptide tau(337-342) within repeat 4, denoted PHF6\*\*. Comparison of TP4-binding with tau aggregation reveals that the same regions of tau are involved in both processes. TP4 inhibits tau aggregation at substoichiometric concentration, demonstrating that it interferes with aggregation nucleation. This study provides residue-level insight into the interaction of tau with an aggregation inhibitor and highlights the structural flexibility of tau.

The microtubule binding protein tau has recently gained increased scientific attention due to its involvement in neurodegenerative diseases. The suggested physiological functions of tau relate mostly to microtubule binding, which occurs through an imperfect repeat domain in the C-terminal part of the protein (1-4). The repeat

domain consists of three (3R) or four (4R) repeats depending on alternative splicing. Although tau is a highly soluble, intrinsically disordered protein (5), it can aggregate into straight or paired helical filaments (PHFs)<sup>6</sup>, which further combine to form neurofibrillary tangles, the hallmarks of several neurodegenerative diseases such as Alzheimer disease and frontotemporal dementia (6,7).

Tau aggregation is a multi-step reaction characterized by conformational conversion of the repeat domain. Aggregation-promoting conditions, such as heparin addition or introduction of the pro-aggregant  $\Delta$ K280 mutation, are associated with increased formation of intramolecular interactions within the repeat domain, accompanied by its compaction (8,9). Tau aggregation progresses through dimerization and oligomerization (10-13). Two motifs with high  $\beta$ -sheet propensity in the repeats R3 and R2, called PHF6 (<sup>306</sup>VQIVYK<sup>311</sup>) and PHF6\* (<sup>275</sup>VQIINK<sup>280</sup>), respectively, are involved in the initiation of the oligomerization process (14-18). PHFs, the products of the aggregation reaction, are characterized by a rigid cross  $\beta$ -sheet core (19,20), built up by the imperfect repeats (21-23), and an outer fuzzy coat formed by the N- and C-terminal parts of the protein (24). Due to its importance for the aggregation process, the repeat domain constitutes an interesting target for interference with tau assembly. For example, methylene blue inhibits tau aggregation by acting on the repeat domain (25).

In this study, we generated an engineered binding protein, termed TP4, to the tau repeat domain and characterized its mode of binding and impact on tau aggregation. TP4 belongs to the class of  $\beta$ -wrapins ( $\beta$ -wrap proteins), which are selected from phage display libraries based on the Z $\beta$ <sub>3</sub> scaffold (26). Z $\beta$ <sub>3</sub> is a disulfide-linked homodimeric protein derived from the Z domain of protein A (27,28). Z $\beta$ <sub>3</sub> binds the amyloid- $\beta$  peptide (A $\beta$ ) with nanomolar affinity, stabilizing a  $\beta$ -hairpin conformation of A $\beta$  and inhibiting A $\beta$  aggregation (28). Evidence obtained by protein engineering, NMR spectroscopy, MD simulations, and FTIR spectroscopy suggests that the  $\beta$ -hairpin conformation observed in complex with the binding protein is also transiently populated in free A $\beta$  monomers and constitutes a component of A $\beta$  oligomers and protofibrils (29-32). The  $\beta$ -wrapin

AS69 selected to bind the protein  $\alpha$ -synuclein involved in Parkinson disease likewise stabilizes a  $\beta$ -hairpin of the target protein and inhibits  $\alpha$ -synuclein aggregation at substoichiometric concentration (26).

This work presents the  $\beta$ -wrapin TP4, which targets the repeat domain of tau. NMR spectroscopy of the complex of TP4 with the repeat domain of the four-repeat tau isoform reveals two alternative conformations of bound tau. TP4 is able to inhibit aggregation of tau at substoichiometric concentration.

## EXPERIMENTAL PROCEDURES

### *Cloning and expression of tau constructs*

The amino acid numbering of all constructs is that of the isoform htau40 (full-length tau) containing 441 residues. Codon-optimized tau K18 $\Delta$ K280(AA) DNA sequences (human tau from Q244 to N368) were cloned into pET24a vector (Merck Millipore) using NdeI and BamHI (Thermo Fisher) restriction sites. The K18 constructs used in this study comprised exactly the four repeat domains, i.e. residues htau(244-368), but not the C-terminal residues <sup>369</sup>KKIE<sup>372</sup> included in the K18 construct as originally defined (1). K18AA proline mutants were prepared by site-directed mutagenesis using phosphorylated primers, one of them containing the mutation at its 5' end (33). The vector was amplified with the high-fidelity polymerase Velocity (Bioline) and religated. Full-length tau in the pET28 vector was a kind gift of Susanne Aillean Funke (Research Centre Jülich). For expression, the constructs were transformed into *E. coli* BL21 (DE3) cells. Cells were grown either in lysogeny broth or, for labeled protein, in minimal medium M9 containing 1 g/l <sup>15</sup>N ammonium chloride and/or 2 g/l <sup>13</sup>C glucose until an OD<sub>600</sub> of approx. 0.8 was reached. Expression was then induced with 1 mM IPTG for 4 h at 37°C. Cell pellets were stored at -20°C until further processing.

### *Purification of tau constructs*

Cell pellets were resuspended in 50 mM Tris HCl, pH 8.2, containing protease inhibitor tablets (Roche), 1 mM MgCl<sub>2</sub>, and 250 U/ml Benzonase (Merck). Cells were disrupted using a high pressure-based system (2.9 kbar, Constant

Systems). After clearing the solution from cell debris (40,000x g, 40 min, 4°C), a first purification step was performed by cation exchange chromatography using a HiTrap SP FF 5 ml column (GE Healthcare) connected to an Äkta Purifier system (GE Healthcare) with a high salt buffer to elute bound protein in a linear gradient (50 mM Tris HCl, pH 8.2, 1 M NaCl). Further purification was achieved by size exclusion chromatography (SEC) using a HiLoad Superdex 75 16/60 column (GE Healthcare) with 50 mM NH<sub>4</sub>CO<sub>3</sub> as running buffer to enable subsequent lyophilization of the purified proteins. Protein aliquots were stored at -80°C. Protein concentration was measured by UV absorption at 280 nm using a calculated extinction coefficient of 1490 M<sup>-1</sup> cm<sup>-1</sup>. Full-length tau protein was purified essentially in the same way. Cells were resuspended in 0.5 M NaCl, 20 mM Pipes, pH 6.5, and 2 mM dithiothreitol (DTT), containing protease inhibitor tablets (Roche). After cell disruption and centrifugation the solution was heated up to 80°C for 15 min. The denatured proteins were removed by centrifugation (as above) and the solution was dialyzed overnight against 50 mM NaCl, 20 mM Pipes, pH 6.5, 2 mM DTT. The same buffer containing 1 M NaCl was used to elute protein from cation exchange chromatography. For SEC, 20 mM sodium phosphate (NaPi), 50 mM NaCl, pH 7.4, was used as running buffer and the purified protein was stored at -20°C.

#### ***Biotinylation of tau K18ΔK280***

For phage display selection, the tau construct K18ΔK280 was biotinylated using NHS-LC-Biotin (Thermo Scientific). A lyophilized tau K18ΔK280 aliquot was resuspended in 100 mM NaPi, pH 7.0, and subjected to SEC using a Superdex 75 10/300 column with the same buffer as running buffer to ensure the monomeric state of the tau construct. Freshly prepared NHS-Biotin solution was added to a 5-fold molar excess and the reaction was incubated for 16 h at 4°C in the presence of 5 mM DTT. The reaction was stopped by removal of the biotinylation reagent using a HiTrap desalting column (GE Healthcare). The biotinylated protein was separated by an avidin agarose column (Thermo Scientific) and the biotinylation state was determined by a HABA assay (Thermo Scientific) to be 2 moles of biotin per mole of tau K18ΔK280 monomer.

#### ***Cloning of the library***

A new β-wrapin library was constructed by overlapping PCR using primers encoding AQHDEA peptide derived from the region E of protein A followed by the randomized ZAβ<sub>3</sub> gene. The NNK degenerate codon (where N stands for any of four nucleotides and K for G, T) was employed for generating diversity at amino acid positions 16, 17, 18, 19, 30, 34, 45 of ZAβ<sub>3</sub>, whereas the DTS degenerate codon (where D stands for A, G, T and S for C, G) was used for amino acid exchange at positions 27 and 31. The primers used were:

L1:

GCGCAACACGATGAAGCCGTAGATAACAA  
ATTCAACAAAGAAATGGCGAGTGCG,

L2:

GATCCGGGTTTAAGTTAGGKNNKNNKNNK  
NNCTCCCCACCCGCACTCGCCATTTCTTTG,

L3:

CCTAACTTAAACCCGGATCAADTSTGCGCC  
NNKDTSCATAGTNNKCATGATGACCCAAG  
CCAAAGC,

L4:

TTTCGGCGCCTGAGCATCATTAGCTTTTT  
AGCTTCTGCKNNCAAGTTAGCGCTTTGGCT  
TGGGTCATC.

The gene pool was cloned between SacI and XhoI of the pComb3HSS vector (provided by C. F. Barbas, The Scripps Research Institute, La Jolla, USA). In addition to the library insert, the pComb3HSS vector contained the coding sequence for c-myc-tag and albumin-binding domain from streptococcal protein G directly cloned between XhoI and SpeI. The library was transformed into electrocompetent *E. coli* XL1-Blue cells (Stratagene) resulting in 2.3 x 10<sup>9</sup> transformants.

#### ***Phage display selection***

The phage library was produced by superinfection of bacteria harboring the library with M13KO7 phage (New England Biolabs) and precipitation by PEG/NaCl. The library was subjected to four successive rounds of panning against biotinylated tau K18ΔK280 with decreasing target concentrations (500, 300, 50 and 1 nM, respectively) and increasing washing stringency (2-, 5-, 10- and 20-times of PBST-BSA (PBS, 0.1% (w/v) Tween 20, 3% (w/v) BSA), respectively, and once with PBS). In order to

*Alternative conformations of the tau repeat domain*

remove streptavidin-binding phage, a negative selection in which the phage preparation was incubated with streptavidin magnetic beads at room temperature for 1 h preceded each selection round. In the first panning round, the incubation was carried out overnight at 4°C whereas the subsequent selection rounds were done for 1 h at room temperature. The phage-target complexes were captured on streptavidin magnetic beads and following washing, bound phages were eluted by lowering the pH to 2.0. After neutralization with 1 M Tris HCl, pH 8.0, the eluted phages were amplified in *E. coli* XL1-Blue cells and subjected to the following panning round. After the fourth selection round, the DNA pool was subcloned into pET302/NT-His vector (Life Technologies) and DNA from 91 single colonies was sequenced.

**Purification of TP4**

TP4 containing an N-terminal His6-tag was expressed from pET302/NT-His vector in *E. coli* BL21(DE3) cells. Cells were grown in lysogeny broth and protein expression was induced with 1 mM IPTG at OD<sub>600</sub> of 0.6-0.8 for 5 h at 37°C. Following centrifugation at 4,000x g, the cell pellet was resuspended in 50 mM NaPi, pH 8.0, 500 mM NaCl, containing EDTA-free protease inhibitor (Roche) and lysed using a high pressure-based system (2.9 kbar, Constant Systems). After clearing the solution from cell debris (40,000x g, 40 min, 4°C), a first purification step was performed by immobilized metal ion affinity chromatography (HisTrap FF column, GE Healthcare). The dimeric fraction of TP4 was collected from a HiLoad Superdex 75 16/60 column (GE Healthcare) in 20 mM NaPi, 50 mM NaCl, pH 7.4. To facilitate concentration determination of TP4, a tryptophan was introduced between the methionine and the N-terminal His6-tag by site-directed mutagenesis (33).

**Aβ(1-40) preparation**

Aβ(1-40) was recombinantly produced with an N-terminal methionine by coexpression with ZAβ<sub>3</sub> as described previously (34).

**Isothermal titration calorimetry (ITC)**

ITC was performed on a Microcal iTC200 calorimeter (GE Healthcare) at 10°C. Binding parameters were obtained from a nonlinear least-squares fit to a 1:1 binding model. K18 variants

were used at a concentration of ~70 μM as titrant in the cell and TP4 at approximately 10-fold higher concentration as titrant in the syringe, except for K18AA I277P V339P, which was used at a concentration of ~560 μM as titrant in the syringe and titrated into 31 μM TP4. Binding of K18AA to ZAβ<sub>3</sub> was tested by using ZAβ<sub>3</sub> at a concentration of ~70 μM as titrant in the cell and K18AA at approximately 10-fold higher concentration as titrant in the syringe. The buffer was 20 mM NaPi, 50 mM NaCl, pH 7.4. The heat of post-saturation injections was averaged and subtracted from each injection to correct for heats of dilution and mixing. Data were processed using MicroCal Origin software provided with the calorimeter.

**NMR spectroscopy**

NMR data were collected at 5°C using a 900 MHz spectrometer (Varian) equipped with a cryogenically cooled Z-axis pulse-field-gradient triple resonance probe. NMR samples contained ca. 150 μM [U-<sup>13</sup>C, <sup>15</sup>N]-K18AA and the indicated amounts of [NA]-TP4 in 20 mM NaPi, 50 mM NaCl, pH 7.0. NMR data were processed using NMRPipe (35) and analyzed with CcpNmr (36). Backbone assignments, obtained using BEST-TROSY experiments (37) and standard triple resonance heteronuclear NMR techniques, were in agreement with prior assignments of tau K18 (15,38).

**Circular dichroism spectroscopy**

Far-UV CD spectra were measured on a JASCO J-815 spectropolarimeter using protein samples at a concentration of 10 μM in 1 mm Suprasil Quartz cuvettes (Hellma). The buffer was 20 mM NaPi, 50 mM NaCl, pH 7.4. To obtain melting curves, spectra were recorded from 5°C to 60°C in 5°C intervals.

**Aggregation assay**

The aggregation of K18AA was monitored with the dye Thioflavin T (ThT). Samples were prepared in 20 mM NaPi, 50 mM NaCl, pH 7.4, with or without addition of 10 μM heparin. Lyophilized and resuspended tau was subjected to SEC using a Superdex 75 10/300 column to ensure the monomeric state of the tau construct. The final reaction contained 50 μM of K18AA, 60 μM ThT,

*Alternative conformations of the tau repeat domain*

0.05%  $\text{NaN}_3$ , and the indicated concentration of TP4. Aggregation was performed in 96-well round bottom plates (Nunc), containing one 2 mm glass bead per well and sealed with a polyolefine tape (Nunc), incubated in an Infinite M1000 plate reader (Tecan) at 25°C, with orbital shaking applied for ~10% of the incubation time. ThT fluorescence was recorded every 30 minutes at 480 nm (excitation 440 nm, bandwidth 5 nm).

**Transmission electron microscopy**

Samples from the aggregation assay were diluted to a K18AA concentration of 4  $\mu\text{M}$ , and 20  $\mu\text{l}$  were applied to formvar/carbon coated copper grids (S162, Plano), followed by incubation for 3 min. The grids were washed three times with  $\text{H}_2\text{O}$  and once with 2% aqueous uranyl acetate, followed by 1 min incubation with 2% aqueous uranyl acetate for negative staining. The grids were dried overnight. The samples were examined with a Libra 120 electron microscope (Zeiss) operating at 120 kV.

**RESULTS**

*Selection of a  $\beta$ -wrapin to tau by phage display* - For this study, a new  $\beta$ -wrapin library was generated by site-directed mutagenesis of the  $\text{ZA}\beta_3$  gene. In the library, the residues of  $\text{ZA}\beta_3$  that constitute the binding surface in the complex with  $\text{A}\beta$  were randomized (Fig. 1). While most of these residues were replaced by all 20 amino acids, residues 27 and 31 in both subunits were substituted only by hydrophobic amino acids in order to preserve the hydrophobic interface between the subunits (Fig. 1). The library size was  $2.3 \times 10^9$  transformants.

As target for phage display selections the tau construct K18 $\Delta$ K280 was used (Fig. 2). The deletion of Lys-280 found in Frontotemporal dementia with parkinsonism-17 patients was included as it increases the population of aggregation-prone conformations of the repeat domain (9,17), which might serve as primary molecular recognition features of the intrinsically disordered tau. In total, four selection rounds on biotinylated K18 $\Delta$ K280 were performed. After selection, 91 clones were sequenced unveiling one dominant sequence with 84% occurrence, corresponding to  $\beta$ -wrapin TP4 (Fig. 1b). The hydrophobic nature of the randomized residues in

the  $\alpha 2$ -helix was conserved in TP4. Apart from the randomized positions, TP4 contained one additional mutation, namely N52S. TP4 was purified as a disulfide-linked homodimer after recombinant expression. The affinity of TP4 for different tau constructs was determined by ITC (Table 1, Fig. 3). To prevent the formation of oxidation products of tau K18 $\Delta$ K280 during the biophysical characterization, Cys-291 and Cys-322 were replaced by alanine residues. The resulting construct, referred to as K18AA (Fig. 2), exhibited an affinity of 260 nM for TP4 (Table 1). Sub-micromolar affinity to TP4 was also observed for full-length htau40 without the  $\Delta$ K280 deletion (Fig. 3). In contrast, ITC did not detect any heats of binding when  $\text{ZA}\beta_3$  was titrated with K18AA, demonstrating that the affinity for tau was generated by the phage display selection.

*Partially folded conformation in the K18:TP4 complex* - The free and bound states of K18AA and TP4 were characterized by CD spectroscopy (Fig. 4). In contrast to the CD spectrum of the original  $\text{ZA}\beta_3$  scaffold, which features minima at 208 nm and 221 nm characteristic for  $\alpha$ -helical secondary structure, CD of TP4 exhibited a minimum at 201 nm indicative of largely disordered conformation (Fig. 4a). This might be a consequence of the selection of residues with lower  $\beta$ -sheet propensity and lower hydrophobicity in the  $\beta$ -strand region of the scaffold. K18AA has an ellipticity minimum at 197 nm in agreement with the intrinsically disordered nature of K18 (Fig. 4b). The CD spectrum of the K18AA:TP4 complex differs from the sum of the CD spectra of the free components. Upon binding, the ellipticity decreases in the wavelength range around 220 nm, whereas it increases in the wavelength range around 200 nm, indicative of partially folded conformation in the K18AA:TP4 complex (Fig. 4b). Thermal melting experiments demonstrated low thermostability of the K18AA:TP4 complex with thermal denaturation occurring in the temperature range from 10°C to 40°C at 10  $\mu\text{M}$  protein concentration (Fig. 4c).

*Two alternative conformations of K18 in complex with TP4* - We used NMR spectroscopy to determine the binding site of K18 interacting with TP4. Several resonance signals in the ( $^1\text{H}$ - $^{15}\text{N}$ )-HSQC spectrum of [ $^{15}\text{N}$ ]-K18AA

*Alternative conformations of the tau repeat domain*

disappeared when [NA]-TP4 was added at 1:1 molar ratio, indicative of an epitope that features intermediate exchange in the bound state (Fig. 5). The disappearing resonances were assigned to the region tau(300-317), whose center corresponds to the PHF6 motif and in which residual  $\beta$ -structure was detected by NMR of the free K18 monomer (15) (Fig. 6a). A ( $^1\text{H}$ - $^{15}\text{N}$ )-HSQC titration experiment confirmed the 1:1 stoichiometry of the K18AA:TP4 interaction (Fig. 6a). The titration experiment moreover revealed that the regions N- and C-terminal of tau(300-317) were also affected by the binding of TP4. These regions spanned approximately the sequence stretches tau(268-299) and tau(318-349), respectively. Like tau(300-317), both tau(268-299) and tau(318-349) contain a stretch of approximately 10 amino acids shown previously to exhibit residual  $\beta$ -structure in the free K18 monomer (15). In the case of tau(268-299), this stretch includes the PHF6\* motif, while tau(318-349) contains a corresponding hexapeptide motif, <sup>337</sup>VEVKSE<sup>342</sup>, which we refer to as PHF6\*\* in this study. The ( $^1\text{H}$ - $^{15}\text{N}$ )-HSQC peak heights in the regions tau(268-299) and tau(318-349) decreased by ca. 50% upon addition of an equimolar amount of TP4 (Fig. 6a). Further addition of TP4 resulted only in a minor further decrease of the peak heights. The titration experiments thus demonstrated that the region tau(300-317) invariably underwent a conformational change upon binding, whereas each of the regions tau(268-299) and tau(318-349) did so in only about half of the K18AA:TP4 complexes, remaining in a disordered free state-like conformation in the rest of the complexes.

A plausible explanation for this observation is that partial folding of K18AA in each individual complex with TP4 involves one of two alternative binding sites, either tau(268-317) or tau(300-349) (Fig. 8a). Partially folded K18AA might be stabilized by contacts between tau(300-317) and the involved adjacent region, potentially established through the sites exhibiting residual  $\beta$ -structure in the free state (Fig. 8b). To test this hypothesis, we decreased the  $\beta$ -sheet propensity of the critical regions by generating proline mutants. Proline mutations were introduced at the third position of the hexapeptide motifs PHF6\* (in R2), PHF6 (in R3), and PHF6\*\* (in R4) (Fig. 2). In total, four proline mutants of K18AA were generated: I277P, I308P, V339P, and the double

mutant I277P V339P. The I308P mutation decreases the  $\beta$ -sheet propensity of PHF6. Introduction of the I308P mutation into K18AA eliminated the affinity for TP4 as measured by ITC (Table 1). Consequently, the decrease in the peak heights in the ( $^1\text{H}$ - $^{15}\text{N}$ )-HSQC spectrum of K18AA I308P upon equimolar addition of TP4 was small compared to K18AA (Fig. 6b). These findings underscore the importance of the PHF6 motif for the K18AA:TP4 interaction. The mutations placed in PHF6\* and PHF6\*\*, I277P and V339P, respectively, resulted in only a small decrease in the affinity to TP4 when introduced individually (Table 1). In bound K18AA I277P, an increased fraction of the tau(268-299) region and a decreased fraction of the tau(318-349) region remained in the disordered free state-like conformation compared to bound K18AA (Fig. 6c). This agrees with preferential binding of TP4 to the binding site tau(300-349) of the I277P mutant (Fig. 8a). Conversely, bound K18AA V339P exhibited a decreased fraction of the tau(268-299) region and an increased fraction of the tau(318-349) region in the disordered free state-like conformation compared to bound K18AA (Fig. 6c), in agreement with preferential binding of TP4 to the binding site tau(268-317) of the V339P mutant (Fig. 8a). When the I277P and V339P mutations were introduced together, binding to TP4 was strongly impaired (Table 1). Both regions tau(268-299) and tau(318-349) remained largely in the disordered free state-like conformation upon binding of the I277P V339P double mutant to TP4 (Fig. 6d). Taken together, the analysis of the proline mutants demonstrated that sub-micromolar binding of TP4 requires the integrity of the PHF6 motif and of one of the motifs PHF6\* or PHF6\*\*, consistent with the existence of two alternative conformations of bound K18AA as depicted schematically in Figure 8b.

The conformations diagrammed in Figure 8b are incompatible with an intramolecular disulfide bond between the two cysteine residues in the repeat domain, Cys-291 and Cys-322. In line with this, pre-oxidation of K18 $\Delta$ K280 by prolonged incubation in the absence of DTT, which would lead to "compact monomers" incompetent for assembly (10,39), strongly decreased the binding affinity of TP4 (Table 1).

*Alternative conformations of the tau repeat domain*

*TP4 inhibits K18 aggregation* - The fluorescence of the dye ThT increases with the formation of tau fibrils (40). To evaluate the effect of TP4 binding on the aggregation of K18AA, ThT fluorescence was monitored during incubation of K18AA in the absence and presence of TP4. In incubations without addition of the aggregation promoter heparin, K18AA fibrillation was potently inhibited both at a 1:1 and a 1:10 molar ratio of TP4 (Fig. 7a). The absence of aggregates during the prolonged lag-time of TP4-containing aggregation reactions was confirmed by electron microscopy (Fig. 7b,c). In the presence of heparin, K18AA aggregated without a discernible lag-phase when TP4 was absent or present at 1:10 molar ratio (Fig. 7a). Addition of TP4 at equimolar ratio, however, led to the emergence of a distinct lag-phase.

**DISCUSSION**

The present study reports the selection of the engineered binding protein TP4 targeting the repeat domain of tau. TP4 was obtained from a new  $\beta$ -wrapin phage display library generated by site-directed mutagenesis of the scaffold protein ZA $\beta_3$ , a binder to a  $\beta$ -hairpin motif of the A $\beta$  peptide. TP4 binds K18 and full-length htau40 with nanomolar affinity. The structural analysis of the K18AA:TP4 interaction revealed the presence of two alternative binding sites in K18, one comprising the region tau(268-317), the other the region tau(300-349) (Fig. 8a). The two binding sites are bound with approximately the same frequency by TP4 according to the ( $^1\text{H}$ - $^{15}\text{N}$ )-HSQC titration data (Fig. 6). The determination of the high-resolution NMR structures of the K18AA:TP4 complexes was precluded by the absence of resonance signals of the bound state due to intermediate exchange. However, the presence of two sequence stretches with high  $\beta$ -structure propensity in each of the binding regions suggests the presence of  $\beta$ -hairpin motifs in bound K18, similar to the structures of A $\beta$  bound to the  $\beta$ -wrapin scaffold protein ZA $\beta_3$  (28) and of  $\alpha$ -synuclein bound to the  $\beta$ -wrapin AS69 (26). For the binding site tau(268-317), the regions around PHF6\* and PHF6 could contribute the  $\beta$ -strands to a  $\beta$ -hairpin, whereas the regions around PHF6 and PHF6\*\* could do so for the binding site tau(300-

349) (Fig. 8). In line with this, a decrease in the  $\beta$ -sheet propensity of any of the hexapeptide motifs by amino acid exchanges to proline resulted in a reduced binding affinity of TP4 to the affected binding site(s).

The binding of tau to TP4 features striking similarities to tau self-assembly. For both tau aggregation and TP4 binding, the PHF6 hexapeptide is of utmost importance. PHF6 is a mandatory element of the TP4 binding sites as well as of the tau fibril core (14,18,20,41,42). Replacement of Val-308 in PHF6 by a proline suppresses PHF formation (17) as well as TP4 binding. In contrast to PHF6, the PHF6\* motif of only a subset of the tau molecules is incorporated into the fibril core, whereas it remains in a disordered conformation in the rest of the tau molecules (42). Similarly, PHF6\* is a binding site constituent in only a subset of the K18:TP4 complexes, while it remains in disordered conformation in the other part. Analogous observations were made for PHF6\*\*, which can adopt folded as well as disordered conformations both in fibrils (43) and in K18:TP4 complexes. The formation of an intramolecular disulfide bond in K18 involving the cysteine residues at position 291 and 322 retards tau aggregation due to the resulting restriction to conformations incompatible with fibril formation (10,44). Similarly, intramolecular disulfide bond formation in K18 resulted in a strong decrease in affinity to TP4. Taken together, these findings show that TP4 recruits exactly those sequence regions that are involved in tau self-assembly. The findings furthermore suggest that aggregation-prone conformations, previously proposed to trigger tau assembly (8,45), might share structural characteristics, e.g. certain intramolecular tertiary contacts, with TP4-bound tau. Aggregation-prone conformations have been detected for example by single-molecule force spectroscopy and by single molecule Förster resonance energy transfer (8,9). The relationship between the  $\beta$ -hairpin conformations of TP4-bound tau suggested in this study and the conformation of tau within filaments is illustrated in Fig. 8c. The  $\beta$ -hairpin features intramolecular backbone hydrogen bonds between the  $\beta$ -strands, whereas the  $\beta$ -sheets of tau filaments are intermolecular, with parallel, in-register orientation (20,42,46).

*Alternative conformations of the tau repeat domain*

Tau can adopt two alternative conformations in complex with TP4. A similar conformational heterogeneity of tau aggregation intermediates would have consequences for the later steps of the aggregation reaction. For example, it could be crucial for the occurrence of conformation-based seeding barriers which have been observed for different tau isoforms (47,48). Structural heterogeneity has also been observed in tau oligomers (16).

TP4 inhibits the aggregation of the repeat domain at stoichiometric concentration (Fig. 7). This can be explained by the sequestration of the aggregation-prone regions of tau by TP4. Moreover, TP4 inhibits aggregation at substoichiometric concentration, demonstrating that it interferes with the nucleation steps of the aggregation reaction. The substoichiometric inhibition cannot be explained simply by monomer removal from the aggregation reaction and the mechanism of substoichiometric inhibition is not provided by the present data. It is, however, tempting to speculate that TP4 might interact with high affinity with tau conformers in oligomeric aggregation intermediates which are similar in structure to TP4-bound tau monomers. The aggregation promoter heparin counteracts the substoichiometric inhibition by TP4 (Fig. 7). Heparin is known to greatly accelerate the nucleation step of tau aggregation (49,50). Under these conditions, the capacity of substoichiometric TP4 concentrations to interfere with the formation and/or growth of nuclei might be exceeded.

This study provides residue-level insight into structural properties of tau interacting with an aggregation inhibitor, revealing two alternative conformations of bound tau. The obtained data elucidates how aggregation can be halted at the stage of monomeric tau.

## REFERENCES

1. Gustke, N., Trinczek, B., Biernat, J., Mandelkow, E. M., and Mandelkow, E. (1994) Domains of tau protein and interactions with microtubules. *Biochemistry* **33**, 9511-9522
2. Lee, G., Neve, R. L., and Kosik, K. S. (1989) The microtubule binding domain of tau protein. *Neuron* **2**, 1615-1624
3. Morris, M., Maeda, S., Vossel, K., and Mucke, L. (2011) The many faces of tau. *Neuron* **70**, 410-426
4. Mukrasch, M. D., von Bergen, M., Biernat, J., Fischer, D., Griesinger, C., Mandelkow, E., and Zweckstetter, M. (2007) The "jaws" of the tau-microtubule interaction. *J. Biol. Chem.* **282**, 12230-12239
5. Schweers, O., Schonbrunn-Hanebeck, E., Marx, A., and Mandelkow, E. (1994) Structural studies of tau protein and Alzheimer paired helical filaments show no evidence for beta-structure. *J. Biol. Chem.* **269**, 24290-24297
6. Ballatore, C., Lee, V. M., and Trojanowski, J. Q. (2007) Tau-mediated neurodegeneration in Alzheimer's disease and related disorders. *Nat. Rev. Neurosci.* **8**, 663-672
7. Lee, V. M., Balin, B. J., Otvos, L., Jr., and Trojanowski, J. Q. (1991) A68: a major subunit of paired helical filaments and derivatized forms of normal Tau. *Science* **251**, 675-678
8. Elbaum-Garfinkle, S., and Rhoades, E. (2012) Identification of an aggregation-prone structure of tau. *J. Am. Chem. Soc.* **134**, 16607-16613
9. Wegmann, S., Scholer, J., Bippes, C. A., Mandelkow, E., and Müller, D. J. (2011) Competing interactions stabilize pro- and anti-aggregant conformations of human Tau. *J. Biol. Chem.* **286**, 20512-20524
10. Barghorn, S., and Mandelkow, E. (2002) Toward a unified scheme for the aggregation of tau into Alzheimer paired helical filaments. *Biochemistry* **41**, 14885-14896
11. Cowan, C. M., Quraisha, S., and Mudher, A. (2012) What is the pathological significance of tau oligomers? *Biochem. Soc. Trans.* **40**, 693-697
12. Patterson, K. R., Remmers, C., Fu, Y., Brooker, S., Kanaan, N. M., Vana, L., Ward, S., Reyes, J. F., Philibert, K., Glucksman, M. J., and Binder, L. I. (2011) Characterization of prefibrillar Tau oligomers in vitro and in Alzheimer disease. *J. Biol. Chem.* **286**, 23063-23076
13. Sahara, N., Maeda, S., Murayama, M., Suzuki, T., Dohmae, N., Yen, S. H., and Takashima, A. (2007) Assembly of two distinct dimers and higher-order oligomers from full-length tau. *Eur. J. Neurosci.* **25**, 3020-3029
14. Li, W., and Lee, V. M. (2006) Characterization of two VQIXXK motifs for tau fibrillization in vitro. *Biochemistry* **45**, 15692-15701
15. Mukrasch, M. D., Biernat, J., von Bergen, M., Griesinger, C., Mandelkow, E., and Zweckstetter, M. (2005) Sites of tau important for aggregation populate  $\beta$ -structure and bind to microtubules and polyanions. *J. Biol. Chem.* **280**, 24978-24986
16. Peterson, D. W., Zhou, H., Dahlquist, F. W., and Lew, J. (2008) A soluble oligomer of tau associated with fiber formation analyzed by NMR. *Biochemistry* **47**, 7393-7404
17. von Bergen, M., Barghorn, S., Li, L., Marx, A., Biernat, J., Mandelkow, E. M., and Mandelkow, E. (2001) Mutations of tau protein in frontotemporal dementia promote aggregation of paired helical filaments by enhancing local  $\beta$ -structure. *J. Biol. Chem.* **276**, 48165-48174
18. von Bergen, M., Friedhoff, P., Biernat, J., Heberle, J., Mandelkow, E. M., and Mandelkow, E. (2000) Assembly of tau protein into Alzheimer paired helical filaments depends on a local sequence motif ((306)VQIVYK(311)) forming  $\beta$  structure. *Proc. Natl. Acad. Sci. U. S. A.* **97**, 5129-5134
19. Berriman, J., Serpell, L. C., Oberg, K. A., Fink, A. L., Goedert, M., and Crowther, R. A. (2003) Tau filaments from human brain and from in vitro assembly of recombinant protein show cross- $\beta$  structure. *Proc. Natl. Acad. Sci. U. S. A.* **100**, 9034-9038

*Alternative conformations of the tau repeat domain*

20. Daebel, V., Chinnathambi, S., Biernat, J., Schwalbe, M., Habenstein, B., Loquet, A., Akoury, E., Tepper, K., Müller, H., Baldus, M., Griesinger, C., Zweckstetter, M., Mandelkow, E., Vijayan, V., and Lange, A. (2012)  $\beta$ -Sheet core of tau paired helical filaments revealed by solid-state NMR. *J. Am. Chem. Soc.* **134**, 13982-13989
21. Jakes, R., Novak, M., Davison, M., and Wischik, C. M. (1991) Identification of 3- and 4-repeat tau isoforms within the PHF in Alzheimer's disease. *EMBO J.* **10**, 2725-2729
22. Li, L., von Bergen, M., Mandelkow, E. M., and Mandelkow, E. (2002) Structure, stability, and aggregation of paired helical filaments from tau protein and FTDP-17 mutants probed by tryptophan scanning mutagenesis. *J. Biol. Chem.* **277**, 41390-41400
23. von Bergen, M., Barghorn, S., Müller, S. A., Pickhardt, M., Biernat, J., Mandelkow, E. M., Davies, P., Aebi, U., and Mandelkow, E. (2006) The core of tau-paired helical filaments studied by scanning transmission electron microscopy and limited proteolysis. *Biochemistry* **45**, 6446-6457
24. Bibow, S., Mukrasch, M. D., Chinnathambi, S., Biernat, J., Griesinger, C., Mandelkow, E., and Zweckstetter, M. (2011) The dynamic structure of filamentous tau. *Angew. Chem. Int. Ed.* **50**, 11520-11524
25. Akoury, E., Pickhardt, M., Gajda, M., Biernat, J., Mandelkow, E., and Zweckstetter, M. (2013) Mechanistic basis of phenothiazine-driven inhibition of Tau aggregation. *Angew. Chem. Int. Ed.* **52**, 3511-3515
26. Mirecka, E. A., Shaykhalishahi, H., Gauhar, A., Akgül, S., Lecher, J., Willbold, D., Stoldt, M., and Hoyer, W. (2014) Sequestration of a  $\beta$ -hairpin for control of  $\alpha$ -synuclein aggregation. *Angew. Chem. Int. Ed.*, DOI: 10.1002/anie.201309001
27. Grönwall, C., Jonsson, A., Lindstrom, S., Gunneriusson, E., Ståhl, S., and Herne, N. (2007) Selection and characterization of Affibody ligands binding to Alzheimer amyloid  $\beta$  peptides. *J. Biotechnol.* **128**, 162-183
28. Hoyer, W., Grönwall, C., Jonsson, A., Ståhl, S., and Härd, T. (2008) Stabilization of a  $\beta$ -hairpin in monomeric Alzheimer's amyloid- $\beta$  peptide inhibits amyloid formation. *Proc. Natl. Acad. Sci. U. S. A.* **105**, 5099-5104
29. Cerf, E., Sarroukh, R., Tamamizu-Kato, S., Breydo, L., Derclaye, S., Dufrene, Y. F., Narayanaswami, V., Goormaghtigh, E., Ruyschaert, J. M., and Raussens, V. (2009) Antiparallel  $\beta$ -sheet: a signature structure of the oligomeric amyloid  $\beta$ -peptide. *Biochem. J.* **421**, 415-423
30. Rosenman, D. J., Connors, C. R., Chen, W., Wang, C., and Garcia, A. E. (2013) A $\beta$  monomers transiently sample oligomer and fibril-like configurations: ensemble characterization using a combined MD/NMR approach. *J. Mol. Biol.* **425**, 3338-3359
31. Sandberg, A., Luheshi, L. M., Sollvander, S., Pereira de Barros, T., Macao, B., Knowles, T. P., Biverstal, H., Lendel, C., Ekholm-Petterson, F., Dubnovitsky, A., Lannfelt, L., Dobson, C. M., and Härd, T. (2010) Stabilization of neurotoxic Alzheimer amyloid- $\beta$  oligomers by protein engineering. *Proc. Natl. Acad. Sci. U. S. A.* **107**, 15595-15600
32. Scheidt, H. A., Morgado, I., and Huster, D. (2012) Solid-state NMR reveals a close structural relationship between amyloid- $\beta$  protofibrils and oligomers. *J. Biol. Chem.* **287**, 22822-22826
33. Hemsley, A., Arnheim, N., Toney, M. D., Cortopassi, G., and Galas, D. J. (1989) A simple method for site-directed mutagenesis using the polymerase chain reaction. *Nucleic Acids Res.* **17**, 6545-6551
34. Macao, B., Hoyer, W., Sandberg, A., Brorsson, A. C., Dobson, C. M., and Härd, T. (2008) Recombinant amyloid beta-peptide production by coexpression with an affibody ligand. *BMC Biotechnol.* **8**, 82
35. Delaglio, F., Grzesiek, S., Vuister, G. W., Zhu, G., Pfeifer, J., and Bax, A. (1995) NMRPipe: a multidimensional spectral processing system based on UNIX pipes. *J. Biomol. NMR* **6**, 277-293

*Alternative conformations of the tau repeat domain*

36. Vranken, W. F., Boucher, W., Stevens, T. J., Fogh, R. H., Pajon, A., Llinas, M., Ulrich, E. L., Markley, J. L., Ionides, J., and Laue, E. D. (2005) The CCPN data model for NMR spectroscopy: development of a software pipeline. *Proteins* **59**, 687-696
37. Solyom, Z., Schwarten, M., Geist, L., Konrat, R., Willbold, D., and Brutscher, B. (2013) BEST-TROSY experiments for time-efficient sequential resonance assignment of large disordered proteins. *J. Biomol. NMR* **55**, 311-321
38. Fischer, D., Mukrasch, M. D., Biernat, J., Bibow, S., Blackledge, M., Griesinger, C., Mandelkow, E., and Zweckstetter, M. (2009) Conformational changes specific for pseudophosphorylation at serine 262 selectively impair binding of tau to microtubules. *Biochemistry* **48**, 10047-10055
39. Schweers, O., Mandelkow, E. M., Biernat, J., and Mandelkow, E. (1995) Oxidation of cysteine-322 in the repeat domain of microtubule-associated protein tau controls the in vitro assembly of paired helical filaments. *Proc. Natl. Acad. Sci. U. S. A.* **92**, 8463-8467
40. Friedhoff, P., Schneider, A., Mandelkow, E. M., and Mandelkow, E. (1998) Rapid assembly of Alzheimer-like paired helical filaments from microtubule-associated protein tau monitored by fluorescence in solution. *Biochemistry* **37**, 10223-10230
41. Andronesi, O. C., von Bergen, M., Biernat, J., Seidel, K., Griesinger, C., Mandelkow, E., and Baldus, M. (2008) Characterization of Alzheimer's-like paired helical filaments from the core domain of tau protein using solid-state NMR spectroscopy. *J. Am. Chem. Soc.* **130**, 5922-5928
42. Margittai, M., and Langen, R. (2006) Side chain-dependent stacking modulates tau filament structure. *J. Biol. Chem.* **281**, 37820-37827
43. Siddiqua, A., and Margittai, M. (2010) Three- and four-repeat Tau coassemble into heterogeneous filaments: an implication for Alzheimer disease. *J. Biol. Chem.* **285**, 37920-37926
44. Walker, S., Ullman, O., and Stultz, C. M. (2012) Using intramolecular disulfide bonds in tau protein to deduce structural features of aggregation-resistant conformations. *J. Biol. Chem.* **287**, 9591-9600
45. Chirita, C. N., Congdon, E. E., Yin, H., and Kuret, J. (2005) Triggers of full-length tau aggregation: a role for partially folded intermediates. *Biochemistry* **44**, 5862-5872
46. Sawaya, M. R., Sambashivan, S., Nelson, R., Ivanova, M. I., Sievers, S. A., Apostol, M. I., Thompson, M. J., Balbirnie, M., Wiltzius, J. J., McFarlane, H. T., Madsen, A. O., Riek, C., and Eisenberg, D. (2007) Atomic structures of amyloid cross- $\beta$  spines reveal varied steric zippers. *Nature* **447**, 453-457
47. Dinkel, P. D., Siddiqua, A., Huynh, H., Shah, M., and Margittai, M. (2011) Variations in filament conformation dictate seeding barrier between three- and four-repeat tau. *Biochemistry* **50**, 4330-4336
48. Siddiqua, A., Luo, Y., Meyer, V., Swanson, M. A., Yu, X., Wei, G., Zheng, J., Eaton, G. R., Ma, B., Nussinov, R., Eaton, S. S., and Margittai, M. (2012) Conformational basis for asymmetric seeding barrier in filaments of three- and four-repeat tau. *J. Am. Chem. Soc.* **134**, 10271-10278
49. Friedhoff, P., von Bergen, M., Mandelkow, E. M., Davies, P., and Mandelkow, E. (1998) A nucleated assembly mechanism of Alzheimer paired helical filaments. *Proc. Natl. Acad. Sci. U. S. A.* **95**, 15712-15717
50. Ramachandran, G., and Udgaonkar, J. B. (2011) Understanding the kinetic roles of the inducer heparin and of rod-like protofibrils during amyloid fibril formation by Tau protein. *J. Biol. Chem.* **286**, 38948-38959

*Acknowledgments* We thank Susanne Aileen Funke for the kind gift of the full-length tau containing vector and Carina Stein for excellent work in the laboratory. This work was supported by the Ministerium für Innovation, Wissenschaft und Forschung des Landes Nordrhein-Westfalen.

**FOOTNOTES**

<sup>1</sup>Institute of Physical Biology, Heinrich-Heine-Universität, 40204 Düsseldorf, Germany

<sup>2</sup>Institute of Structural Biochemistry (ICS-6), Research Centre Jülich, 52425 Jülich, Germany

<sup>3</sup>CAESAR Research Center, 53175 Bonn, Germany

<sup>4</sup>German Center for Neurodegenerative Diseases (DZNE), 53175 Bonn, Germany

<sup>5</sup>Present address: Max-Delbrück-Centrum für Molekulare Medizin, Robert-Rössle-Strasse 10, 13125 Berlin, Germany

<sup>6</sup>The abbreviations used are: aa, amino acid; A $\beta$ , amyloid- $\beta$  peptide; CD, circular dichroism; ITC, isothermal titration calorimetry; K18 $\Delta$ K280, four-repeat-domain tau (residues 244-368) with deletion of Lys-280; K18AA, as construct K18 $\Delta$ K280 with additional C291A and C322A exchanges; PHF, paired helical filament; SEC, size exclusion chromatography; ThT, Thioflavin T.

**FIGURE LEGENDS**

**FIGURE 1.** Library design and selected  $\beta$ -wrapin TP4. (a) Ribbon schematic of the  $ZA\beta_3$  scaffold (grey) in complex with  $A\beta(1-40)$  (red) (pdb entry 2OTK). The side-chains of  $ZA\beta_3$  residues that were randomized in the library are shown as light blue (exchanged to all 20 amino acids) or dark blue (exchanged to hydrophobic residues only) spheres. The disulfide bond connecting the two subunits  $ZA\beta_3$  and  $ZA\beta_3'$  is depicted in yellow. The secondary structure elements of  $ZA\beta_3$  are labeled as in ref. (28). (b) Amino acid sequence of the selected  $\beta$ -wrapin TP4 aligned to  $ZA\beta_3$ . The positions of helical and  $\beta$ -sheet secondary structure in  $A\beta$ -bound  $ZA\beta_3$  are indicated by cylinders and an arrow, respectively. Randomized and exchanged amino acids are printed in bold with the same color coding as in (a).

**FIGURE 2.** Tau isoform and tau constructs used in this study. The domain organization of the tau isoform htau40 and of the construct K18 is displayed. Deletions and mutations in the constructs K18 $\Delta$ K280, K18AA, and in the K18AA proline mutants are indicated in red. htau40 is the longest human tau isoform. htau40 and K18 contain four imperfect repeats designated R1 to R4. The positions of the hexapeptide motifs PHF6, PHF6\*, and PHF6\*\* are highlighted in yellow.

**FIGURE 3.** Affinity of TP4 for htau40 determined by ITC. Titration of 680  $\mu$ M TP4 into 68  $\mu$ M htau40 monitored by ITC at 10°C, yielding an affinity of  $K_d = 580 \pm 20$  nM.

**FIGURE 4.** Partial folding and thermostability of the K18AA:TP4 complex analyzed by far-UV CD spectroscopy. (a) Spectra of free TP4 and  $ZA\beta_3$ . (b) Spectra of free TP4, free K18AA, K18AA:TP4 complex, and the signal gained upon binding, i.e., the calculated difference between the complex spectrum and the sum of the spectra of the free components. (c) Thermal melting of the K18AA:TP4 complex compared to the sum of free components, monitored at 201 nm and 221 nm. The concentration of all proteins was 10  $\mu$ M.

**FIGURE 5.** NMR of the K18AA:TP4 interaction. ( $^1\text{H}$ - $^{15}\text{N}$ )-HSQC spectra of [ $U$ - $^{15}\text{N}$ ]-K18AA recorded at 5°C in the absence (red) and presence (blue) of an excess of [ $NA$ ]-TP4.

**FIGURE 6.** Identification of two alternative binding sites by NMR. Changes in the peak height in the ( $^1\text{H}$ - $^{15}\text{N}$ )-HSQC NMR spectrum of [ $U$ - $^{15}\text{N}$ ]-labeled K18AA and its proline mutants I277P, I308P, V339P, and I277P V339P, upon addition of [ $NA$ ]-TP4, recorded at 5°C. (a) Titration of K18AA with TP4. The repeat domain organization is shown on top of the diagram. The positions of the hexapeptide motifs PHF6\*, PHF6, and PHF6\*\* are indicated by striped boxes. Previously detected stretches of residual  $\beta$ -structure in the free K18 monomer (15), containing the hexapeptide motifs, are highlighted in yellow. (b)-(d) Comparison of the TP4 complexes of K18AA and the K18AA proline mutants. The complexes were prepared from equimolar amounts of TP4 and the respective tau construct.

**FIGURE 7.** Inhibition of tau K18AA aggregation. (a) ThT time course of the aggregation of 50  $\mu$ M K18AA at 25°C in the absence (upper panel) and presence (lower panel) of 10  $\mu$ M of the aggregation promoter heparin. K18AA aggregation in the absence of TP4 (black) was compared with aggregation in the presence of TP4 at stoichiometric (blue) and substoichiometric (magenta) concentration (duplicate experiments). (b,c) TEM of K18AA samples incubated in the absence of heparin for 52 h, either without (b) or with (c) addition of TP4 at stoichiometric concentration.

**FIGURE 8.** Binding sites and hypothetical conformations of TP4-bound tau K18. (a) Two alternative TP4-binding sites in K18. The repeat domain organization is shown in the top line with each repeat labeled in a different color. The positions of the hexapeptide motifs PHF6, PHF6\*, and PHF6\*\* are indicated by numbered boxes. Previously detected stretches of residual  $\beta$ -structure in the free K18 monomer (15), comprising the hexapeptide motifs, are highlighted in yellow. Binding site 1 corresponds to tau(268-317), binding site 2 to tau(300-368). (b) Schematic of two hypothetical conformations of TP4-

*Alternative conformations of the tau repeat domain*

bound tau K18AA, corresponding to the two identified binding sites. The models were constructed assuming the presence of intramolecular tertiary contacts between the hexapeptide motifs, which thus were aligned. The positions of the cysteines in K18, Cys-291 and Cys-322, are indicated by black circles. (c) Comparison of the  $\beta$ -hairpin conformation of TP4-bound tau suggested in this study with the conformation of tau within filaments. Each tau molecule contributes a few  $\beta$ -strands to the fibril core, which assemble into parallel, in-register, intermolecular  $\beta$ -sheets. Backbone hydrogen bonding is indicated by blue dashed lines.

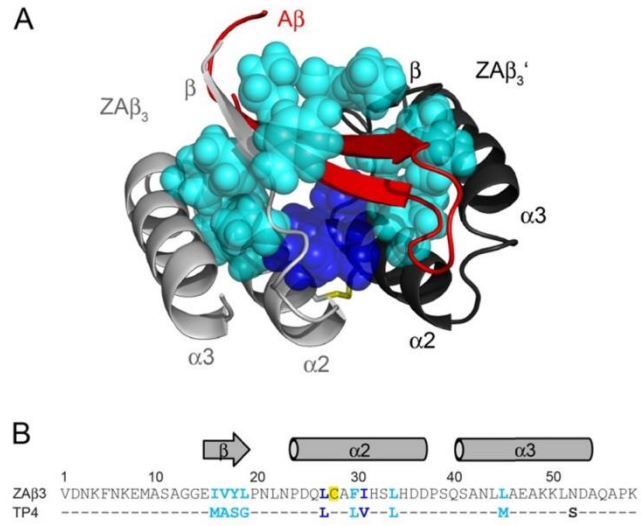
*Alternative conformations of the tau repeat domain*

**Table 1. ITC of K18AA variants.** ITC was performed at 10°C. The given parameters result from a nonlinear least-squares fit to a 1:1 binding model. K18 variants were used at a concentration of ~70  $\mu\text{M}$  as titrant in the cell and TP4 at approximately 10-fold higher concentration as titrant in the syringe, except for K18AA I277P V339P, which was used at a concentration of ~560  $\mu\text{M}$  as titrant in the syringe and titrated into 31  $\mu\text{M}$  TP4. n.d., no binding detectable.

Variant	$K_d$ ( $\mu\text{M}$ )	$n$	$\Delta H$ ( $\text{kcal mol}^{-1}$ )
K18AA	$0.26 \pm 0.03$	$1.00 \pm 0.01$	$-36.7 \pm 0.3$
K18AA I308P	n.d.		
K18AA I277P	$0.74 \pm 0.07$	$1.20 \pm 0.01$	$-27.3 \pm 0.2$
K18AA V339P	$0.50 \pm 0.05$	$0.95 \pm 0.01$	$-25.0 \pm 0.2$
K18AA I277P V339P	$9.6 \pm 1.1$	$1.26 \pm 0.04$	$-4.7 \pm 0.2$
K18 $\Delta$ K280 oxidized	$11.0 \pm 0.6$	$1.15 \pm 0.01$	$-25.1 \pm 0.3$

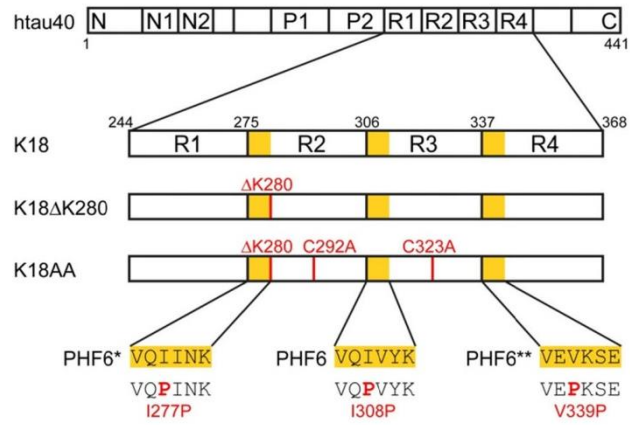
*Alternative conformations of the tau repeat domain*

FIGURE 1



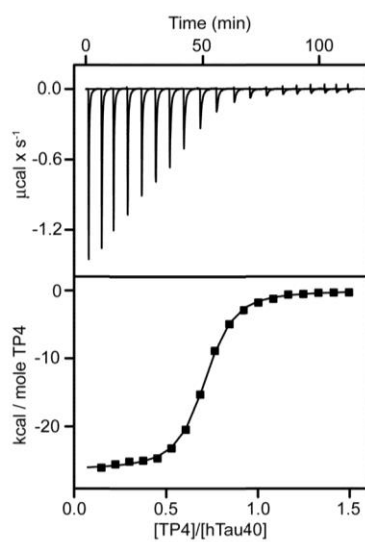
*Alternative conformations of the tau repeat domain*

FIGURE 2



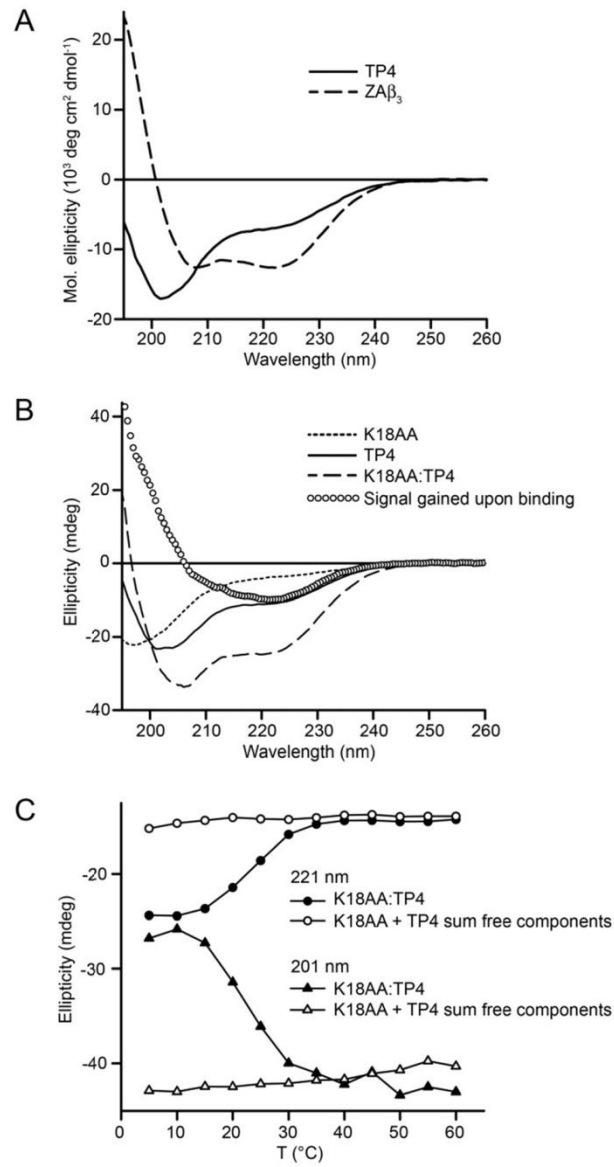
*Alternative conformations of the tau repeat domain*

FIGURE 3



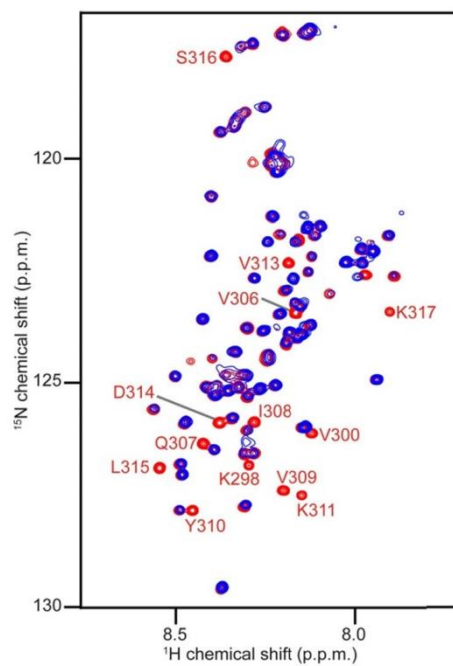
*Alternative conformations of the tau repeat domain*

FIGURE 4



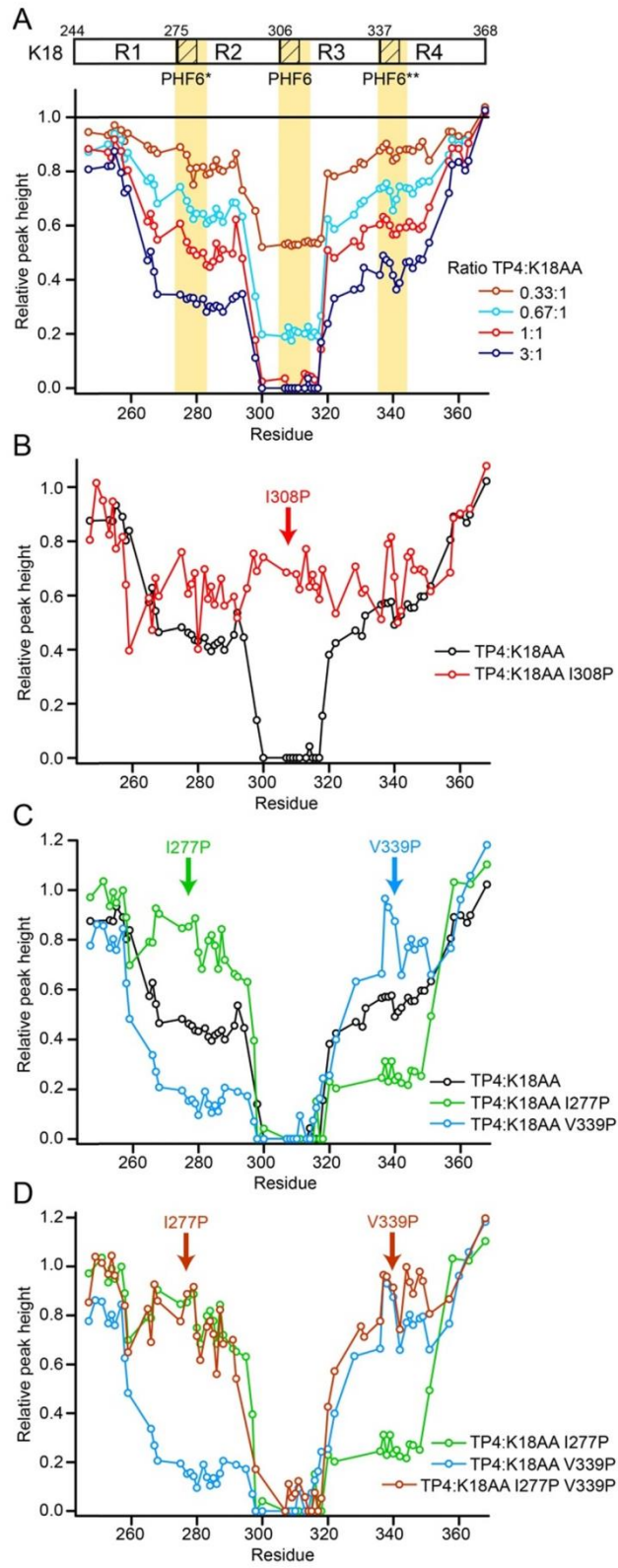
*Alternative conformations of the tau repeat domain*

FIGURE 5



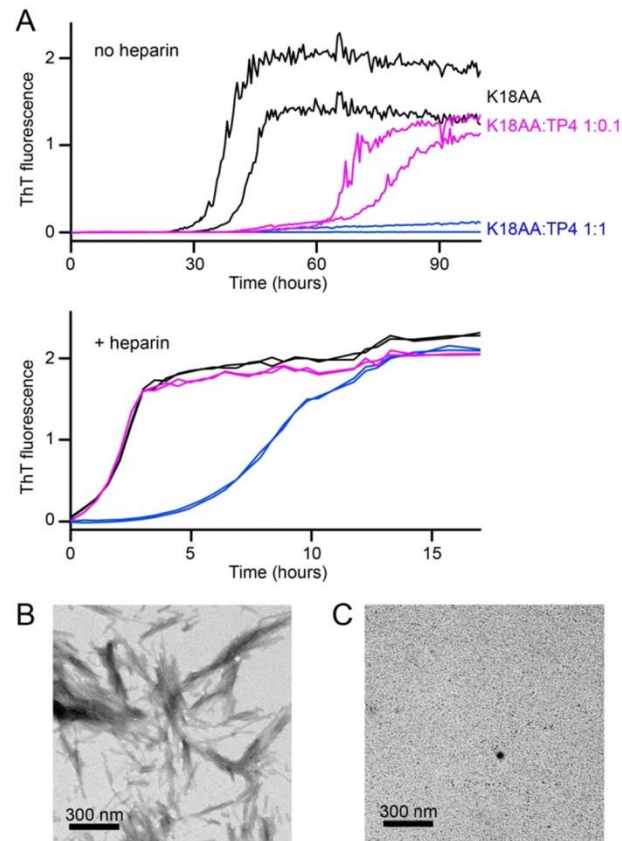
*Alternative conformations of the tau repeat domain*

FIGURE 6



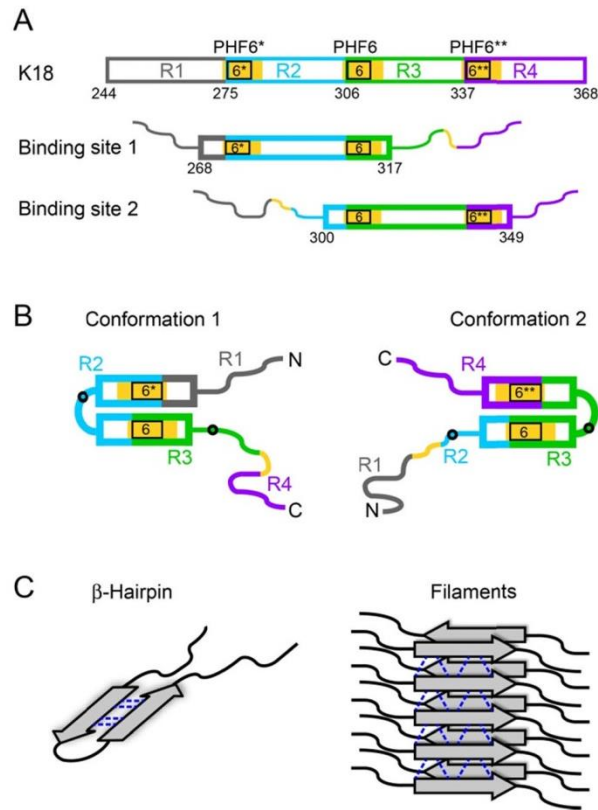
*Alternative conformations of the tau repeat domain*

FIGURE 7



*Alternative conformations of the tau repeat domain*

FIGURE 8



---

## DISCUSSION

### 2.1 Two Proteins Involved in Alzheimer Disease

AD is a fatal neurological disorder with increasing case numbers worldwide due to an aging population, since age is the risk factor number one to develop AD (190). Symptoms of AD are memory loss, movement disabilities and cognitive dysfunction, which finally lead to death (1). The AD brain is characterized by neuronal loss along with protein aggregates, senile plaques and neurofibrillary tangles, built up of two major proteins, namely the A $\beta$  peptide, a cleavage product of the APP, and the microtubule-binding protein tau, respectively. The identification of patients suffering from AD symptoms without observable plaques and tangles in the brain and patients with a severe plaque and tangle load without AD symptoms questioned the neurotoxic relevance of these deposits (91,92). The finding that the load of AD brain with oligomeric species correlates strongly with the severity of cognitive dysfunction led to the hypothesis that aggregation intermediates act as the neurotoxic agent (94-98). So far, small protein assemblies of different sizes have been isolated, starting with dimers (57,99) up to higher molecular weight oligomers (12,101). These intermediates were shown to have cytotoxic potential (98,102,104,136) and injection into the brains of rodent models resulted in AD pathogenesis (104,105,146,149,150) indicating a role in the development of AD. How exactly oligomers mediate their toxic function is rather speculative. Oligomers per se might be neurotoxic by forming a membrane-pore leading to cell leakage (4,6,140) or their neurotoxicity is mediated through a receptor such as cellular PrP (137) or acetylcholine receptors (141,142) initiating an intracellular signaling cascade. What has become clear is that tau plays a central role in A $\beta$ -mediated toxicity. Tau aggregates are found alone in tauopathies but also accompany A $\beta$  aggregates or  $\alpha$ -synuclein aggregates in AD and  $\alpha$ -synucleinopathies, respectively. Furthermore, mice deficient of tau cannot develop AD (131). It is still uncertain which protein induces and which protein mediates toxicity, but it is hypothesized that A $\beta$  induces tau aggregation and tau executes neurotoxicity (191). For drug development it is essentially important to understand the toxic mechanism behind AD pathology. This includes a precise characterization of the two

---

involved proteins and their individual aggregation pathways including the aggregation intermediates.

## 2.2 Characterization of Amyloid- $\beta$ Aggregation Intermediates

Two chapters of this thesis, chapter 1 and chapter 2, deal with aggregation intermediates of A $\beta$ . Chapter 1 focuses on determining the dissociation constant of monomers dissociating from the protofibril, an oligomeric A $\beta$  species. The assay was based on an engineered binding protein, ZA $\beta$ <sub>3</sub>W, that specifically binds to A $\beta$  monomers (108) and thus hinders monomers from reassociating with the protofibril and from incorporation into mature amyloid fibrils. Upon binding of A $\beta$ , ZA $\beta$ <sub>3</sub>W folds simultaneously into a more compact structure bringing a water-exposed tryptophan into a hydrophobic environment (cp. chapter 1). This rearrangement of tryptophan 18 enables differentiation of the A $\beta$ -free and A $\beta$ -bound form of ZA $\beta$ <sub>3</sub>W by the fluorescence emission maximum and permits to follow the dissociation of protofibrils into monomers. The protofibrils employed in the assay were obtained by size exclusion chromatography (SEC) and were of different size and morphology (spherical and linear) as observed by transmission electron microscopy (EM). The dissociation of the A $\beta$  protofibrils followed exponential decay kinetics in our experiments, which principally could have two possible explanations: 1) An exponential size distribution in the protofibril sample would yield a decay that resembles an exponential function (192), or 2) the dissociation of subunits from the protofibril is not limited to the protofibril's end, but dissociation occurs at all possible positions of the protofibril's surface. The first explanation can be excluded as an exponential size distribution is not given in our sample because of SEC preparation and, importantly, analytical ultracentrifugation (AUC) analysis of the protofibril fraction showed a distinct distribution of species with a maximum at 7.6 S. Thus, the observed exponential decay can only be explained by the dissociation of subunits at all possible positions of the protofibril's surface. A subunit released from the protofibril could be a monomer or a smaller oligomeric species that subsequently decomposes into monomers. The latter alternative is more conceivable as monomers within the protofibril are integrated into a strong network of non-covalent bonds with other neighboring monomers.

But the exact mechanism of the protofibril dissolution, e.g. whether it is a one step or a multi-step process, as well as the precise nature of the rate-limiting step, cannot be retrieved from these data as they are limited to the occurrence of monomeric A $\beta$ .

The time course of protofibril dissociation could be fit to a monoexponential function conveying a single  $k_{off}$  value for the protofibril sample and assuming the same kinetic stability for all protofibrils in the sample. To test whether the monoexponential fit is the best fit to the obtained data, an alternative global triexponential fit was performed assuming different protofibrillar structures with different kinetic stabilities that occur in different proportionalities in the samples. This global fit performed as well as the individual monoexponential decay fits. Thus, variations between the different protofibril batches might result from differences in the composition of protofibrillar species. As environmental conditions are critical for the stability of aggregates (29), an effect of the solution conditions on the energy barrier of the dissociation cannot be excluded as well.

Neither the monoexponential nor the triexponential fits covered a fast monomer dissociation phase occurring between the elution of protofibrils from SEC and ZA $\beta_3$ W addition. This fast dissociation might result from the fast dissociation of loosely attached monomers ("dock"-phase, cp.1.3.2).

Interestingly, protofibrils built of the less aggregation-prone A $\beta$ 1-40 variant showed a comparable macroscopic dissociation constant as A $\beta$ 1-42. This is surprising in so far as A $\beta$ 1-40 requires higher concentration and longer incubation time for fibrillization (193,194). A comparable  $k_{off}$  value indicates that the energy barrier to be overcome between the protofibrillar and monomeric state is equal for A $\beta$ 1-42 and A $\beta$ 1-40 and implies that intermolecular interactions in the protofibril are similar for A $\beta$ 1-42 and A $\beta$ 1-40 protofibrils, which is a prerequisite for the formation of mixed assemblies (195). Two models are proposed to explain the comparable energy barrier between monomeric and protofibrillar species (Fig. 8). Model one supposes a higher energy for the A $\beta$ 1-42 peptide than A $\beta$ 1-40 as a monomer but the same energetic minimum for both variants in the protofibril, model two presumes the same energy level for the monomer but a lower energetic minimum for A $\beta$ 1-42 inside the protofibril than for A $\beta$ 1-40.

The  $k_{off}$  values and the high activation energy of the protofibrillar dissociation process characterize the protofibril as a rather stable aggregation intermediate. Nonetheless, the mature amyloid fibril demonstrated an even higher stability towards dissociation in our assay supporting a rather inert character of the mature amyloid fibril (185,196).

In summary, chapter 1 demonstrates that protofibrils independent of the A $\beta$  variant have a similar energy barrier to dissociation. Furthermore, the data show that protofibril dissociation does not only occur from the ends of the protofibril. This finding should be taken into account when developing new concepts of the protofibrillar structure. The elucidation of a detailed protofibril structure would help to clarify the exact mechanism of protofibril formation and dissociation and thus help to understand the aggregation mechanism of the A $\beta$  peptides.

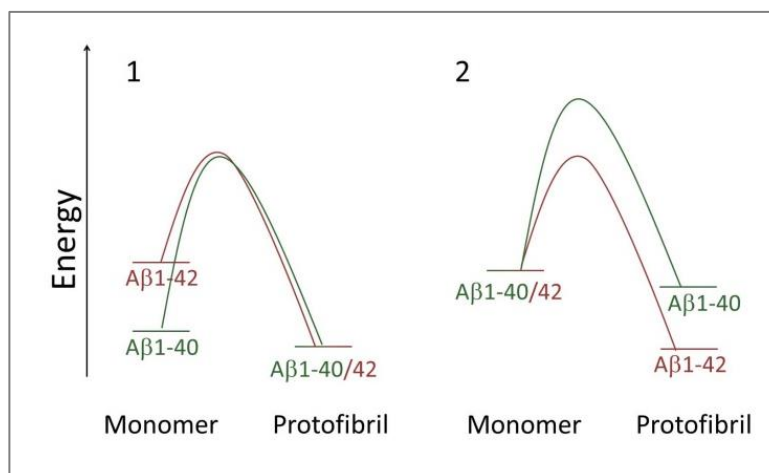


**Figure 8: The energy barrier between monomer and protofibril compared for A $\beta$ 1-40 and A $\beta$ 1-42.**  
**1**, A possible explanation for the similar energy barrier for monomers dissociating from the protofibril for the two A $\beta$  peptides is a difference in the energy of the monomeric species and/or **2**, a difference of energy in the protofibril.

Chapter 2 is dedicated to the characterization of a synthetic A $\beta$  dimer in order to understand aggregational properties of the A $\beta$  peptide. As dimeric A $\beta$  species have been isolated and correlated to neuronal death and shown to induce synaptic toxicity (105,197), their characterization is critical for the neurotoxic processes of AD. Therefore, chapter 2 focuses on the attempt to obtain structural information of an A $\beta$  dimer and to identify first interaction points between A $\beta$  molecules. Interestingly, the A $\beta$ 1-40 aggregation was

influenced by the presence of the synthetic A $\beta$ 1-40 dimer. A low increase of ThT signal might indicate that the A $\beta$ 1-40 dimer stabilizes oligomeric species and thus prolongs fibril formation. To understand the importance of assemblies of different sizes and their influence on AD progression, it is important to study this feature of the A $\beta$ 1-40 dimer in depth.

### 2.2.1 Outlook

The characterization of the synthetic A $\beta$  dimer will be driven forward by NMR experiments to elucidate structural properties of the dimer. This will be done by the introduction of point mutations on primary sequence level to differentiate the two A $\beta$  subunits of the dimer, assignment of the NMR signals of the relevant atoms, and identification of the interactions between the two subunits. Furthermore, the two phases of the co-aggregation of A $\beta$ 1-40 and A $\beta$ 1-40 dimer will be analyzed by SEC and EM to clarify the different intensity of the ThT signal and the inhibitory mechanism exercised by the A $\beta$ 1-40 dimer. It is thinkable that protofibrils or other oligomeric species occur in the first phase showing a low ThT signal. These can be detected and purified by SEC. Subsequent analysis of the protofibril peak by SDS gel electrophoresis will yield the composition of the protofibril, e.g. A $\beta$ 1-40 alone or A $\beta$ 1-40 dimer alone or both. The effect of the A $\beta$ 1-40 dimer can also be analyzed by the protofibril dissociation assay presented in chapter 1. It would also be interesting to test the kinetic stability of mixed A $\beta$ 1-40 and A $\beta$ 1-42 protofibrils, which might be relevant in AD, by this assay.

## 2.3 A Novel Binding Protein to tau

Chapter 3 is dedicated to the second amyloidogenic protein involved in Alzheimer disease and many other neurodegenerative diseases, the microtubule binding protein tau. In these disorders, tau aggregates into filaments of different macroscopic appearance, e.g. straight or paired helical filaments. The filaments are characterized by an outer flexible coat (34) formed by the non-structured N- and C-terminal parts of the protein. The rigid core of the fibril is formed by four imperfect repeat domains (R1, R2, R3, R4) also involved in microtubule binding (19). Two amino acid motifs, PHF6 and PHF6\* in the MTBR have been

shown to initiate filament formation (24,25). The isolated MTBR aggregates into filaments *in vitro* and aggregation can be enhanced by a point mutation, deletion of Lys-280, identified in familiar forms of tauopathies (7). For selection of an engineered binding protein a construct containing the four repeat domains and the deletion of Lys-280 (K18ΔK280) was employed as a target to increase the possibility of detecting disease-relevant structures of tau in complex with the engineered binding protein. Based on a  $\beta$ -wrapin scaffold library derived from ZA $\beta_3$ , a homodimer sequestering the A $\beta$  peptide (108,109), several rounds of phage display were performed to select a binding protein to tau. A binder, called TP4, with nanomolar affinity to the employed construct as well as to full-length tau was identified. The first selection round was carried out at 4°C (while the subsequent rounds were performed at room temperature), which might explain the selection of a TP4:tau complex with low thermostability. The structural determination of the complex via NMR at low temperatures was hindered by missing resonances of TP4-bound tau. NMR at higher temperatures, as successfully performed for  $\alpha$ -synuclein in complex with a  $\beta$ -wrapin protein (198), was not possible because of the aforementioned low thermostability of the complex. Due to a high ratio of unstructured protein parts, structural elucidation of the complex by crystallization and X-ray analysis is unlikely as well.

NMR titration experiments indicate that TP4 binds two conformations of tau, involving different regions of the MTBR, with approximately the same frequency. Interestingly, both conformations sequester the PHF6 motif, strengthening the importance of this motif in the aggregation of tau, in particular considering the inhibitory effect of TP4 on tau aggregation. In one of the tau conformations in complex with TP4, TP4 binds to the region 268 to 317 including the C-terminal part of R1, R2 with the PHF6\* motif and the N-terminal part of R3 with the PHF6 motif. We hypothesize that in this conformation PHF6 and PHF6\* interact with each other. The second conformation incorporates the C-terminal part of R2, R3 with the PHF6 motif and the N-terminal part of R4, which also contains a region of high sequence similarity to PHF6 and PHF6\* and a high tendency to form  $\beta$ -structure (23) denoted as PHF6\*\* in chapter 3. We hypothesize that in this conformation PHF6 and PHF6\*\* interact. An interaction of these motifs in aggregation intermediate species was supposed by Peterson *et al.* (117) and would be in line with findings that tau oligomerization includes a compaction of the repeat domain (54,55). A  $\beta$ -hairpin fold of the tau conformations in

complex with TP4 can only be deduced from the following indicators: 1) The repeat domain of tau includes motifs (PHF6, PHF6\* and PHF6\*\*) which have a propensity to form  $\beta$ -strands (23), and an increase of  $\beta$ -sheet structure during oligomerization has been reported for tau (61,199); 2) the introduction of proline mutations disturbing any secondary structure formation hinders binding of TP4 to the affected region; 3) previously determined structures of amyloidogenic proteins bound to  $\beta$ -wrapins revealed  $\beta$ -hairpin folds of the bound proteins (108,198).

The  $\beta$ -strands of tau suggested to be established in complex with TP4 are similar to those that have been identified for the tau fibril core (37,200), although the  $\beta$ -strands in the fibril are arranged in a parallel in register manner. In tau oligomers an increase of  $\beta$ -sheet structure has also been detected (61) and thus, the TP4-trapped conformation of tau might also reflect a conformation of tau within oligomers. Moreover, our proposed tau conformations are in line with the suggested interaction of PHF motifs in tau oligomers (117). For A $\beta$  incorporated into oligomers, a  $\beta$ -hairpin fold has been suggested as well (108,110) and the finding that neurotoxic tau oligomers can be produced by seeding with A $\beta$  oligomers indicates a certain structural similarity of these aggregation intermediates (61). As proposed for A $\beta$  (108,110), fibril formation might then require a structural rearrangement on the pathway from tau oligomers to fibrils.

The proposed conformations of tau in complex with TP4 are not compatible with an intramolecular disulfide bridge formed by the cysteine residues 291 and 322, which is in line with studies indicating an inhibitory effect of oxidized tau (71,72,100), although intermolecular disulfide formation as observed in tau dimers (100) and fibrils (37) probably might not interfere with TP4 binding.

In line with our finding of alternative conformations of tau, Margittai & Langen (201) and Siddiqua & Margittai (51) found that PHF6\* and PHF6\*\* do not always contribute to the  $\beta$ -sheet structure of the fibril core. For PHF6\*, the deletion of lysine 280 increases the involvement of PHF6\* in the fibril core and its adaption of  $\beta$ -sheet structure (201). These findings might contribute to clarify the molecular basis for observed seeding barriers between 3R and 4R tau (52,202).

---

In summary, the engineered binding protein TP4 presented in chapter 3, has helped to reveal structural properties of the AD-relevant protein tau on the residue-level and demonstrates the structural flexibility of tau, which might be crucial for drug development.

### 2.3.1 Outlook

The usage of TP4 is limited by the low temperature stability of the formed complex. This hinders most likely the elucidation of a high-resolution NMR structure and its examination in cell culture or animal models of AD. A thermostable, nanomolar binder for tau is thus desirable. Therefore, a new phage display selection at elevated temperature should be performed. Additionally, phage display selection on two new tau constructs is planned. In these new constructs, the two alternative conformations of tau are separated from each other by deleting either R2 (PHF6\*) or R4 (PHF6\*\*) leading to the constructs K19 and R123, respectively.

As the conformations of tau found in complex with TP4 suggest an interaction of PHF6 motifs, it is tempting to speculate that this interaction is the aggregation-initiating step. Investigation of this hypothesis includes the analyses of different combinations of the PHF6 motifs and their potential to initiate aggregation.

## 2.4 Diverse Applications of Engineered Binding Proteins

Binding proteins, and in particular engineered binding proteins, have been used for a wide range of applications in the fields of therapy, diagnosis and imaging, biotechnology and biological research (Fig. 9). This thesis presents examples of how to employ engineered binding proteins as tools in biological research and biotechnology.

ZA $\beta$ <sub>3</sub>, an affibody sequestering the A $\beta$  peptide, was employed in several ways in this thesis. First, it was co-expressed with the A $\beta$  peptide facilitating expression and subsequent purification of A $\beta$  peptides based on the study of Macao *et al.* (42) (chapter 1-2). This method was also used for recombinant expression of designed A $\beta$  dimers (chapter 2). The successful expression of the A $\beta$ <sub>1-40</sub> dimer was based on the co-expression with ZA $\beta$ <sub>3</sub>,

demonstrating that co-expression can be a valuable strategy to obtain recombinant proteins, as also illustrated by other examples of protein co-expression yielding higher amounts of soluble proteins (203,204). Alternatively, solubility tags may be attached to the protein, which particularly in the case of small peptides requires a proteolysis step to remove the tag (64,205,206).

Furthermore, a mutated variant of  $\text{ZA}\beta_3$ ,  $\text{ZA}\beta_3\text{W}$ , was used as a fluorescent detector for monomeric  $\text{A}\beta$  in a study that analyzed the dissociation of  $\text{A}\beta$  protofibrils into monomers (chapter 1).  $\text{ZA}\beta_3\text{W}$  enabled us to study the dissociation process as an isolated reaction step and to retrieve kinetic information of a transient aggregation intermediate. The result indicates that the protofibril is a rather stable species and that its disaggregation is not necessarily limited to the ends. Thus, this assay in a way helped also to obtain structural information of the protofibril. The application of binding proteins for structural determination is well known, especially as a co-crystallization agent (207). The NMR structure of  $\text{A}\beta$  in complex with  $\text{ZA}\beta_3$  provided the first high-resolution structure of  $\text{A}\beta$  in solution (108). The finding that  $\text{A}\beta$  adopts a  $\beta$ -hairpin fold in complex with  $\text{ZA}\beta_3$  has contributed to the understanding of the aggregation mechanism and pointed to the relevance of this conformation for  $\text{A}\beta$  in aggregation intermediates. An  $\text{A}\beta$  disulfide-bridged construct derived from the  $\text{A}\beta$   $\beta$ -hairpin in complex with  $\text{ZA}\beta_3$  formed stable oligomers but no fibrils, demonstrating a connection between the  $\beta$ -hairpin fold observed in complex with  $\text{ZA}\beta_3$  and the oligomeric  $\text{A}\beta$  conformation (112).

The selection of an engineered binding protein to tau pursued a similar aim: With the help of a  $\beta$ -wrapin, structural properties of the tau protein, in particular of the aggregation-relevant domains, should be investigated. This was successful as the selected binder, TP4, bound to two different conformations of tau, demonstrating the structural flexibility of the tau repeat domain and underlining findings of structural diversity in the tau fibril (51,52,201,202).

In summary, in this thesis engineered binding proteins were exploited as useful tools to derive structural and mechanistic information on two proteins relevant for AD pathogenesis, demonstrating how affinity proteins can help to understand the aggregation pathway and its intermediates.

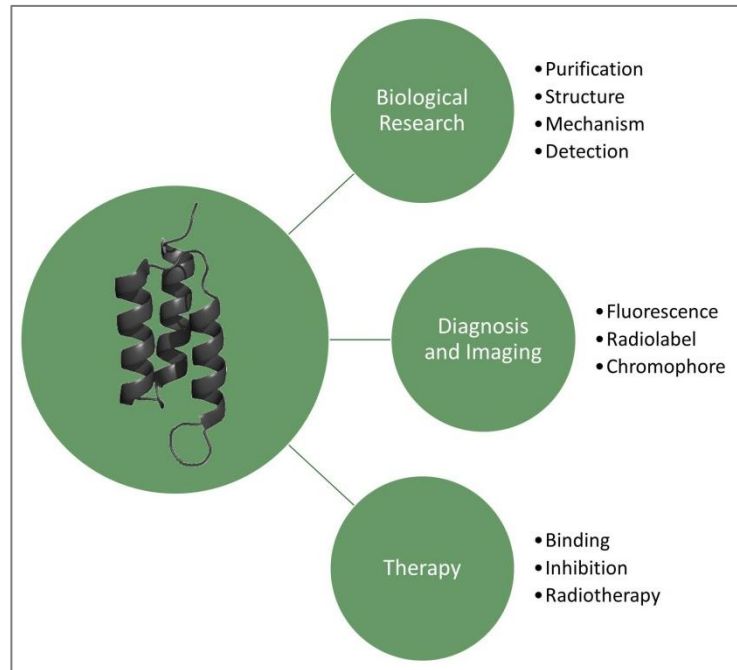


**Figure 9: Possibilities of employing engineered binding proteins.** In this thesis, engineered binding proteins were used for purification and as a tool to derive information on the conformations and aggregation mechanism of amyloidogenic proteins. Further applications can be found in the literature. Based on (165,178).

## REFERENCES

1. Soto, C. (2003) Unfolding the role of protein misfolding in neurodegenerative diseases. *Nature reviews. Neuroscience* **4**, 49-60
2. de Groot, N. S., Sabate, R., and Ventura, S. (2009) Amyloids in bacterial inclusion bodies. *Trends in biochemical sciences* **34**, 408-416
3. WHO. (2012) Dementia. World Health Organization
4. Glabe, C. G., and Kaye, R. (2006) Common structure and toxic function of amyloid oligomers implies a common mechanism of pathogenesis. *Neurology* **66**, S74-78
5. Skovronsky, D. M., Lee, V. M., and Trojanowski, J. Q. (2006) Neurodegenerative diseases: new concepts of pathogenesis and their therapeutic implications. *Annual review of pathology* **1**, 151-170
6. Gendreau, K. L., and Hall, G. F. (2013) Tangles, Toxicity, and Tau Secretion in AD - New Approaches to a Vexing Problem. *Frontiers in neurology* **4**, 160
7. von Bergen, M., Barghorn, S., Li, L., Marx, A., Biernat, J., Mandelkow, E. M., and Mandelkow, E. (2001) Mutations of tau protein in frontotemporal dementia promote aggregation of paired helical filaments by enhancing local beta-structure. *The Journal of biological chemistry* **276**, 48165-48174
8. McKeith, I. (2004) Dementia with Lewy bodies. *Dialogues in clinical neuroscience* **6**, 333-341
9. Ludolph, A. C., Kassubek, J., Landwehrmeyer, B. G., Mandelkow, E., Mandelkow, E. M., Burn, D. J., Caparros-Lefebvre, D., Frey, K. A., de Yébenes, J. G., Gasser, T., Heutink, P., Höglinger, G., Jamrozik, Z., Jellinger, K. A., Kazantsev, A., Kretzschmar, H., Lang, A. E., Litvan, I., Lucas, J. J., McGeer, P. L., Melquist, S., Oertel, W., Otto, M., Paviour, D., Reum, T., Saint-Raymond, A., Steele, J. C., Tolnay, M., Tumani, H., van Swieten, J. C., Vanier, M. T., Vonsattel, J. P., Wagner, S., Wszolek, Z. K., and Reinsberg Working Group for Tauopathies With, P. (2009) Tauopathies with parkinsonism: clinical spectrum, neuropathologic basis, biological markers, and treatment options. *European journal of neurology : the official journal of the European Federation of Neurological Societies* **16**, 297-309
10. Muñoz, D. G., Dickson, D. W., Bergeron, C., Mackenzie, I. R., Delacourte, A., and Zhukareva, V. (2003) The neuropathology and biochemistry of frontotemporal dementia. *Annals of neurology* **54 Suppl 5**, S24-28
11. Nalivaeva, N. N., and Turner, A. J. (2013) The amyloid precursor protein: a biochemical enigma in brain development, function and disease. *FEBS letters* **587**, 2046-2054
12. Haass, C., and Selkoe, D. J. (2007) Soluble protein oligomers in neurodegeneration: lessons from the Alzheimer's amyloid beta-peptide. *Nature reviews. Molecular cell biology* **8**, 101-112
13. De Strooper, B. (2010) Proteases and proteolysis in Alzheimer disease: a multifactorial view on the disease process. *Physiological reviews* **90**, 465-494
14. Morris, M., Maeda, S., Vossel, K., and Mucke, L. (2011) The many faces of tau. *Neuron* **70**, 410-426
15. Cáceres, A., and Kosik, K. S. (1990) Inhibition of neurite polarity by tau antisense oligonucleotides in primary cerebellar neurons. *Nature* **343**, 461-463
16. Biernat, J., Wu, Y. Z., Timm, T., Zheng-Fischhofer, Q., Mandelkow, E., Meijer, L., and Mandelkow, E. M. (2002) Protein kinase MARK/PAR-1 is required for neurite outgrowth and establishment of neuronal polarity. *Molecular biology of the cell* **13**, 4013-4028
17. Frappier, T. F., Georgieff, I. S., Brown, K., and Shelanski, M. L. (1994) tau Regulation of microtubule-microtubule spacing and bundling. *Journal of neurochemistry* **63**, 2288-2294
18. Lee, G., Newman, S. T., Gard, D. L., Band, H., and Panchamoorthy, G. (1998) Tau interacts with src-family non-receptor tyrosine kinases. *Journal of cell science* **111 ( Pt 21)**, 3167-3177
19. Mandelkow, E. M., Schweers, O., Drewes, G., Biernat, J., Gustke, N., Trinczek, B., and Mandelkow, E. (1996) Structure, microtubule interactions, and phosphorylation of tau protein. *Annals of the New York Academy of Sciences* **777**, 96-106

20. Goedert, M. (2004) Tau protein and neurodegeneration. *Seminars in cell & developmental biology* **15**, 45-49
21. Ballatore, C., Lee, V. M., and Trojanowski, J. Q. (2007) Tau-mediated neurodegeneration in Alzheimer's disease and related disorders. *Nature reviews. Neuroscience* **8**, 663-672
22. Schweers, O., Schonbrunn-Hanebeck, E., Marx, A., and Mandelkow, E. (1994) Structural studies of tau protein and Alzheimer paired helical filaments show no evidence for beta-structure. *The Journal of biological chemistry* **269**, 24290-24297
23. Mukrasch, M. D., Biernat, J., von Bergen, M., Griesinger, C., Mandelkow, E., and Zweckstetter, M. (2005) Sites of tau important for aggregation populate {beta}-structure and bind to microtubules and polyanions. *The Journal of biological chemistry* **280**, 24978-24986
24. Li, W., and Lee, V. M. (2006) Characterization of two VQIXXK motifs for tau fibrillization in vitro. *Biochemistry* **45**, 15692-15701
25. von Bergen, M., Friedhoff, P., Biernat, J., Heberle, J., Mandelkow, E. M., and Mandelkow, E. (2000) Assembly of tau protein into Alzheimer paired helical filaments depends on a local sequence motif ((306)VQIVYK(311)) forming beta structure. *Proceedings of the National Academy of Sciences of the United States of America* **97**, 5129-5134
26. Biernat, J., Gustke, N., Drewes, G., Mandelkow, E. M., and Mandelkow, E. (1993) Phosphorylation of Ser262 strongly reduces binding of tau to microtubules: distinction between PHF-like immunoreactivity and microtubule binding. *Neuron* **11**, 153-163
27. Eisenberg, D., and Jucker, M. (2012) The amyloid state of proteins in human diseases. *Cell* **148**, 1188-1203
28. Sunde, M., Serpell, L. C., Bartlam, M., Fraser, P. E., Pepys, M. B., and Blake, C. C. (1997) Common core structure of amyloid fibrils by synchrotron X-ray diffraction. *Journal of molecular biology* **273**, 729-739
29. Miller, Y., Ma, B., and Nussinov, R. (2010) Polymorphism in Alzheimer Abeta amyloid organization reflects conformational selection in a rugged energy landscape. *Chemical reviews* **110**, 4820-4838
30. Wegmann, S., Jung, Y. J., Chinnathambi, S., Mandelkow, E. M., Mandelkow, E., and Muller, D. J. (2010) Human Tau isoforms assemble into ribbon-like fibrils that display polymorphic structure and stability. *The Journal of biological chemistry* **285**, 27302-27313
31. Jakes, R., Novak, M., Davison, M., and Wischik, C. M. (1991) Identification of 3- and 4-repeat tau isoforms within the PHF in Alzheimer's disease. *The EMBO journal* **10**, 2725-2729
32. Li, L., von Bergen, M., Mandelkow, E. M., and Mandelkow, E. (2002) Structure, stability, and aggregation of paired helical filaments from tau protein and FTDP-17 mutants probed by tryptophan scanning mutagenesis. *The Journal of biological chemistry* **277**, 41390-41400
33. von Bergen, M., Barghorn, S., Muller, S. A., Pickhardt, M., Biernat, J., Mandelkow, E. M., Davies, P., Aebi, U., and Mandelkow, E. (2006) The core of tau-paired helical filaments studied by scanning transmission electron microscopy and limited proteolysis. *Biochemistry* **45**, 6446-6457
34. Wegmann, S., Medalsy, I. D., Mandelkow, E., and Muller, D. J. (2013) The fuzzy coat of pathological human Tau fibrils is a two-layered polyelectrolyte brush. *Proceedings of the National Academy of Sciences of the United States of America* **110**, E313-321
35. Kirschner, D. A., Abraham, C., and Selkoe, D. J. (1986) X-ray diffraction from intraneuronal paired helical filaments and extraneuronal amyloid fibers in Alzheimer disease indicates cross-(3 conformation. *Proceedings of the National Academy of Sciences of the United States of America* **83**, 503-507
36. Berriman, J., Serpell, L. C., Oberg, K. A., Fink, A. L., Goedert, M., and Crowther, R. A. (2003) Tau filaments from human brain and from in vitro assembly of recombinant protein show cross-beta structure. *Proceedings of the National Academy of Sciences of the United States of America* **100**, 9034-9038
37. Daebel, V., Chinnathambi, S., Biernat, J., Schwalbe, M., Habenstein, B., Loquet, A., Akoury, E., Tepper, K., Muller, H., Baldus, M., Griesinger, C., Zweckstetter, M., Mandelkow, E., Vijayan,

- V., and Lange, A. (2012) beta-Sheet core of tau paired helical filaments revealed by solid-state NMR. *Journal of the American Chemical Society* **134**, 13982-13989
38. Giannetti, A. M., Lindwall, G., Chau, M. F., Radeke, M. J., Feinstein, S. C., and Kohlstaedt, L. A. (2000) Fibers of tau fragments, but not full length tau, exhibit a cross beta-structure: implications for the formation of paired helical filaments. *Protein science : a publication of the Protein Society* **9**, 2427-2435
39. Goux, W. J., Kopplin, L., Nguyen, A. D., Leak, K., Rutkofsky, M., Shanmuganandam, V. D., Sharma, D., Inouye, H., and Kirschner, D. A. (2004) The formation of straight and twisted filaments from short tau peptides. *The Journal of biological chemistry* **279**, 26868-26875
40. Sawaya, M. R., Sambashivan, S., Nelson, R., Ivanova, M. I., Sievers, S. A., Apostol, M. I., Thompson, M. J., Balbirnie, M., Wiltzius, J. J., McFarlane, H. T., Madsen, A. O., Riek, C., and Eisenberg, D. (2007) Atomic structures of amyloid cross-beta spines reveal varied steric zippers. *Nature* **447**, 453-457
41. Luhrs, T., Ritter, C., Adrian, M., Riek-Loher, D., Bohrmann, B., Dobeli, H., Schubert, D., and Riek, R. (2005) 3D structure of Alzheimer's amyloid-beta(1-42) fibrils. *Proceedings of the National Academy of Sciences of the United States of America* **102**, 17342-17347
42. Macao, B., Hoyer, W., Sandberg, A., Brorsson, A. C., Dobson, C. M., and Hard, T. (2008) Recombinant amyloid beta-peptide production by coexpression with an affibody ligand. *BMC biotechnology* **8**, 82
43. Barghorn, S., Zheng-Fischhofer, Q., Ackmann, M., Biernat, J., von Bergen, M., Mandelkow, E. M., and Mandelkow, E. (2000) Structure, microtubule interactions, and paired helical filament aggregation by tau mutants of frontotemporal dementias. *Biochemistry* **39**, 11714-11721
44. Astbury, W. T., Dickinson, S., and Bailey, K. (1935) The X-ray interpretation of denaturation and the structure of the seed globulins. *The Biochemical journal* **29**, 2351-2360
45. Bonar, L., Cohen, A. S., and Skinner, M. M. (1969) Characterization of the amyloid fibril as a cross-beta protein. *Proceedings of the Society for Experimental Biology and Medicine. Society for Experimental Biology and Medicine* **131**, 1373-1375
46. Tsemekhman, K., Goldschmidt, L., Eisenberg, D., and Baker, D. (2007) Cooperative hydrogen bonding in amyloid formation. *Protein science : a publication of the Protein Society* **16**, 761-764
47. Balbirnie, M., Grothe, R., and Eisenberg, D. S. (2001) An amyloid-forming peptide from the yeast prion Sup35 reveals a dehydrated beta-sheet structure for amyloid. *Proceedings of the National Academy of Sciences of the United States of America* **98**, 2375-2380
48. Sievers, S. A., Karanicolas, J., Chang, H. W., Zhao, A., Jiang, L., Zirafi, O., Stevens, J. T., Munch, J., Baker, D., and Eisenberg, D. (2011) Structure-based design of non-natural amino-acid inhibitors of amyloid fibril formation. *Nature* **475**, 96-100
49. Buchete, N. V., and Hummer, G. (2007) Structure and dynamics of parallel beta-sheets, hydrophobic core, and loops in Alzheimer's A beta fibrils. *Biophysical journal* **92**, 3032-3039
50. Colletier, J. P., Laganowsky, A., Landau, M., Zhao, M., Soriaga, A. B., Goldschmidt, L., Flot, D., Cascio, D., Sawaya, M. R., and Eisenberg, D. (2011) Molecular basis for amyloid-beta polymorphism. *Proceedings of the National Academy of Sciences of the United States of America* **108**, 16938-16943
51. Siddiqua, A., and Margittai, M. (2010) Three- and four-repeat Tau coassemble into heterogeneous filaments: an implication for Alzheimer disease. *The Journal of biological chemistry* **285**, 37920-37926
52. Siddiqua, A., Luo, Y., Meyer, V., Swanson, M. A., Yu, X., Wei, G., Zheng, J., Eaton, G. R., Ma, B., Nussinov, R., Eaton, S. S., and Margittai, M. (2012) Conformational basis for asymmetric seeding barrier in filaments of three- and four-repeat tau. *Journal of the American Chemical Society* **134**, 10271-10278

53. Maeda, S., Sahara, N., Saito, Y., Murayama, M., Yoshiike, Y., Kim, H., Miyasaka, T., Murayama, S., Ikai, A., and Takashima, A. (2007) Granular tau oligomers as intermediates of tau filaments. *Biochemistry* **46**, 3856-3861
54. Elbaum-Garfinkle, S., and Rhoades, E. (2012) Identification of an aggregation-prone structure of tau. *Journal of the American Chemical Society* **134**, 16607-16613
55. Wegmann, S., Scholer, J., Bippes, C. A., Mandelkow, E., and Muller, D. J. (2011) Competing interactions stabilize pro- and anti-aggregant conformations of human Tau. *The Journal of biological chemistry* **286**, 20512-20524
56. Nelson, R., Sawaya, M. R., Balbirnie, M., Madsen, A. O., Riek, C., Grothe, R., and Eisenberg, D. (2005) Structure of the cross-beta spine of amyloid-like fibrils. *Nature* **435**, 773-778
57. Patterson, K. R., Remmers, C., Fu, Y., Brooker, S., Kanaan, N. M., Vana, L., Ward, S., Reyes, J. F., Philibert, K., Glucksman, M. J., and Binder, L. I. (2011) Characterization of prefibrillar Tau oligomers in vitro and in Alzheimer disease. *The Journal of biological chemistry* **286**, 23063-23076
58. Lee, J., Culyba, E. K., Powers, E. T., and Kelly, J. W. (2011) Amyloid-beta forms fibrils by nucleated conformational conversion of oligomers. *Nature chemical biology* **7**, 602-609
59. Gong, Y., Chang, L., Viola, K. L., Lacor, P. N., Lambert, M. P., Finch, C. E., Krafft, G. A., and Klein, W. L. (2003) Alzheimer's disease-affected brain: presence of oligomeric A beta ligands (ADDLs) suggests a molecular basis for reversible memory loss. *Proceedings of the National Academy of Sciences of the United States of America* **100**, 10417-10422
60. Jan, A., Hartley, D. M., and Lashuel, H. A. (2010) Preparation and characterization of toxic Abeta aggregates for structural and functional studies in Alzheimer's disease research. *Nature protocols* **5**, 1186-1209
61. Lasagna-Reeves, C. A., Castillo-Carranza, D. L., Guerrero-Muoz, M. J., Jackson, G. R., and Kaye, R. (2010) Preparation and characterization of neurotoxic tau oligomers. *Biochemistry* **49**, 10039-10041
62. LeVine, H., 3rd. (1993) Thioflavine T interaction with synthetic Alzheimer's disease beta-amyloid peptides: detection of amyloid aggregation in solution. *Protein science : a publication of the Protein Society* **2**, 404-410
63. Friedhoff, P., Schneider, A., Mandelkow, E. M., and Mandelkow, E. (1998) Rapid assembly of Alzheimer-like paired helical filaments from microtubule-associated protein tau monitored by fluorescence in solution. *Biochemistry* **37**, 10223-10230
64. Hortschansky, P., Schroeckh, V., Christopeit, T., Zandomenighi, G., and Fandrich, M. (2005) The aggregation kinetics of Alzheimer's beta-amyloid peptide is controlled by stochastic nucleation. *Protein science : a publication of the Protein Society* **14**, 1753-1759
65. Friedhoff, P., von Bergen, M., Mandelkow, E. M., Davies, P., and Mandelkow, E. (1998) A nucleated assembly mechanism of Alzheimer paired helical filaments. *Proceedings of the National Academy of Sciences of the United States of America* **95**, 15712-15717
66. von Bergen, M., Barghorn, S., Biernat, J., Mandelkow, E. M., and Mandelkow, E. (2005) Tau aggregation is driven by a transition from random coil to beta sheet structure. *Biochimica et biophysica acta* **1739**, 158-166
67. Walker, L. C., Diamond, M. I., Duff, K. E., and Hyman, B. T. (2013) Mechanisms of protein seeding in neurodegenerative diseases. *JAMA neurology* **70**, 304-310
68. Jomova, K., Vondrakova, D., Lawson, M., and Valko, M. (2010) Metals, oxidative stress and neurodegenerative disorders. *Molecular and cellular biochemistry* **345**, 91-104
69. Nilsberth, C., Westlind-Danielsson, A., Eckman, C. B., Condron, M. M., Axelman, K., Forsell, C., Sten, C., Luthman, J., Teplow, D. B., Younkin, S. G., Naslund, J., and Lannfelt, L. (2001) The 'Arctic' APP mutation (E693G) causes Alzheimer's disease by enhanced Abeta protofibril formation. *Nature neuroscience* **4**, 887-893
70. Norlin, N., Hellberg, M., Filippov, A., Sousa, A. A., Grobner, G., Leapman, R. D., Almqvist, N., and Antzutkin, O. N. (2012) Aggregation and fibril morphology of the Arctic mutation of

- Alzheimer's Aβ peptide by CD, TEM, STEM and in situ AFM. *Journal of structural biology* **180**, 174-189
71. Walker, S., Ullman, O., and Stultz, C. M. (2012) Using intramolecular disulfide bonds in tau protein to deduce structural features of aggregation-resistant conformations. *The Journal of biological chemistry* **287**, 9591-9600
  72. Barghorn, S., and Mandelkow, E. (2002) Toward a unified scheme for the aggregation of tau into Alzheimer paired helical filaments. *Biochemistry* **41**, 14885-14896
  73. Fischer, D., Mukrasch, M. D., Biernat, J., Bibow, S., Blackledge, M., Griesinger, C., Mandelkow, E., and Zweckstetter, M. (2009) Conformational changes specific for pseudophosphorylation at serine 262 selectively impair binding of tau to microtubules. *Biochemistry* **48**, 10047-10055
  74. Chang, E., Kim, S., Schafer, K. N., and Kuret, J. (2011) Pseudophosphorylation of tau protein directly modulates its aggregation kinetics. *Biochimica et biophysica acta* **1814**, 388-395
  75. Abraha, A., Ghoshal, N., Gamblin, T. C., Cryns, V., Berry, R. W., Kuret, J., and Binder, L. I. (2000) C-terminal inhibition of tau assembly in vitro and in Alzheimer's disease. *Journal of cell science* **113 Pt 21**, 3737-3745
  76. Khlistunova, I., Biernat, J., Wang, Y., Pickhardt, M., von Bergen, M., Gazova, Z., Mandelkow, E., and Mandelkow, E. M. (2006) Inducible expression of Tau repeat domain in cell models of tauopathy: aggregation is toxic to cells but can be reversed by inhibitor drugs. *The Journal of biological chemistry* **281**, 1205-1214
  77. Park, S. Y., and Ferreira, A. (2005) The generation of a 17 kDa neurotoxic fragment: an alternative mechanism by which tau mediates beta-amyloid-induced neurodegeneration. *The Journal of neuroscience : the official journal of the Society for Neuroscience* **25**, 5365-5375
  78. Saido, T. C., Iwatsubo, T., Mann, D. M., Shimada, H., Ihara, Y., and Kawashima, S. (1995) Dominant and differential deposition of distinct beta-amyloid peptide species, Aβ<sub>42</sub>(pE), in senile plaques. *Neuron* **14**, 457-466
  79. Kuo, Y. M., Emmerling, M. R., Woods, A. S., Cotter, R. J., and Roher, A. E. (1997) Isolation, chemical characterization, and quantitation of Aβ<sub>42</sub>-pyroglutamate peptide from neuritic plaques and vascular amyloid deposits. *Biochemical and biophysical research communications* **237**, 188-191
  80. Russo, C., Violani, E., Salis, S., Venezia, V., Dolcini, V., Damonte, G., Benatti, U., D'Arrigo, C., Patrone, E., Carlo, P., and Schettini, G. (2002) Pyroglutamate-modified amyloid beta-peptides--Aβ<sub>42</sub>(pE)--strongly affect cultured neuron and astrocyte survival. *Journal of neurochemistry* **82**, 1480-1489
  81. Schlenzig, D., Ronicke, R., Cynis, H., Ludwig, H. H., Scheel, E., Reymann, K., Saido, T., Hause, G., Schilling, S., and Demuth, H. U. (2012) N-Terminal pyroglutamate formation of Aβ<sub>38</sub> and Aβ<sub>40</sub> enforces oligomer formation and potency to disrupt hippocampal long-term potentiation. *Journal of neurochemistry* **121**, 774-784
  82. Roher, A. E., Lowenson, J. D., Clarke, S., Wolkow, C., Wang, R., Cotter, R. J., Reardon, I. M., Zurcher-Neely, H. A., Heinrichson, R. L., Ball, M. J., and et al. (1993) Structural alterations in the peptide backbone of beta-amyloid core protein may account for its deposition and stability in Alzheimer's disease. *The Journal of biological chemistry* **268**, 3072-3083
  83. Hou, L., Lee, H. G., Han, F., Tedesco, J. M., Perry, G., Smith, M. A., and Zagorski, M. G. (2013) Modification of amyloid-beta<sub>1-42</sub> fibril structure by methionine-35 oxidation. *Journal of Alzheimer's disease : JAD* **37**, 9-18
  84. Mrak, R. E., Griffin, S. T., and Graham, D. I. (1997) Aging-associated changes in human brain. *Journal of neuropathology and experimental neurology* **56**, 1269-1275
  85. Garvey, M., and Morgado, I. (2013) Peptide concentration alters intermediate species in amyloid beta fibrillation kinetics. *Biochemical and biophysical research communications* **433**, 276-280
  86. Chen, W. T., Liao, Y. H., Yu, H. M., Cheng, I. H., and Chen, Y. R. (2011) Distinct effects of Zn<sup>2+</sup>, Cu<sup>2+</sup>, Fe<sup>3+</sup>, and Al<sup>3+</sup> on amyloid-beta stability, oligomerization, and aggregation: amyloid-

- beta destabilization promotes annular protofibril formation. *The Journal of biological chemistry* **286**, 9646-9656
87. Dahse, K., Garvey, M., Kovermann, M., Vogel, A., Balbach, J., Fandrich, M., and Fahr, A. (2010) DHPC strongly affects the structure and oligomerization propensity of Alzheimer's Abeta(1-40) peptide. *Journal of molecular biology* **403**, 643-659
  88. Hellstrand, E., Sparr, E., and Linse, S. (2010) Retardation of Abeta fibril formation by phospholipid vesicles depends on membrane phase behavior. *Biophysical journal* **98**, 2206-2214
  89. Kampers, T., Friedhoff, P., Biernat, J., Mandelkow, E. M., and Mandelkow, E. (1996) RNA stimulates aggregation of microtubule-associated protein tau into Alzheimer-like paired helical filaments. *FEBS letters* **399**, 344-349
  90. King, M. E., Gamblin, T. C., Kuret, J., and Binder, L. I. (2000) Differential assembly of human tau isoforms in the presence of arachidonic acid. *Journal of neurochemistry* **74**, 1749-1757
  91. Nelson, P. T., Braak, H., and Markesbery, W. R. (2009) Neuropathology and cognitive impairment in Alzheimer disease: a complex but coherent relationship. *Journal of neuropathology and experimental neurology* **68**, 1-14
  92. Katzman, R., Terry, R., DeTeresa, R., Brown, T., Davies, P., Fuld, P., Renbing, X., and Peck, A. (1988) Clinical, pathological, and neurochemical changes in dementia: a subgroup with preserved mental status and numerous neocortical plaques. *Annals of neurology* **23**, 138-144
  93. Hyman, B. T., Marzloff, K., and Arriagada, P. V. (1993) The lack of accumulation of senile plaques or amyloid burden in Alzheimer's disease suggests a dynamic balance between amyloid deposition and resolution. *Journal of neuropathology and experimental neurology* **52**, 594-600
  94. Naslund, J., Haroutunian, V., Mohs, R., Davis, K. L., Davies, P., Greengard, P., and Buxbaum, J. D. (2000) Correlation between elevated levels of amyloid beta-peptide in the brain and cognitive decline. *JAMA : the journal of the American Medical Association* **283**, 1571-1577
  95. Lue, L. F., Kuo, Y. M., Roher, A. E., Brachova, L., Shen, Y., Sue, L., Beach, T., Kurth, J. H., Rydel, R. E., and Rogers, J. (1999) Soluble amyloid beta peptide concentration as a predictor of synaptic change in Alzheimer's disease. *Am J Pathol* **155**, 853-862
  96. McLean, C. A., Cherny, R. A., Fraser, F. W., Fuller, S. J., Smith, M. J., Beyreuther, K., Bush, A. I., and Masters, C. L. (1999) Soluble pool of Abeta amyloid as a determinant of severity of neurodegeneration in Alzheimer's disease. *Annals of neurology* **46**, 860-866
  97. Wang, J., Dickson, D. W., Trojanowski, J. Q., and Lee, V. M. (1999) The levels of soluble versus insoluble brain Abeta distinguish Alzheimer's disease from normal and pathologic aging. *Experimental neurology* **158**, 328-337
  98. Lasagna-Reeves, C. A., Castillo-Carranza, D. L., Sengupta, U., Sarmiento, J., Troncoso, J., Jackson, G. R., and Kaye, R. (2012) Identification of oligomers at early stages of tau aggregation in Alzheimer's disease. *FASEB journal : official publication of the Federation of American Societies for Experimental Biology* **26**, 1946-1959
  99. Jin, M., Shepardson, N., Yang, T., Chen, G., Walsh, D., and Selkoe, D. J. (2011) Soluble amyloid beta-protein dimers isolated from Alzheimer cortex directly induce Tau hyperphosphorylation and neuritic degeneration. *Proceedings of the National Academy of Sciences of the United States of America* **108**, 5819-5824
  100. Schweers, O., Mandelkow, E. M., Biernat, J., and Mandelkow, E. (1995) Oxidation of cysteine-322 in the repeat domain of microtubule-associated protein tau controls the in vitro assembly of paired helical filaments. *Proceedings of the National Academy of Sciences of the United States of America* **92**, 8463-8467
  101. Ren, Y., and Sahara, N. (2013) Characteristics of tau oligomers. *Frontiers in neurology* **4**, 102
  102. Lambert, M. P., Barlow, A. K., Chromy, B. A., Edwards, C., Freed, R., Liosatos, M., Morgan, T. E., Rozovsky, I., Trommer, B., Viola, K. L., Wals, P., Zhang, C., Finch, C. E., Krafft, G. A., and Klein, W. L. (1998) Diffusible, nonfibrillar ligands derived from Abeta1-42 are potent central

- nervous system neurotoxins. *Proceedings of the National Academy of Sciences of the United States of America* **95**, 6448-6453
103. Walsh, D. M., Klyubin, I., Fadeeva, J. V., Cullen, W. K., Anwyl, R., Wolfe, M. S., Rowan, M. J., and Selkoe, D. J. (2002) Naturally secreted oligomers of amyloid beta protein potently inhibit hippocampal long-term potentiation in vivo. *Nature* **416**, 535-539
104. Lesne, S., Koh, M. T., Kotilinek, L., Kaye, R., Glabe, C. G., Yang, A., Gallagher, M., and Ashe, K. H. (2006) A specific amyloid-beta protein assembly in the brain impairs memory. *Nature* **440**, 352-357
105. Shankar, G. M., Li, S., Mehta, T. H., Garcia-Munoz, A., Shepardson, N. E., Smith, I., Brett, F. M., Farrell, M. A., Rowan, M. J., Lemere, C. A., Regan, C. M., Walsh, D. M., Sabatini, B. L., and Selkoe, D. J. (2008) Amyloid-beta protein dimers isolated directly from Alzheimer's brains impair synaptic plasticity and memory. *Nature medicine* **14**, 837-842
106. Hartley, D. M., Walsh, D. M., Ye, C. P., Diehl, T., Vasquez, S., Vassilev, P. M., Teplow, D. B., and Selkoe, D. J. (1999) Protofibrillar intermediates of amyloid beta-protein induce acute electrophysiological changes and progressive neurotoxicity in cortical neurons. *The Journal of neuroscience : the official journal of the Society for Neuroscience* **19**, 8876-8884
107. Yu, L., Edalji, R., Harlan, J. E., Holzman, T. F., Lopez, A. P., Labkovsky, B., Hillen, H., Barghorn, S., Ebert, U., Richardson, P. L., Miesbauer, L., Solomon, L., Bartley, D., Walter, K., Johnson, R. W., Hajduk, P. J., and Olejniczak, E. T. (2009) Structural characterization of a soluble amyloid beta-peptide oligomer. *Biochemistry* **48**, 1870-1877
108. Hoyer, W., Gronwall, C., Jonsson, A., Stahl, S., and Hard, T. (2008) Stabilization of a beta-hairpin in monomeric Alzheimer's amyloid-beta peptide inhibits amyloid formation. *Proceedings of the National Academy of Sciences of the United States of America* **105**, 5099-5104
109. Gronwall, C., Jonsson, A., Lindstrom, S., Gunneriusson, E., Stahl, S., and Herne, N. (2007) Selection and characterization of Affibody ligands binding to Alzheimer amyloid beta peptides. *Journal of biotechnology* **128**, 162-183
110. Rosenman, D. J., Connors, C. R., Chen, W., Wang, C., and Garcia, A. E. (2013) Abeta monomers transiently sample oligomer and fibril-like configurations: ensemble characterization using a combined MD/NMR approach. *Journal of molecular biology* **425**, 3338-3359
111. Habicht, G., Haupt, C., Friedrich, R. P., Hortschansky, P., Sachse, C., Meinhardt, J., Wieligmann, K., Gellermann, G. P., Brodhun, M., Gotz, J., Halbhuber, K. J., Rocken, C., Horn, U., and Fandrich, M. (2007) Directed selection of a conformational antibody domain that prevents mature amyloid fibril formation by stabilizing Abeta protofibrils. *Proceedings of the National Academy of Sciences of the United States of America* **104**, 19232-19237
112. Sandberg, A., Luheshi, L. M., Sollvander, S., Pereira de Barros, T., Macao, B., Knowles, T. P., Biverstal, H., Lendel, C., Ekholm-Petterson, F., Dubnovitsky, A., Lannfelt, L., Dobson, C. M., and Hard, T. (2010) Stabilization of neurotoxic Alzheimer amyloid-beta oligomers by protein engineering. *Proceedings of the National Academy of Sciences of the United States of America* **107**, 15595-15600
113. Cerf, E., Sarroukh, R., Tamamizu-Kato, S., Breydo, L., Derclaye, S., Dufrene, Y. F., Narayanaswami, V., Goormaghtigh, E., Ruyschaert, J. M., and Raussens, V. (2009) Antiparallel beta-sheet: a signature structure of the oligomeric amyloid beta-peptide. *The Biochemical journal* **421**, 415-423
114. Mufson, E. J., Ward, S., and Binder, L. (2013) Prefibrillar Tau Oligomers in Mild Cognitive Impairment and Alzheimer's Disease. *Neuro-degenerative diseases*
115. Berger, Z., Roder, H., Hanna, A., Carlson, A., Rangachari, V., Yue, M., Wszolek, Z., Ashe, K., Knight, J., Dickson, D., Andorfer, C., Rosenberry, T. L., Lewis, J., Hutton, M., and Janus, C. (2007) Accumulation of pathological tau species and memory loss in a conditional model of tauopathy. *The Journal of neuroscience : the official journal of the Society for Neuroscience* **27**, 3650-3662

116. Santacruz, K., Lewis, J., Spires, T., Paulson, J., Kotilinek, L., Ingelsson, M., Guimaraes, A., DeTure, M., Ramsden, M., McGowan, E., Forster, C., Yue, M., Orne, J., Janus, C., Mariash, A., Kuskowski, M., Hyman, B., Hutton, M., and Ashe, K. H. (2005) Tau suppression in a neurodegenerative mouse model improves memory function. *Science* **309**, 476-481
117. Peterson, D. W., Zhou, H., Dahlquist, F. W., and Lew, J. (2008) A soluble oligomer of tau associated with fiber formation analyzed by NMR. *Biochemistry* **47**, 7393-7404
118. Bucciantini, M., Giannoni, E., Chiti, F., Baroni, F., Formigli, L., Zurdo, J., Taddei, N., Ramponi, G., Dobson, C. M., and Stefani, M. (2002) Inherent toxicity of aggregates implies a common mechanism for protein misfolding diseases. *Nature* **416**, 507-511
119. Kaye, R., Head, E., Thompson, J. L., McIntire, T. M., Milton, S. C., Cotman, C. W., and Glabe, C. G. (2003) Common structure of soluble amyloid oligomers implies common mechanism of pathogenesis. *Science* **300**, 486-489
120. Campioni, S., Mannini, B., Zampagni, M., Pensalfini, A., Parrini, C., Evangelisti, E., Relini, A., Stefani, M., Dobson, C. M., Cecchi, C., and Chiti, F. (2010) A causative link between the structure of aberrant protein oligomers and their toxicity. *Nature chemical biology* **6**, 140-147
121. Keshet, B., Yang, I. H., and Good, T. A. (2010) Can size alone explain some of the differences in toxicity between beta-amyloid oligomers and fibrils? *Biotechnology and bioengineering* **106**, 333-337
122. Mattson, M. P. (2000) Apoptosis in neurodegenerative disorders. *Nature reviews. Molecular cell biology* **1**, 120-129
123. Stokin, G. B., Lillo, C., Falzone, T. L., Brusch, R. G., Rockenstein, E., Mount, S. L., Raman, R., Davies, P., Masliah, E., Williams, D. S., and Goldstein, L. S. (2005) Axonopathy and transport deficits early in the pathogenesis of Alzheimer's disease. *Science* **307**, 1282-1288
124. Hiruma, H., Katakura, T., Takahashi, S., Ichikawa, T., and Kawakami, T. (2003) Glutamate and amyloid beta-protein rapidly inhibit fast axonal transport in cultured rat hippocampal neurons by different mechanisms. *The Journal of neuroscience : the official journal of the Society for Neuroscience* **23**, 8967-8977
125. Roy, S., Zhang, B., Lee, V. M., and Trojanowski, J. Q. (2005) Axonal transport defects: a common theme in neurodegenerative diseases. *Acta neuropathologica* **109**, 5-13
126. Zempel, H., Luedtke, J., Kumar, Y., Biernat, J., Dawson, H., Mandelkow, E., and Mandelkow, E. M. (2013) Amyloid-beta oligomers induce synaptic damage via Tau-dependent microtubule severing by TTL6 and spastin. *The EMBO journal* **32**, 2920-2937
127. Loo, D. T., Copani, A., Pike, C. J., Whitemore, E. R., Walencewicz, A. J., and Cotman, C. W. (1993) Apoptosis is induced by beta-amyloid in cultured central nervous system neurons. *Proceedings of the National Academy of Sciences of the United States of America* **90**, 7951-7955
128. Yankner, B. A. (1996) Mechanisms of neuronal degeneration in Alzheimer's disease. *Neuron* **16**, 921-932
129. Itagaki, S., McGeer, P. L., Akiyama, H., Zhu, S., and Selkoe, D. (1989) Relationship of microglia and astrocytes to amyloid deposits of Alzheimer disease. *Journal of neuroimmunology* **24**, 173-182
130. Rapoport, M., Dawson, H. N., Binder, L. I., Vitek, M. P., and Ferreira, A. (2002) Tau is essential to beta-amyloid-induced neurotoxicity. *Proceedings of the National Academy of Sciences of the United States of America* **99**, 6364-6369
131. Roberson, E. D., Searce-Levie, K., Palop, J. J., Yan, F., Cheng, I. H., Wu, T., Gerstein, H., Yu, G. Q., and Mucke, L. (2007) Reducing endogenous tau ameliorates amyloid beta-induced deficits in an Alzheimer's disease mouse model. *Science* **316**, 750-754
132. Hedden, T., Van Dijk, K. R., Becker, J. A., Mehta, A., Sperling, R. A., Johnson, K. A., and Buckner, R. L. (2009) Disruption of functional connectivity in clinically normal older adults harboring amyloid burden. *The Journal of neuroscience : the official journal of the Society for Neuroscience* **29**, 12686-12694

133. Tsai, J., Grutzendler, J., Duff, K., and Gan, W. B. (2004) Fibrillar amyloid deposition leads to local synaptic abnormalities and breakage of neuronal branches. *Nature neuroscience* **7**, 1181-1183
134. Carulla, N., Caddy, G. L., Hall, D. R., Zurdo, J., Gairi, M., Feliz, M., Giralt, E., Robinson, C. V., and Dobson, C. M. (2005) Molecular recycling within amyloid fibrils. *Nature* **436**, 554-558
135. Jan, A., Adolfsson, O., Allaman, I., Buccarello, A. L., Magistretti, P. J., Pfeifer, A., Muhs, A., and Lashuel, H. A. (2011) Abeta42 neurotoxicity is mediated by ongoing nucleated polymerization process rather than by discrete Abeta42 species. *The Journal of biological chemistry* **286**, 8585-8596
136. Winner, B., Jappelli, R., Maji, S. K., Desplats, P. A., Boyer, L., Aigner, S., Hetzer, C., Loher, T., Vilar, M., Campioni, S., Tzitzilonis, C., Soragni, A., Jessberger, S., Mira, H., Consiglio, A., Pham, E., Masliah, E., Gage, F. H., and Riek, R. (2011) In vivo demonstration that alpha-synuclein oligomers are toxic. *Proceedings of the National Academy of Sciences of the United States of America* **108**, 4194-4199
137. Lauren, J., Gimbel, D. A., Nygaard, H. B., Gilbert, J. W., and Strittmatter, S. M. (2009) Cellular prion protein mediates impairment of synaptic plasticity by amyloid-beta oligomers. *Nature* **457**, 1128-1132
138. Wang, L., Chiang, H. C., Wu, W., Liang, B., Xie, Z., Yao, X., Ma, W., Du, S., and Zhong, Y. (2012) Epidermal growth factor receptor is a preferred target for treating amyloid-beta-induced memory loss. *Proceedings of the National Academy of Sciences of the United States of America* **109**, 16743-16748
139. Wang, H., Ren, C. H., Gunawardana, C. G., and Schmitt-Ulms, G. (2013) Overcoming barriers and thresholds - signaling of oligomeric Abeta through the prion protein to Fyn. *Molecular neurodegeneration* **8**, 24
140. Roychaudhuri, R., Yang, M., Hoshi, M. M., and Teplow, D. B. (2009) Amyloid beta-protein assembly and Alzheimer disease. *The Journal of biological chemistry* **284**, 4749-4753
141. Gomez-Ramos, A., Diaz-Hernandez, M., Rubio, A., Miras-Portugal, M. T., and Avila, J. (2008) Extracellular tau promotes intracellular calcium increase through M1 and M3 muscarinic receptors in neuronal cells. *Molecular and cellular neurosciences* **37**, 673-681
142. Gomez-Ramos, A., Diaz-Hernandez, M., Rubio, A., Diaz-Hernandez, J. I., Miras-Portugal, M. T., and Avila, J. (2009) Characteristics and consequences of muscarinic receptor activation by tau protein. *European neuropsychopharmacology : the journal of the European College of Neuropsychopharmacology* **19**, 708-717
143. Aguzzi, A., and Rajendran, L. (2009) The transcellular spread of cytosolic amyloids, prions, and prionoids. *Neuron* **64**, 783-790
144. Prusiner, S. B. (1998) Prions. *Proceedings of the National Academy of Sciences of the United States of America* **95**, 13363-13383
145. Luers, L., Bannach, O., Stohr, J., Wordehoff, M. M., Wolff, M., Nagel-Steger, L., Riesner, D., Willbold, D., and Birkmann, E. (2013) Seeded fibrillation as molecular basis of the species barrier in human prion diseases. *PLoS one* **8**, e72623
146. Hamaguchi, T., Eisele, Y. S., Varvel, N. H., Lamb, B. T., Walker, L. C., and Jucker, M. (2012) The presence of Abeta seeds, and not age per se, is critical to the initiation of Abeta deposition in the brain. *Acta neuropathologica* **123**, 31-37
147. Jucker, M., and Walker, L. C. (2011) Pathogenic protein seeding in Alzheimer disease and other neurodegenerative disorders. *Annals of neurology* **70**, 532-540
148. Eisele, Y. S., Obermuller, U., Heilbronner, G., Baumann, F., Kaeser, S. A., Wolburg, H., Walker, L. C., Staufienbiel, M., Heikenwalder, M., and Jucker, M. (2010) Peripherally applied Abeta-containing inoculates induce cerebral beta-amyloidosis. *Science* **330**, 980-982
149. Clavaguera, F., Grueninger, F., and Tolnay, M. (2013) Intercellular transfer of tau aggregates and spreading of tau pathology: Implications for therapeutic strategies. *Neuropharmacology*
150. Iba, M., Guo, J. L., McBride, J. D., Zhang, B., Trojanowski, J. Q., and Lee, V. M. (2013) Synthetic tau fibrils mediate transmission of neurofibrillary tangles in a transgenic mouse model of

- Alzheimer's-like tauopathy. *The Journal of neuroscience : the official journal of the Society for Neuroscience* **33**, 1024-1037
151. Clavaguera, F., Bolmont, T., Crowther, R. A., Abramowski, D., Frank, S., Probst, A., Fraser, G., Stalder, A. K., Beibel, M., Staufenbiel, M., Jucker, M., Goedert, M., and Tolnay, M. (2009) Transmission and spreading of tauopathy in transgenic mouse brain. *Nature cell biology* **11**, 909-913
152. Frost, B., Jacks, R. L., and Diamond, M. I. (2009) Propagation of tau misfolding from the outside to the inside of a cell. *The Journal of biological chemistry* **284**, 12845-12852
153. Robert, R., and Wark, K. L. (2012) Engineered antibody approaches for Alzheimer's disease immunotherapy. *Archives of biochemistry and biophysics* **526**, 132-138
154. Janeway, C. A., and Janeway, C. (2002) *Immunologie. Immunobiologie <dt.>*,
155. Gill, D. S., and Damle, N. K. (2006) Biopharmaceutical drug discovery using novel protein scaffolds. *Current opinion in biotechnology* **17**, 653-658
156. Borrebaeck, C. A. (2000) Antibodies in diagnostics - from immunoassays to protein chips. *Immunology today* **21**, 379-382
157. Michaud, G. A., Salcius, M., Zhou, F., Bangham, R., Bonin, J., Guo, H., Snyder, M., Predki, P. F., and Schweitzer, B. I. (2003) Analyzing antibody specificity with whole proteome microarrays. *Nature biotechnology* **21**, 1509-1512
158. Holliger, P., Prospero, T., and Winter, G. (1993) "Diabodies": small bivalent and bispecific antibody fragments. *Proceedings of the National Academy of Sciences of the United States of America* **90**, 6444-6448
159. Baeuerle, P. A., and Reinhardt, C. (2009) Bispecific T-cell engaging antibodies for cancer therapy. *Cancer research* **69**, 4941-4944
160. Holliger, P., and Hudson, P. J. (2005) Engineered antibody fragments and the rise of single domains. *Nature biotechnology* **23**, 1126-1136
161. Holt, L. J., Herring, C., Jespers, L. S., Woolven, B. P., and Tomlinson, I. M. (2003) Domain antibodies: proteins for therapy. *Trends in biotechnology* **21**, 484-490
162. Colby, D. W., Chu, Y., Cassady, J. P., Duennwald, M., Zazulak, H., Webster, J. M., Messer, A., Lindquist, S., Ingram, V. M., and Wittrup, K. D. (2004) Potent inhibition of huntingtin aggregation and cytotoxicity by a disulfide bond-free single-domain intracellular antibody. *Proceedings of the National Academy of Sciences of the United States of America* **101**, 17616-17621
163. Harmsen, M. M., and De Haard, H. J. (2007) Properties, production, and applications of camelid single-domain antibody fragments. *Applied microbiology and biotechnology* **77**, 13-22
164. Cortez-Retamozo, V., Backmann, N., Senter, P. D., Wernery, U., De Baetselier, P., Muyldermans, S., and Revets, H. (2004) Efficient cancer therapy with a nanobody-based conjugate. *Cancer research* **64**, 2853-2857
165. Gronwall, C., and Stahl, S. (2009) Engineered affinity proteins--generation and applications. *Journal of biotechnology* **140**, 254-269
166. Nord, K., Nilsson, J., Nilsson, B., Uhlen, M., and Nygren, P. A. (1995) A combinatorial library of an alpha-helical bacterial receptor domain. *Protein engineering* **8**, 601-608
167. Koide, A., Bailey, C. W., Huang, X., and Koide, S. (1998) The fibronectin type III domain as a scaffold for novel binding proteins. *Journal of molecular biology* **284**, 1141-1151
168. Xu, L., Aha, P., Gu, K., Kuimelis, R. G., Kurz, M., Lam, T., Lim, A. C., Liu, H., Lohse, P. A., Sun, L., Weng, S., Wagner, R. W., and Lipovsek, D. (2002) Directed evolution of high-affinity antibody mimics using mRNA display. *Chemistry & biology* **9**, 933-942
169. Lipovsek, D. (2011) Adnectins: engineered target-binding protein therapeutics. *Protein engineering, design & selection : PEDS* **24**, 3-9
170. Beste, G., Schmidt, F. S., Stibora, T., and Skerra, A. (1999) Small antibody-like proteins with prescribed ligand specificities derived from the lipocalin fold. *Proceedings of the National Academy of Sciences of the United States of America* **96**, 1898-1903

171. Schlehuber, S., Beste, G., and Skerra, A. (2000) A novel type of receptor protein, based on the lipocalin scaffold, with specificity for digoxigenin. *Journal of molecular biology* **297**, 1105-1120
172. Schlehuber, S., and Skerra, A. (2005) Anticalins as an alternative to antibody technology. *Expert opinion on biological therapy* **5**, 1453-1462
173. Nygren, P. A., and Skerra, A. (2004) Binding proteins from alternative scaffolds. *Journal of immunological methods* **290**, 3-28
174. Schlatter, D., Brack, S., Banner, D. W., Batey, S., Benz, J., Bertschinger, J., Huber, W., Joseph, C., Rufer, A., van der Klooster, A., Weber, M., Grabulovski, D., and Hennig, M. (2012) Generation, characterization and structural data of chymase binding proteins based on the human Fyn kinase SH3 domain. *mAbs* **4**, 497-508
175. Nilsson, B., Moks, T., Jansson, B., Abrahmsen, L., Elmlblad, A., Holmgren, E., Henrichson, C., Jones, T. A., and Uhlen, M. (1987) A synthetic IgG-binding domain based on staphylococcal protein A. *Protein engineering* **1**, 107-113
176. Wikman, M., Steffen, A. C., Gunneriusson, E., Tolmachev, V., Adams, G. P., Carlsson, J., and Stahl, S. (2004) Selection and characterization of HER2/neu-binding affibody ligands. *Protein engineering, design & selection : PEDS* **17**, 455-462
177. Nilsson, F. Y., and Tolmachev, V. (2007) Affibody molecules: new protein domains for molecular imaging and targeted tumor therapy. *Current opinion in drug discovery & development* **10**, 167-175
178. Lofblom, J., Feldwisch, J., Tolmachev, V., Carlsson, J., Stahl, S., and Frejd, F. Y. (2010) Affibody molecules: engineered proteins for therapeutic, diagnostic and biotechnological applications. *FEBS letters* **584**, 2670-2680
179. Citron, M. (2004) Strategies for disease modification in Alzheimer's disease. *Nature reviews. Neuroscience* **5**, 677-685
180. Wilcock, D. M., Alamed, J., Gottschall, P. E., Grimm, J., Rosenthal, A., Pons, J., Ronan, V., Symmonds, K., Gordon, M. N., and Morgan, D. (2006) Deglycosylated anti-amyloid-beta antibodies eliminate cognitive deficits and reduce parenchymal amyloid with minimal vascular consequences in aged amyloid precursor protein transgenic mice. *The Journal of neuroscience : the official journal of the Society for Neuroscience* **26**, 5340-5346
181. Zameer, A., Kasturirangan, S., Emadi, S., Nimmagadda, S. V., and Sierks, M. R. (2008) Anti-oligomeric Abeta single-chain variable domain antibody blocks Abeta-induced toxicity against human neuroblastoma cells. *Journal of molecular biology* **384**, 917-928
182. Robert, R., Dolezal, O., Waddington, L., Hattarki, M. K., Cappai, R., Masters, C. L., Hudson, P. J., and Wark, K. L. (2009) Engineered antibody intervention strategies for Alzheimer's disease and related dementias by targeting amyloid and toxic oligomers. *Protein engineering, design & selection : PEDS* **22**, 199-208
183. Lafaye, P., Achour, I., England, P., Duyckaerts, C., and Rougeon, F. (2009) Single-domain antibodies recognize selectively small oligomeric forms of amyloid beta, prevent Abeta-induced neurotoxicity and inhibit fibril formation. *Molecular immunology* **46**, 695-704
184. Hoyer, W., and Hard, T. (2008) Interaction of Alzheimer's A beta peptide with an engineered binding protein--thermodynamics and kinetics of coupled folding-binding. *Journal of molecular biology* **378**, 398-411
185. Luheshi, L. M., Hoyer, W., de Barros, T. P., van Dijk Hard, I., Brorsson, A. C., Macao, B., Persson, C., Crowther, D. C., Lomas, D. A., Stahl, S., Dobson, C. M., and Hard, T. (2010) Sequestration of the Abeta peptide prevents toxicity and promotes degradation in vivo. *PLoS biology* **8**, e1000334
186. Bradbury, A. R., and Marks, J. D. (2004) Antibodies from phage antibody libraries. *Journal of immunological methods* **290**, 29-49
187. Hoogenboom, H. R., Griffiths, A. D., Johnson, K. S., Chiswell, D. J., Hudson, P., and Winter, G. (1991) Multi-subunit proteins on the surface of filamentous phage: methodologies for displaying antibody (Fab) heavy and light chains. *Nucleic acids research* **19**, 4133-4137

188. Viti, F., Nilsson, F., Demartis, S., Huber, A., and Neri, D. (2000) Design and use of phage display libraries for the selection of antibodies and enzymes. *Methods in enzymology* **326**, 480-505
189. Azzazy, H. M., and Highsmith, W. E., Jr. (2002) Phage display technology: clinical applications and recent innovations. *Clinical biochemistry* **35**, 425-445
190. Querfurth, H. W., and LaFerla, F. M. (2010) Alzheimer's Disease. *The New England Journal of Medicine* **362**, 329-344
191. Mann, D. M., and Hardy, J. (2013) Amyloid or tau: the chicken or the egg? *Acta neuropathologica*
192. Lee, C. F. (2014) Discussion on The Off-rate of Monomers Dissociating from Amyloid- $\beta$  Protofibrils. (Hoyer, W. ed.
193. Burdick, D., Soreghan, B., Kwon, M., Kosmoski, J., Knauer, M., Henschen, A., Yates, J., Cotman, C., and Glabe, C. (1992) Assembly and aggregation properties of synthetic Alzheimer's A4/beta amyloid peptide analogs. *The Journal of biological chemistry* **267**, 546-554
194. Jarrett, J. T., Berger, E. P., and Lansbury, P. T., Jr. (1993) The C-terminus of the beta protein is critical in amyloidogenesis. *Annals of the New York Academy of Sciences* **695**, 144-148
195. Kempis, P. (2013) *Analyse des Amyloid-Beta Peptids mit suprauflösender optischer Mikroskopie*,
196. Martins, I. C., Kuperstein, I., Wilkinson, H., Maes, E., Vanbrabant, M., Jonckheere, W., Van Gelder, P., Hartmann, D., D'Hooge, R., De Strooper, B., Schymkowitz, J., and Rousseau, F. (2008) Lipids revert inert Abeta amyloid fibrils to neurotoxic protofibrils that affect learning in mice. *EMBO J* **27**, 224-233
197. Shankar, G. M., Bloodgood, B. L., Townsend, M., Walsh, D. M., Selkoe, D. J., and Sabatini, B. L. (2007) Natural oligomers of the Alzheimer amyloid-beta protein induce reversible synapse loss by modulating an NMDA-type glutamate receptor-dependent signaling pathway. *The Journal of neuroscience : the official journal of the Society for Neuroscience* **27**, 2866-2875
198. Mirecka, E. A., Shaykhalishahi, H., Gauhar, A., Akgül, S., Lecher, J., Willbold, D., Stoldt, M., and Hoyer, W. (2014) Sequestration of a b-hairpin enables control of a-synuclein aggregation. *Angew Chem Int Ed Engl*.
199. Chirita, C. N., Congdon, E. E., Yin, H., and Kuret, J. (2005) Triggers of full-length tau aggregation: a role for partially folded intermediates. *Biochemistry* **44**, 5862-5872
200. Andronesi, O. C., von Bergen, M., Biernat, J., Seidel, K., Griesinger, C., Mandelkow, E., and Baldus, M. (2008) Characterization of Alzheimer's-like paired helical filaments from the core domain of tau protein using solid-state NMR spectroscopy. *Journal of the American Chemical Society* **130**, 5922-5928
201. Margittai, M., and Langen, R. (2006) Side chain-dependent stacking modulates tau filament structure. *The Journal of biological chemistry* **281**, 37820-37827
202. Dinkel, P. D., Siddiqua, A., Huynh, H., Shah, M., and Margittai, M. (2011) Variations in filament conformation dictate seeding barrier between three- and four-repeat tau. *Biochemistry* **50**, 4330-4336
203. Bossi, S., Ferranti, B., Martinelli, C., Capasso, P., and de Marco, A. (2010) Antibody-mediated purification of co-expressed antigen-antibody complexes. *Protein expression and purification* **72**, 55-58
204. Schlieker, C., Bukau, B., and Mogk, A. (2002) Prevention and reversion of protein aggregation by molecular chaperones in the E. coli cytosol: implications for their applicability in biotechnology. *Journal of biotechnology* **96**, 13-21
205. Lee, E. K., Hwang, J. H., Shin, D. Y., Kim, D. I., and Yoo, Y. J. (2005) Production of recombinant amyloid-beta peptide 42 as an ubiquitin extension. *Protein expression and purification* **40**, 183-189

- 
206. Thapa, A., Shahnawaz, M., Karki, P., Raj Dahal, G., Sharoar, M. G., Yub Shin, S., Sup Lee, J., Cho, B., and Park, I. S. (2008) Purification of inclusion body-forming peptides and proteins in soluble form by fusion to *Escherichia coli* thermostable proteins. *BioTechniques* **44**, 787-796
  207. Hogbom, M., Eklund, M., Nygren, P. A., and Nordlund, P. (2003) Structural basis for recognition by an in vitro evolved affibody. *Proceedings of the National Academy of Sciences of the United States of America* **100**, 3191-3196

**ABBREVIATIONS**

3R	three-repeat tau
4R	four-repeat tau
A $\beta$	amyloid- $\beta$ peptide
AD	Alzheimer disease
AFM	atomic force microscopy
AICD	APP intracellular domain
Ala	alanine
APP	amyloid precursor protein
Asp	aspartate
AUC	analytical ultracentrifugation
BACE-1	$\beta$ -site of APP cleaving enzyme, $\beta$ -secretase
c.p.	compare
CDR(s)	complementarity-determining region(s)
C <sub>H</sub>	constant domain of the heavy chain
C <sub>L</sub>	constant domain of the light chain
$\Delta$ K280	deletion of lysine at position 280
e.g.	<i>exempli gratia</i> , for example
EM	transmission electron microscopy
FTDP-17	frontotemporal dementia with parkinsonism linked to chromosome-17
Glu	glutamate
HER2	human epidermal growth factor receptor 2
htau23	fetal isoform of tau
htau40	longest tau isoform
i.e.	<i>id est</i> , that is
K18	construct of tau including only the 4R-MTBR
kDa	kilo Dalton
Lys	lysine
Met	methionine
MTBR	microtubule-binding domain
NFT(s)	neurofibrillary tangle(s)
NMR	nuclear magnetic resonance spectroscopy
PHF(s)	paired helical filament(s)
PHF6	hexapeptide motif in R3
PHF6*	hexapeptide motif in R2
PHF6**	hexapeptide motif in R4
PrP	prion protein
R2	repeat 2
R3	repeat 3
SDS	sodium dodecyl sulfate
SEC	size exclusion chromatography
ThT	Thioflavine T
TP4	$\beta$ -wrapin binder to tau
TSEs	transmissible spongiform encephalopathies
Val	valine
VEGFR2	human vascular endothelial growth factor receptor 2
V <sub>H</sub>	variable domain of the heavy chain
V <sub>L</sub>	variable domain of the light chain

---

**LIST OF FIGURES AND TABLES**

Table 1: Selected features of some neurodegenerative diseases associated with amyloid deposition.....	9
Figure 1: Cleavage of APP.....	11
Figure 2: Isoforms and constructs of tau. ....	12
Figure 3: The amyloid fibril structure.....	14
Figure 4: Amyloid aggregation. ....	17
Figure 5: Representative illustrations of selected binding protein scaffolds. ....	27
Figure 6: The ZA $\beta_3$ :A $\beta$ 1-40 complex.....	30
Figure 7: Schematic of the phage display procedure.....	32
Figure 8: The energy barrier between monomer and protofibril compared for A $\beta$ 1-40 and A $\beta$ 1-42. ....	83
Figure 9: Possibilities of employing engineered binding proteins. ....	89

## DANKSAGUNG

Mein erster Dank geht an Wolfgang Hoyer, der mir ein spannendes Thema für meine Doktorarbeit angeboten hat und mich in seiner Bearbeitung unterstützt hat. Lieber Wolfgang, ich danke dir für zahlreiche Diskussionen, Gedanken und auch lustige Momente.

Ich danke meinen Kollegen, insbesondere Hamed Shaykalishahi und Aziz Gauhar für die gute Zusammenarbeit. Ich danke Ewa Mirecka und Stephen Marino für die Erstellung der Bibliothek auf die ein Teil dieser Arbeit aufbaut. Des Weiteren danke ich Mathias Stoldt, Carina Stein, Küpra Tökösz, und Jacqueline Richter für die gute und produktive Zusammenarbeit.

Ich danke den Mitarbeitern des Instituts für Physikalische Biologie für eine gute Atmosphäre bei der Arbeit. Ein besonderer Dank gilt Barbara Schulten, die das Herz des Labors ist und es am Laufen hält, genauso wie Elke Reinartz. Dies gilt ebenso für Oliver Bannach, der die Computer am Laufen hält und mit dem es viel Spaß gemacht hat den Praktikumsversuch durchzuführen.

Ich danke Jendrik Marbach für etliche kleine „Krisen“gespräche und die coolen Segeltörns-jetzt Karribick! Ich danke meinen lieben Freunden für ihr Verständnis, Unterstützung und Aufmunterung!

Ich danke Karin und Günter Ellinger für stetes Interesse am Voranschreiten meiner Arbeit. Ich danke euch auch besonders für zahlreiche schöne entspannende Abende, Tage und Wochenenden. Und nicht zu vergessen, für einige Bügelaktionen ☺

Meinem Bruder, Wolfram, möchte ich auch für schöne gemeinsame Momente, auch zusammen mit Marina, danken. Und du wirst es auch bald geschafft haben!

Meinem Onkel Thomas, seiner Frau Gaby und ihrer Mutter Rosi danke ich auch für schöne gemeinsame Stunden. Ebenso, danke ich Nora Ellinger und freue mich schon wieder auf Eierlikör und Michels Buffet in 2014!

Ein besonderer Dank geht an meine Oma, die immer an mich geglaubt, mir immer Mut zugesprochen und für mich gebetet hat.

Meinen Eltern, Cornelia und Burghard Grüning, danke ich ganz besonders. Sie haben mich größtmöglich unterstützt, mich angetrieben wenn es nötig war und sonst für den entsprechenden Ausgleich zur Arbeit gesorgt. Ich hab euch lieb! Auch hier darf man Reparatur-, Baumaßnahmen und Bügelaktionen nicht unerwähnt lassen ☺

Mein Dank an Philipp Ellinger ist nicht mit Worten auszudrücken. Ich kann nicht glücklicher sein als ihn an meiner Seite zu wissen. Und nur ein Bär kann so stark sein, wie er es in dieser Zeit sein musste. Ich danke dir! Kuss

Vielen Dank!

**Erklärung an Eides statt**

Ich versichere an Eides statt, dass die Dissertation von mir selbstständig und ohne unzulässige fremde Hilfe unter Beachtung der „Grundsätze zur Sicherung guter wissenschaftlicher Praxis an der Heinrich-Heine-Universität Düsseldorf“ erstellt worden ist. Die Dissertation wurde in der vorgelegten oder in ähnlicher Form noch bei keiner anderen Institution eingereicht. Ich habe bisher keine erfolglosen Promotionsversuche unternommen.

Düsseldorf, den

---

Clara Grüning